arXiv:hep-lat/0211011v1 5 Nov 2002

The Renormalised Quark Mass in the Schrödinger Functional of Lattice QCD

A One–Loop Calculation with a Non–Vanishing Background Field

D I S S E R T A T I O N

zur Erlangung des akademischen Grades
doctor rerum naturalium
(Dr. rer. nat.)
im Fach Physik

eingereicht an der
Mathematisch-Naturwissenschaftlichen Fakultät I
der Humboldt-Universität zu Berlin

von
Dipl.-Phys. Stefan Kurth
geboren am 10.04.1971 in Berlin

Präsident der Humboldt-Universität zu Berlin:
Prof. Dr. J. Mlynek

Dekan der Mathematisch-Naturwissenschaftlichen Fakultät I:
Prof. Dr. M. Linscheid

Gutachter:

1. Prof. Dr. Ulrich Wolff
2. Prof. Dr. Michael Müller-Preußker
3. Dr. Peter Weisz

eingereicht am:	06.06.2002
Tag der mündlichen Prüfung:	04.09.2002

Abstract

The renormalised quark mass in the Schrödinger functional is studied perturbatively with a non–vanishing background field.

The framework in which the calculations are done is the Schrödinger functional. Its definition and basic properties are reviewed and it is shown how to make the theory converge faster towards its continuum limit by O(a) improvement. It is explained how the Schrödinger functional scheme avoids the implications of treating a large energy range on a single lattice in order to determine the scale dependence of renormalised quantities. The description of the scale dependence by the step scaling function is introduced both for the renormalised coupling and the renormalised quark masses. The definition of the renormalised coupling in the Schrödinger functional is reviewed, and the concept of the renormalised mass being defined by the axial current and density via the PCAC–relation is explained. The running of the renormalised mass described by its step scaling function is presented as a consequence of the fact that the renormalisation constant of the axial density is scale dependent.

The central part of the thesis is the expansion of several correlation functions up to 1–loop order. The expansion coefficients are used to compute the critical quark mass at which the renormalised mass vanishes, as well as the 1–loop coefficient of the renormalisation constant of the axial density. Using the result for this renormalisation constant, the 2–loop anomalous dimension is obtained by conversion from the $\overline{\mathrm{MS}}$–scheme.

Another important application of perturbation theory carried out in this thesis is the determination of discretisation errors. The critical quark mass at 1–loop order is used to compute the deviation of the coupling's step scaling function from its continuum limit at 2–loop order. Several lattice artefacts of the current quark mass, defined by the PCAC relation with the unrenormalised axial current and density, are computed at 1–loop order. An essential property of the renormalised quark mass being computed in this thesis at 1–loop order is the deviation of its step scaling function from the continuum limit, which was so far only known for the zero background field case.

Keywords:
lattice QCD, renormalised quark mass, perturbation theory, O(a) improvement

Zusammenfassung

Diese Arbeit befasst sich mit störungstheoretischen Rechnungen zur renormierten Quarkmasse im Schrödinger-Funktional mit nicht verschwindendem Hintergrundfeld.

Als Grundlage der Rechnungen werden das Schrödinger-Funktional und seine grundlegenden Eigenschaften erläutert. Auch die O(a)-Verbesserung, die zu einem schnelleren Erreichen des Kontinuumslimes führen soll, wird in diesem Zusammenhang dargestellt. Des weiteren wird erklärt, auf welche Weise das Schrödinger-Funktional dazu dient, das Skalenverhalten renormierter Größen über einen großen Energiebereich zu untersuchen. Das Skalenverhalten sowohl der renormierten Kopplung als auch der renormierten Quarkmassen wird in diesem Schema durch Step-Scaling-Funktionen beschrieben. Die Definition der renormierten Kopplung wird dargestellt, ebenso die Definition der renormierten Masse, die mit Hilfe der PCAC-Relation über den Axialvektorstrom und die Pseudoskalardichte erfolgt. Die Skalenabhängigkeit der renormierten Masse wird auf die Skalenabhängigkeit der Renormierungskonstanten der Pseudoskalardichte zurückgeführt.

Breiten Raum nimmt die Berechnung verschiedener Korrelationsfunktionen bis zur Ein-Loop-Ordnung in Störungstheorie ein. Mit Hilfe der so ermittelten Koeffizienten wird die kritische Quarkmasse, bei der die renormierte Masse verschwindet, in Ein-Loop-Näherung berechnet, ebenso der Ein-Loop-Koeffizent der Renormierungskonstanten der Pseudoskalardichte. Mit Hilfe dieses Koeffizienten wird aus der bekannten anomalen Dimension in Zwei-Loop-Ordnung im $\overline{\mathrm{MS}}$-Schema die anomale Dimension im Schrödinger-Funktional berechnet.

Als weitere Anwendung der Störungstheorie werden verschiedene Diskretisierungsfehler bestimmt. Die kritische Quarkmasse in Ein-Loop-Ordnung geht in den Zwei-Loop-Koeffizienten des Diskretisierungfehlers der Step-Scaling-Funktion der renormierten Kopplung ein, der durch die Abweichung dieser Funktion von ihrem Kontinuumslimes definiert ist. Verschiedene Diskretisierungsfehler der Strommasse, die durch die PCAC-Relation mit unrenormiertem Axialvektorstrom und Pseudoskalardichte definiert ist, werden in Ein-Loop-Ordnung berechnet. Ein wichtiger Diskretisierungsfehler der renormierten Quarkmasse ist die Abweichung ihrer Step-Scaling-Funktion vom Kontinuumslimes. Dieser Fehler ist in Ein-Loop-Ordnung bislang nur mit verschwindendem Hintergrundfeld bekannt und wird in dieser Arbeit mit nicht verschwindendem Hintergrundfeld berechnet.

Schlagwörter:
Gitter-QCD, renormierte Quarkmasse, Störungstheorie, O(a)-Verbesserung

Acknowledgements

In one way or another, many people have contributed to this thesis and deserve some words of thanks.

First of all, I would like to thank my supervisor Ulli Wolff, both for taking me as a PhD student and for the guidance afterwards. Writing this thesis would not have been possible without his advice, which I should have asked for more often.

Very important contributions came from Peter Weisz, whose numerical checks were essential for the results in this thesis. During our correspondence, I recognised that the title "Mister Perturbation Theory", given to him by a colleague, is completely justified.

Furthermore, I would like to thank Rainer Sommer, who was so nice to have a critical look at my results even when being on holiday. It were some remarks of his that gave me the important idea that results looking wrong at a first glance are sometimes correct.

A colleague worth mentioning is Juri Rolf, not only for his ability to create a humorous atmosphere in the office we shared, but also for essential checks on the results.

Without Burkhard Bunk and his skills in solving computer problems, the project would have failed right from the beginning. In this context, I would also like to thank Martin Hasenbusch for useful hints on using the right Fortran compiler, and Bernd Gehrmann, both for his help in debugging some programs and for critical reading of the manuscript of this thesis.

Concerning critical looks, I am also grateful to Francesco Knechtli and to my brother Martin for participating in a thorough–going discussion of the results.

Furthermore, I would like to thank all members of the computational physics group at Humboldt University not mentioned so far for contributing to the pleasant atmosphere making my stay here an agreeable time. Gratefully, I also have to mention the Graduiertenkolleg 271 for ensuring my survival on the financial front.

Last but not least, I would like to thank Alice Rolf and Paul Hasenbusch for making my time as a PhD student more entertaining than it would have been without them.

Contents

1 Introduction **1**

2 QCD on the lattice **5**
2.1 Lattice gauge theory 5
2.2 Fermions on the lattice 6
2.2.1 The naïve fermion action 6
2.2.2 Fermion doubling and chiral symmetry 7
2.3 Symanzik's improvement programme 9
2.4 Renormalised parameters 11
2.4.1 The renormalised coupling 11
2.4.2 The renormalised quark masses 12
2.4.3 Finite renormalisations 14

3 The Schrödinger functional **15**
3.1 Motivation 15
3.2 Definition of the Schrödinger functional 16
3.2.1 Formal definition 17
3.2.2 Fermions in the Schrödinger functional 19
3.3 Lattice formulation 20
3.3.1 The Schrödinger functional action on the lattice 20
3.3.2 The background field 21
3.4 O(a) improvement of the Schrödinger functional 23
3.5 The renormalised coupling in the Schrödinger functional 25
3.5.1 Definition of the coupling 25
3.5.2 The step scaling function and its lattice artefacts 26

4 Perturbation theory in the Schrödinger functional **29**
4.1 The gauge fixed action 29
4.1.1 Preliminaries 29
4.1.2 The gauge fixing procedure 31
4.1.3 The total action 33
4.2 Perturbative expansion of the coupling 35
4.2.1 The coupling at 1– and 2–loop order 35

4.2.2 The step scaling function and its lattice artefacts at 1– and 2–loop order . . . 35

5 The current quark mass **37**
5.1 The PCAC relation . . . 37
5.2 The current mass and its lattice artefacts . . . 39
5.3 1–loop expansion of f_{A} and f_{P} . . . 41
5.3.1 Preliminaries . . . 41
5.3.2 The propagators . . . 43
5.3.3 The vertices . . . 45
5.3.4 The diagrams . . . 49
5.3.5 The improvement terms . . . 56
5.4 Calculation of the critical quark mass and the lattice artefacts . . . 61
5.5 Numerical computation of $f_{\mathrm{A}}^{(1)}$ and $f_{\mathrm{P}}^{(1)}$ . . . 63

6 The renormalised quark mass **65**
6.1 The renormalisation constant Z_{P} and its step scaling function . . . 65
6.1.1 The renormalisation constant Z_{P} . . . 65
6.1.2 The step scaling function of the running mass . . . 66
6.1.3 The 2–loop anomalous dimension . . . 68
6.2 The renormalisation constant Z_{P} at 1–loop order . . . 69
6.2.1 Preliminaries . . . 69
6.2.2 The correlation function f_1 at 1–loop order . . . 70
6.2.3 The improvement terms . . . 76
6.2.4 Computation of Z_{P} at 1–loop order . . . 77

7 Results **81**
7.1 The current quark mass . . . 81
7.1.1 The critical quark mass . . . 81
7.1.2 Lattice artefacts of the current mass up to 1–loop order . . . 84
7.2 Lattice artefacts of the step scaling function of the coupling . . . 84
7.3 The renormalised quark mass . . . 88
7.3.1 The renormalisation constant Z_{P} up to 1–loop order . . . 88
7.3.2 Lattice artefacts of Σ_{P} up to 1–loop order . . . 92
7.4 Numerical checks of the results . . . 95

8 Summary **99**

A Notations and conventions **101**
A.1 The Dirac matrices . . . 101
A.2 The basis of the Lie algebra $su(3)$ . . . 102
A.3 The background field . . . 103

B The numerical construction of the propagators **105**
B.1 The gluon and ghost propagators 105
B.2 The quark propagator 107

C The extrapolation procedure **109**

D Tables of expansion coefficients **113**

Bibliography **127**

List of Figures

2.1 The Sheikholeslami–Wohlert term 10

3.1 Strategy for evolving the renormalised coupling to large energy scales 16
3.2 The space time box of the Schrödinger functional 19

5.1 The correlation functions f_{A} and f_{P} 40
5.2 Diagram for f_{A} and f_{P} at tree level 50
5.3 Diagrams contributing to $f_{\mathrm{A}}(x_0)$ and $f_{\mathrm{P}}(x_0)$ at 1–loop order of perturbation theory both at vanishing and non–vanishing background field 52
5.4 Tadpole diagrams contributing to $f_{\mathrm{A}}(x_0)$ and $f_{\mathrm{P}}(x_0)$ at 1–loop order of perturbation theory 55
5.5 Diagrams for $f(\Gamma;\mathbf{p},x_0)^{(1)}_{\mathrm{V}}$, $f(\Gamma;\mathbf{p},x_0)^{(1)}_{\mathrm{Fb}}$, and $\frac{\partial}{\partial m_0}f(\Gamma;\mathbf{p},x_0)^{(0)}$ . . 58
5.6 Diagrams contributing to the improvement term proportional to $c_{\mathrm{t}}^{(1)}$ for f_{A} and f_{P} at 1–loop order 59
5.7 Further diagrams contributing to the improvement term proportional to $c_{\mathrm{t}}^{(1)}$ for f_{A} and f_{P} at 1–loop order 60

6.1 The correlation function f_1 66
6.2 Diagram for f_1 at tree level 70
6.3 Diagrams contributing to f_1 at 1–loop order of perturbation theory 71
6.4 Further diagrams contributing to f_1 at 1–loop order of perturbation theory 73
6.5 More diagrams contributing to f_1 at 1–loop order of perturbation theory 75
6.6 Diagrams for $f^{(1)}_{1,\mathrm{V}}$ and $f^{(1)}_{1,\mathrm{Fb}}$ 76
6.7 Diagrams contributing to $f^{(1)}_{1,\mathrm{Gb}}$ 77
6.8 More diagrams for $f^{(1)}_{1,\mathrm{Gb}}$ 78

7.1 The critical quark mass m_{c} at 1–loop order 83
7.2 The lattice artefacts $d = m_2(L/a) - m_1(L/a)$ and $e = m_1(2L/a) - m_1(L/a)$ at 1–loop order 86

7.3 The lattice artefacts $e = m_1(2L/a) - m_1(L/a)$ and $d = m_2(L/a) - m_1(L/a)$ up to 1–loop order at different values of the renormalised coupling $\bar{g}^2$ 87
7.4 The 2–loop discretisation error δ_2 89
7.5 The finite part Y_{p} of the renormalisation constant Z_{P} at 1–loop order 91
7.6 The 1–loop order discretisation error δ_k of the step scaling function Σ_{P} for $\theta = \pi/5$ and $\rho = 1$ 93
7.7 The 1–loop order discretisation error δ_k of the step scaling function Σ_{P} for various values of θ and ρ 94
7.8 Monte Carlo results for $f_{\mathrm{P}}(T/2)$ and f_1 at $L/a = 6$ 96
7.9 Monte Carlo results for $(f_{\mathrm{P}}(T/2) - f_{\mathrm{P}}^{(0)}(T/2))/g_0^2$ and $(f_1 - f_1^{(0)})/g_0^2$ at $L/a = 6$ 97

List of Tables

7.1 Perturbative results for the critical quark mass m_c up to 1–loop order . . . 82
7.2 The lattice artefacts $d = m_2(L) - m_1(L)$ and $e = m_1(2L) - m_1(L)$ up to 1–loop order . . . 85
7.3 The discretisation errors δ_{ij} up to 2–loop order . . . 88
7.4 The N_f independent and N_f dependent part of $Y_P(L/a)$ . . . 90
7.5 The N_f independent and N_f dependent part of $\delta_k(L/a)$ for $\theta = \pi/5$ and $\rho = 1$ . . . 93
7.6 The N_f independent and N_f dependent part of $\delta_k(L/a)$ for various values of θ and ρ compared to the zero background field values . . 95

A.1 C_a and S_a for the gauge group $SU(3)$ . . . 103
A.2 $\phi_a(x_0)$ and R_a for the gauge group $SU(3)$ . . . 104

D.1 Parts of the 1–loop coefficient $m_1^{(1)}$ for $\theta = \pi/5$ and $\rho = 1$ . . . 114
D.2 Parts of the 1–loop coefficient $m_1^{(1)}$ for $\theta = \pi/5$ and $\rho = 1$ (cont.) . 115
D.3 Parts of the 1–loop coefficient $m_1^{(1)}$ for various values of θ and ρ . 116
D.4 Parts of the 1–loop coefficient $m_1^{(1)}$ for various values of θ and ρ (cont.) . . . 117
D.5 Parts of the 1–loop coefficient $m_1^{(1)}(2L)$ with $m_1(L) = 0$ for $\theta = \pi/5$ and $\rho = 1$ . . . 118
D.6 Parts of the 1–loop coefficient $m_1^{(1)}(2L)$ with $m_1(L) = 0$ for $\theta = \pi/5$ and $\rho = 1$ (cont.) . . . 118
D.7 Parts of m' at 1–loop order with $m_1(L) = 0$ for $\theta = \pi/5$ and $\rho = 1$ 119
D.8 Parts of m' at 1–loop order with $m_1(L) = 0$ for $\theta = \pi/5$ and $\rho = 1$ (cont.) . . . 120
D.9 Parts of the 1–loop coefficient $Z_P^{(1)}$ at $\theta = \pi/5$ and $\rho = 1$ . . . 121
D.10 Parts of the 1–loop coefficient $Z_P^{(1)}$ at $\theta = \pi/5$ and $\rho = 1$ (cont.) . 121
D.11 Parts of the 1–loop coefficient $Z_P^{(1)}$ at various values of θ and ρ . . 122
D.12 Parts of the 1–loop coefficient $Z_P^{(1)}$ at various values of θ and ρ (cont.) . . . 123
D.13 Parts of the 1–loop coefficient $Z_P^{(1)}(2L)$ with $m_1(L) = 0$ at $\theta = \pi/5$ and $\rho = 1$ . . . 124

D.14 Parts of the 1–loop coefficient $Z_{\mathrm{P}}^{(1)}(2L)$ with $m_1(L) = 0$ at $\theta = \pi/5$ and $\rho = 1$ (cont.) 124
D.15 Parts of the 1–loop coefficient $Z_{\mathrm{P}}^{(1)}(2L)$ with $m_1(L) = 0$ at various values of θ and ρ 125
D.16 Parts of the 1–loop coefficient $Z_{\mathrm{P}}^{(1)}(2L)$ with $m_1(L) = 0$ at various values of θ and ρ (cont.) 126

Chapter 1

Introduction

Since the idea of matter consisting of particles was invented by the Greek philosopher Democrit (460–371 B.C.), there has been considerable progress in particle physics. Especially the invention first of quantum mechanics and later of quantum field theories have improved our basic understanding of elementary particles and their interactions. At the same time, large accelerators have made experiments in the high energy regime possible, giving large amounts of results to compare to theoretical predictions.

The modern theoretical framework of particle physics is the Standard Model, which is a gauge theory based on the invariance of the Lagrangian under the gauge group $SU(3)_{\mathrm{c}} \times SU(2)_{\mathrm{I}} \times U(1)_{\mathrm{Y}}$. The $SU(2) \times U(1)$ symmetry associated with the weak isospin I and the weak hypercharge Y describes the unified electroweak interaction [1, 2, 3]. In this context, particles acquire their masses via the Higgs mechanism [4].

The $SU(3)$ is the gauge group of the strong interaction affecting the hadrons. The idea of hadrons consisting of several point–like constituents was raised by Bjorken's analysis of the scaling properties of the structure functions in deep inelastic lepton–nucleon scattering [5]. This Bjorken scaling could be explained by the assumption that the hadrons consist of point-like particles called partons [6, 7]. These partons could then be identified with the so called quarks proposed earlier by Gell–Mann and Zweig in order to explain why hadrons can be classified into multiplets [8, 9]. As a theory for the strong interaction, Fritzsch, Gell–Mann, and Leutwyler proposed a non–Abelian gauge theory containing quarks obeying an $SU(3)$ gauge symmetry, where the associated quantum number is called colour [10].

This theory, called quantum chromodynamics (QCD) and today widely accepted as a model for the strong interaction, does however pose some problems. First of all, the theory is mathematically demanding, making it difficult to get predictions for experimental results. Second, the basic particles of the theory, the quarks, cannot be observed as free particles in nature, due to the phenomenon of confinement, binding them together in colour neutral hadrons.

However, despite of these problems, QCD together with the Feynman path integral approach [11, 12] turned out to be successful in the high energy regime. This is due to a property of non–Abelian gauge theories called asymptotic freedom [13, 14, 15]. Asymptotic freedom means that the coupling becomes small at high energies, allowing us to treat the quarks as free particles and to expand expectation values in powers of the gauge coupling. The coefficients in the expansion may be formally infinite, but can be made finite by regularisation and renormalisation. Regularisation means introducing an artificial momentum cutoff, and renormalisation means removing the divergences before removing the cutoff again. This method gave, for example, good results for the violation of the Bjorken scaling [16, 17, 18] and for QCD corrections to cross sections in electron–positron annihilation [19, 20, 21].

At low energies, perturbation theory cannot be applied, since the gauge coupling is large at these scales. For this case, Wilson introduced the concept of lattice QCD [22]. In this approach, space–time is treated as a four dimensional Euclidean lattice, the inverse lattice spacing a^{-1} serving as an ultraviolet cutoff. Removing the cutoff then corresponds to taking the continuum limit. On the lattice, QCD can be treated like a classical statistical system, where expectation values of observables can be obtained by Monte Carlo simulations. However, due to the limitations of computer power, the simulations are restricted to small lattices, making safe extrapolations to the continuum limit difficult. In order to improve the situation, Symanzik has introduced the concept of systematically removing terms of order a both from the action and from the observables, thus making the theory converge at a rate proportional to a^2 rather than a [23, 24].

In any case, both at high or low energies, the free parameters of the theory like the coupling and the quark masses have to be fixed by a set of observables. Since these observables have to be calculated in the theory, one has to take observables computable in the respective framework, i.e. lattice QCD or perturbation theory. This means that, at low energies, the parameters have to be fixed by low energy quantities like hadron masses, while for high energy perturbative calculations, one has to take high energy quantities like jet cross sections. It is not a priori clear if one set of fixed parameters describes the effects of QCD both at low and at high energy scales.

To study this question is one aim of the ALPHA collaboration. To this end, one has to define the renormalised parameters at low energies on the lattice and then evolve them to high energies, where they can be compared to the quantities defined perturbatively. The technique developed for this purpose is the Schrödinger functional scheme [25], which mainly amounts to defining the renormalised coupling and masses in a four dimensional box of box size L with special boundary conditions, imposing a constant colour electric background field. One thus gets a running coupling and running quark masses depending on the scale $1/L$. Having computed these quantities at some low energy scale, they may be evolved to higher energies step by step, using the so called step scaling function.

In the Schrödinger functional scheme, the renormalised strong coupling is constructed by choosing the boundary conditions to be dependent on a parameter η. The renormalised coupling is then defined as the derivative of an effective action with respect to η. For this reason, a non–vanishing background field is required for the renormalisation of the coupling.

The renormalised quark mass is defined using the PCAC relation, which connects the axial current $A^a_\mu(x)$ and the axial density $P^a(x)$ via

$$\partial_\mu A^a_\mu(x) = 2mP^a(x). \tag{1.1}$$

A renormalised quark mass can be defined using appropriate correlation functions containing the renormalised axial current and density. In contrast to the continuum case, where the axial current does not need to be renormalised, it does get a finite renormalisation in lattice QCD. This is a special consequence of the lattice regularisation, which explicitly breaks the chiral symmetry of the massless continuum theory. The renormalisation needed on the lattice is, however, finite and scale independent. The only divergent and scale dependent renormalisation constant needed for mass renormalisation is the one of the axial density $P^a(x)$. Thus, the running of the mass is completely described by this renormalisation constant. In contrast to the coupling, the mass renormalisation does not refer to the boundary gauge fields and may thus be done both with a vanishing or a non–vanishing background field.

In this scheme, the renormalised coupling and masses can be computed non–perturbatively by Monte Carlo simulations. Because of the high computational costs of simulations in full QCD, first results have been obtained in the quenched approximation [26], where the fermion determinant is constant, which means that the flavour number is set to $N_\mathrm{f} = 0$. There have, however, been recent results in full QCD with two flavours [27]. A less expensive toy model are so called bermions, which is a theory with $N_\mathrm{f} = -2$ [28, 29, 30, 31]. Although this is of course no realistic model of the physical world, bermions may be used to study structural properties of the theory. The original idea of extrapolating from $N_\mathrm{f} = -2$ and $N_\mathrm{f} = 0$ to $N_\mathrm{f} = 2$ did, however, not turn out to be practicable.

In the high energy regime, one wants to compare the renormalised parameters defined in the Schrödinger functional scheme to those commonly used in this energy region, i.e. to renormalised parameters in some perturbative scheme. For this purpose, it is necessary to expand the renormalised coupling and masses in powers of the bare coupling. For the coupling, this has been done both at 1– and 2–loop order [26, 32, 33, 34]. For the mass, however, there has only been a 1–loop calculation with a vanishing background field [35]. One of the aims of this thesis is to do this calculation with a non–vanishing background field. The computation will give the finite part of the renormalisation constant Z_P at 1–loop order as well as the 2–loop anomalous dimension.

Another useful application of perturbation theory on the lattice is the estimation of discretisation errors. For the coupling, the discretisation errors of the step

scaling function have been calculated in [34] up to 2–loop order. The 2–loop coefficient does, however, contain the critical quark mass, at which the renormalised mass vanishes, at 1–loop order. In [34], the known continuum limit of the critical mass was used. In order to get a precise result for the discretisation error, it is, however, necessary to use the critical mass at the finite lattice spacing at which the step scaling function is computed. The calculation of the critical quark mass and the resulting discretisation errors of the step scaling function of the coupling will be done in this theses.

For the quark mass, several lattice artefacts may be considered. One way to estimate the size of the lattice effects is to construct several different unrenormalised masses using different correlation functions containing the axial current and density. The difference of these masses should then be a lattice artefact of order a (or a^2 in the improved theory). For the renormalised quark mass, the deviation of the step scaling function from its continuum limit is of interest. This deviation has already been calculated with a vanishing background field. If one wishes to compute the quark masses in the same runs as the coupling, it is, however, desirable to have an estimate for the discretisation errors of the step scaling function of the running quark mass with a non–vanishing background field. These discretisation errors will be computed in this thesis at 1–loop order.

The thesis is structured as follows: Chapter 2 is an introduction to the basic ideas of lattice QCD. Also Symanzik's O(a)–improvement is presented here. In chapter 3, the Schrödinger functional is defined, and the renormalisation of the coupling constant in this scheme is outlined. The Schrödinger functional is then treated perturbatively in chapter 4, including the details of the gauge fixing and the expansion of the coupling. Chapter 5 describes how to calculate the PCAC mass, serving as a mass later renormalised multiplicatively, on the lattice. The critical bare mass, at which the lattice PCAC mass vanishes, is calculated at 1–loop order by expanding correlation functions containing the axial current and density. In chapter 6, the renormalisation of the mass is studied. The renormalisation constant of the axial density and its step scaling function are calculated at 1–loop order as well as the discretisation errors. The results of all calculations can be found in chapter 7. The thesis closes with a summary in chapter 8. Finally, the appendices A–D contain notational conventions, some computational techniques used in the calculations, and some numerical results.

Chapter 2

QCD on the lattice

2.1 Lattice gauge theory

In this chapter, the basic concepts of lattice gauge theory will be introduced. Of course, only a short overview can be given here, with an emphasis on ideas needed later on in this thesis. More details on quantum fields on the lattice can be found in the literature [36, 37, 38, 39, 40].

Lattice gauge theory is set up on a 4–dimensional hyper-cubic lattice with lattice spacing a. In order to bring quantum field theories onto the lattice, one has to discretise the action of the corresponding Euclidean continuum theory.

In the continuum, the gauge fields are represented by the vector potential $A_\mu(x)$, lying in the Lie algebra of the gauge group.[1] The calculations in this thesis will be done for the case of QCD, where one has the gauge group $SU(3)$, but the construction of the theory is applicable for a general gauge group $SU(N)$. On the lattice, the gauge fields are expressed as parallel transporters between the lattice points. Let $\hat{\mu}$ be a unit vector in direction μ. Then the gauge field on the link between the lattice site x and the lattice site $x + a\hat{\mu}$ is represented by a *link variable* $U(x, \mu)$, which is related to the continuum gauge field $A_\mu(x)$ by

$$U(x, \mu) = e^{aA_\mu(x)}. \tag{2.1}$$

Local gauge transformations are represented by gauge functions $\Omega(x)$ living on the lattice sites x and acting on the link variables according to

$$U(x, \mu) \to U^\Omega(x, \mu) = \Omega(x)U(x, \mu)\Omega(x + a\hat{\mu})^{-1}. \tag{2.2}$$

Clearly, $U(x, \mu)$ is an element of the gauge group, allowing us to take products of link variables on a curve consisting of several links. A special curve giving a gauge invariant combination of link variables is a closed loop consisting of four

[1] Here and in the following, Greek letters denote Lorentz indices from 0 to 3, while Latin indices run from 1 to 3.

links in the μ-ν plane, which is called a *plaquette* p. The product of the link variables around this plaquette is then denoted by

$$U(p) = U(x,\mu)U(x+a\hat{\mu},\nu)U(x+a\hat{\nu},\mu)^{-1}U(x,\nu)^{-1}. \tag{2.3}$$

According to Wilson [22], an appropriate discretisation of the gauge field action is given by

$$S_{\mathrm{G}}[U] = \frac{1}{g_0^2}\sum_p \mathrm{tr}\left\{1 - U(p)\right\}, \tag{2.4}$$

where the sum is to be taken over all *oriented* plaquettes. The Wilson action can be shown to coincide with the continuum action at leading order in the small a expansion.

2.2 Fermions on the lattice

2.2.1 The naïve fermion action

In contrast to the gauge fields, the lattice fermions are not situated on the links but on the lattice sites themselves. They are Grassmann valued fields and carry Dirac, colour, and flavour indices. Thus they differ from the continuum case merely by the fact that they are only defined on discrete lattice sites.

To set up the theory, one has to define an action for the fermions on the lattice. For this purpose, the covariant derivative has to be carried over to the lattice. This may be done using the forward derivative,

$$\nabla_\mu\psi(x) = \frac{1}{a}\left[U(x,\mu)\psi(x+a\hat{\mu}) - \psi(x)\right] \tag{2.5}$$

or the backward derivative,

$$\nabla^*_\mu\psi(x) = \frac{1}{a}\left[\psi(x) - U(x-a\hat{\mu},\mu)^{-1}\psi(x-a\hat{\mu})\right]. \tag{2.6}$$

Using the average of these two derivatives as a discretised version of the covariant derivative, one gets the naïve fermion action

$$S_{\mathrm{F,naïve}}[U,\bar{\psi},\psi] = a^4\sum_x \bar{\psi}(x)(D+m_0)\psi(x), \tag{2.7}$$

where m_0 is the bare quark mass. Strictly speaking, m_0 is a diagonal matrix containing the bare masses of the different quark flavours. In this thesis, however, only degenerate quark masses will be considered. D is the Dirac operator,

$$D = \frac{1}{2}\gamma_\mu\left(\nabla^*_\mu + \nabla_\mu\right), \tag{2.8}$$

where γ_μ are the Dirac matrices, which can be found in appendix A. Of course, one may add terms that vanish in the continuum limit. While (2.8) seems to be the simplest formulation, it turns out to cause some severe problems outlined in the next subsection. For later use, a more complicated expression for the fermion action will be needed due to these difficulties.

2.2.2 Fermion doubling and chiral symmetry

The main problem of the naïve fermion action (2.8) is the phenomenon of *fermion doubling*. This property is easily seen when writing down the propagator one gets from the naïve action in momentum space,

$$S^{-1}(p) = m_0 + \frac{i}{a}\sum_\mu \gamma_\mu \sin(p_\mu a). \tag{2.9}$$

This expression has not only one but 16 zeros in the Brillouin cell in the chiral limit $m_0 \to 0$, and these spurious poles of the propagator cannot be ignored, since they survive in the continuum limit. To make things even worse, they come in pairs with opposite axial charge, thus spoiling the axial anomaly. As a consequence of these problems, the naïve action is obviously not acceptable as a discretised fermion action.

The occurrence of fermion doublers can also be understood as a consequence of the symmetries of the naïve action. In the continuum, the flavour symmetry of the massless action on the classical level is $U(1)_\mathrm{L} \times U(1)_\mathrm{R} \times SU(N_\mathrm{f})_\mathrm{L} \times SU(N_\mathrm{f})_\mathrm{R}$, where N_f is the number of flavours. As a consequence, one has the symmetries $U(1)_\mathrm{V}$ and $SU(N_\mathrm{f})_\mathrm{V}$, which are valid even in the case of non–vanishing masses, and the axial symmetries $U(1)_\mathrm{A}$ and $SU(N_\mathrm{f})_\mathrm{A}$. While $SU(N_\mathrm{f})_\mathrm{V}$ and $U(1)_\mathrm{V}$ remain exact symmetries of the quantised theory giving rise to isospin and baryon number conservation, the $SU(N_\mathrm{f})_\mathrm{A}$ is spontaneously broken, leading to (N_f^2-1) Goldstone bosons, which explains the relative lightness of the pions. The $U(1)_\mathrm{A}$ is broken in the quantised theory by the axial anomaly. The crucial point here is that the naïve fermion action (2.8), instead of $U(1)_\mathrm{L} \times U(1)_\mathrm{R}$, has a much larger symmetry group $U(4)_\mathrm{L} \times U(4)_\mathrm{R}$, where the spurious symmetry transformations exchange the corners of the Brillouin cell.

Several ways have been tried to circumvent the problem of fermion doubling. One possibility is to define only one spin component per lattice site, thus reducing the number of fermions to four, which may then be interpreted as different flavours. These *staggered fermions* introduced by Kogut and Susskind [41, 42] have a major drawback in the fact that gauge interactions break the flavour symmetry at finite lattice spacing. As a consequence, the 16 degrees of freedom on the lattice become a mixture of spin and flavour, making the interpretation of operators in terms of spin and flavour non trivial.

Another possibility is to add a dimension five operator to the fermion action. This term will vanish in the continuum limit and can be chosen such that the

15 spurious flavours become infinitely heavy. A convenient choice was proposed by Wilson [43]. Instead of taking the naïve Dirac operator (2.8), the action of *Wilson fermions* is constructed using the Dirac–Wilson operator

$$D = \frac{1}{2}\left\{\gamma_\mu(\nabla^*_\mu + \nabla_\mu) - a\nabla^*_\mu\nabla_\mu\right\}. \tag{2.10}$$

Using this action, the spurious fermion states get a mass proportional to $1/a$ and thus decouple in the continuum limit.

While the problem of fermion doubling is solved by the Wilson action, it introduces a new difficulty. The chiral symmetry of the massless theory is explicitly broken by the additional term in (2.10). This is easily seen by stating that

$$\gamma_5 D + D\gamma_5 \neq 0. \tag{2.11}$$

This is, of course, a major drawback, because it disables us from treating theories in which chiral eigenstates play a crucial role on the lattice. For these purposes, one would like to have a theory free of doublers and preserving chiral symmetry. The question whether such a theory does exist is answered by the *Nielsen–Ninomiya theorem* [44]. If one uses an action which

- is translation invariant,
- has continuous lattice momenta in the range $[0, 2\pi]$ for $L \to \infty$,
- has only local interactions,
- gives the correct continuum propagator in the continuum limit,
- and preserves chiral symmetry at finite lattice spacing a,

then the theory will have doublers. This means that one has the choice either to get rid of the doublers or to preserve chiral symmetry, but one can not have both at the same time.

A recent development in this field is the resurrection [45] of the Ginsparg–Wilson relation [46] for a chirally invariant formulation. If the Dirac operator satisfies the condition

$$\gamma_5 D + D\gamma_5 = aD\gamma_5 D, \tag{2.12}$$

then it has a symmetry that becomes the chiral symmetry in the continuum limit. Lüscher has presented a detailed analysis how to avoid the implications of the Nielsen–Ninomiya theorem using Ginsparg–Wilson fermions [47].

For our calculations, which do not depend on the chiral symmetry of the theory, it is however simpler to use the Dirac–Wilson operator. The only implications of broken chiral symmetry will be a finite scale independent renormalisation of the axial current and an additional renormalisation of the quark mass.

2.3 Symanzik's improvement programme

The main purpose of lattice gauge theory is to calculate physical quantities on the lattice and then extrapolate to the continuum limit. However, the closer one gets to the continuum limit, the more expensive are Monte Carlo simulations due to critical slowing down. Therefore, it is desirable to make the theory converge faster. This is possible due to the fact that the lattice discretisation of the action is not unique. One may add irrelevant terms that vanish in the continuum limit. This property may be used to cancel $\mathrm{O}(a)$ effects. At small lattice spacing a, one gets an effective action

$$S_{\text{eff}} = S_0 + aS_1 + \mathrm{O}(a^2) \tag{2.13}$$

by Taylor expansion. The principle idea of Symanzik [23, 24] was to subtract the order a term, thus making the theory converge at a rate proportional to a^2.

The pure gauge action can be shown to reach its continuum limit at $\mathrm{O}(a^2)$ without any additional terms, but the quark action does need improvement. For on–shell quantities, the $\mathrm{O}(a)$ contribution can be cancelled by the *Sheikholeslami–Wohlert term* [48]

$$\delta S_{\mathrm{V}}[U, \bar{\psi}, \psi] = a^5 \sum_x \bar{\psi}(x) \delta D_{\mathrm{V}} \psi(x), \tag{2.14}$$

with

$$\delta D_{\mathrm{V}} = c_{\mathrm{sw}} \frac{i}{4} \sigma_{\mu\nu} \hat{F}_{\mu\nu}(x). \tag{2.15}$$

The Dirac structure of the Sheikholeslami–Wohlert term is given by

$$\sigma_{\mu\nu} = \frac{i}{2}[\gamma_\mu, \gamma_\nu], \tag{2.16}$$

and $\hat{F}_{\mu\nu}(x)$ is the lattice field tensor given by

$$\hat{F}_{\mu\nu}(x) = \frac{1}{8a^2} \left\{ Q_{\mu\nu}(x) - Q_{\nu\mu}(x) \right\}, \tag{2.17}$$

with

$$\begin{aligned} Q_{\mu\nu}(x) \;=\; & \Big\{ U(x,\mu) U(x+a\hat{\mu},\nu) U(x+a\hat{\nu},\mu)^{-1} U(x,\nu)^{-1} \\ & + U(x,\nu) U(x+a\hat{\nu}-a\hat{\mu},\mu)^{-1} U(x-a\hat{\mu},\nu)^{-1} U(x-a\hat{\mu},\mu) \\ & + U(x-a\hat{\mu},\mu)^{-1} U(x-a\hat{\nu}-a\hat{\mu},\nu)^{-1} U(x-a\hat{\nu}-a\hat{\mu},\mu) U(x-a\hat{\nu},\nu) \\ & + U(x-a\hat{\nu},\nu)^{-1} U(x-a\hat{\nu},\mu) U(x-a\hat{\nu}+a\hat{\mu},\nu) U(x,\mu)^{-1} \Big\}. \end{aligned} \tag{2.18}$$

The Sheikholeslami–Wohlert term may be visualised by the characteristic shape in figure 2.1. Therefore, it is often called the *clover term.* The improvement

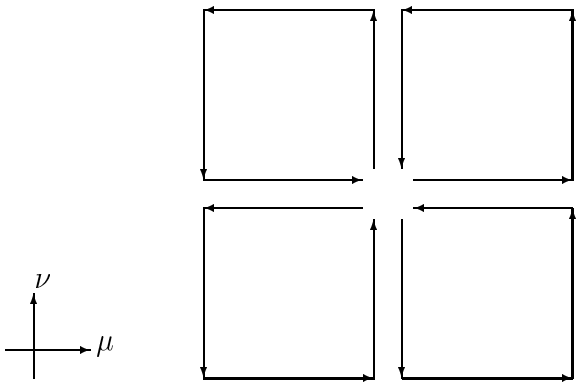

Figure 2.1: *The Sheikholeslami–Wohlert term*

coefficient $c_{\rm sw}$ may be computed in perturbation theory. Up to 1–loop order, the result originally obtained by Wohlert [49] is

$$c_{\rm sw} = 1 + 0.26590(7)g_0^2 + \mathrm{O}(g_0^4), \tag{2.19}$$

independent of $N_{\rm f}$. Values obtained later using the Schrödinger functional [50, 51] are completely compatible with this result. For $N_{\rm f} = 0$ and $N_{\rm f} = 2$, $c_{\rm sw}$ has also been computed non–perturbatively [52, 53]. For $0 \leq g_0 \leq 1$, the results can be represented in good approximation by

$$c_{\rm sw}(g_0)|_{N_{\rm f}=0} = \frac{1 - 0.656g_0^2 - 0.152g_0^4 - 0.054g_0^6}{1 - 0.922g_0^2}, \tag{2.20}$$

$$c_{\rm sw}(g_0)|_{N_{\rm f}=2} = \frac{1 - 0.454g_0^2 - 0.175g_0^4 + 0.012g_0^6 + 0.045g_0^8}{1 - 0.720g_0^2}. \tag{2.21}$$

For the case of $N_{\rm f} = -2$ ("bermions"), one gets good results by linear extrapolation of the results for $N_{\rm f} = 2$ and $N_{\rm f} = 0$ [31].

However, the improvement of the action is not sufficient to improve the expectation value of every composite operator. The operator has to be improved in addition. To achieve this improvement, one has to expand the operator in powers of a and then remove the $\mathrm{O}(a)$ contribution. To this end, one has to write down a basis of operators with the correct dimensions and the symmetries required and subtract them with appropriate improvement coefficients. Often, the number of operators can be reduced by using the equations of motion. An important example is the improvement of the axial current [54], which will play an important role in later chapters.

2.4 Renormalised parameters

It is well known that, in order to get finite results, quantum field theories have to be renormalised, leading to a redefinition of the parameters of the theory, like couplings and fermion masses. The renormalisation is done by first introducing a regularisation, then doing the renormalisation cancelling divergences, and finally removing the cutoff again. This situation does also occur in lattice QCD, where the cutoff is given by the inverse lattice spacing a^{-1}. In the following, the renormalisation of the coupling and the masses will be briefly summarised.

2.4.1 The renormalised coupling

Since, in the continuum, the coupling can only be calculated perturbatively, one has to apply a perturbative renormalisation scheme to compute the renormalised coupling $\bar{g}$. Such schemes are the MOM–scheme [55], the MS–scheme [56], and the $\overline{\text{MS}}$–scheme [57] of dimensional regularisation. The last two schemes differ by the subtraction of a constant in the $\overline{\text{MS}}$–scheme in addition to the divergence, while in the MS–scheme, only the divergence itself is removed. This variety of renormalisation schemes is in contrast to the case of QED, where one naturally chooses the scheme such that the charges and masses of the leptons get their physical values. This is however not possible in QCD, because free quarks cannot be observed.

On the lattice, one can define a renormalised coupling non–perturbatively [36]. One possibility is to consider a pair of a static quark and a static antiquark separated by the distance r. The force $F(r)$ acting between these quarks is the derivative of the static potential $V(r)$, which can be computed from Wilson loops. Defining $\alpha = \bar{g}^2/4\pi$, a physical coupling is given by

$$\alpha_{q\bar{q}}(q) = \frac{1}{C_{\text{F}}} r^2 F(r), \tag{2.22}$$

where $q = 1/r$, and C_{F} is the eigenvalue of the quadratic Casimir operator of the gauge group in the fundamental representation. For $SU(N)$, it is

$$C_{\text{F}} = \frac{N^2 - 1}{2N}. \tag{2.23}$$

For QCD, one thus has $C_{\text{F}} = 4/3$.

What all couplings computed in different renormalisation schemes have in common is the fact that they depend on a renormalisation scale, like q in (2.22). The running of the coupling is described by the Callan–Symanzik equation

$$q\frac{\partial \bar{g}}{\partial q} = \beta(\bar{g}), \tag{2.24}$$

where the β–function has an asymptotic expansion

$$\beta(\bar{g}) \overset{\bar{g}\to 0}{\sim} -\bar{g}^3 \left[b_0 + \bar{g}^2 b_1 + \mathrm{O}(\bar{g}^4)\right]. \tag{2.25}$$

In general, the expansion coefficients will be scheme dependent. The first two, however, are the same in any two mass–independent renormalisation schemes. In these schemes, the renormalisation conditions are imposed at zero quark mass, thus avoiding an implicit dependence of the renormalised coupling and fields on the quark mass. Then b_0 and b_1 are given by

$$b_0 = \frac{1}{(4\pi)^2}\left(11 - \frac{2}{3}N_\mathrm{f}\right), \tag{2.26}$$

$$b_1 = \frac{1}{(4\pi)^4}\left(102 - \frac{38}{3}N_\mathrm{f}\right). \tag{2.27}$$

For energies high enough to make perturbation theory possible and for sufficiently small flavour number N_f, one has asymptotic freedom, which means that the coupling approaches zero in the limit of infinite energy. The asymptotic solution is

$$\bar{g}^2 \overset{q\to\infty}{\sim} \frac{1}{b_0 \ln(q^2/\Lambda^2)} - \frac{b_1 \ln[\ln(q^2/\Lambda^2)]}{b_0^3[\ln(q^2/\Lambda^2)]^2} + \mathrm{O}\left(\frac{\{\ln[\ln(q^2/\Lambda^2)]\}^2}{[\ln(q^2/\Lambda^2)]^3}\right), \tag{2.28}$$

where Λ is a scheme dependent integration constant. In the high energy regime, it may be used to relate different renormalisation schemes to each other.

2.4.2 The renormalised quark masses

Like the coupling, also the quark masses have to be renormalised. In continuum perturbation theory, their renormalisation is incorporated in the MOM–, MS–, or $\overline{\mathrm{MS}}$–scheme. On the lattice, a good choice is the *hadronic scheme*, in which the bare quark masses are eliminated in favour of physical hadron masses. First, one chooses certain values for the bare coupling g_0 and the bare masses am_0^f, where the index f labels the different quark flavours u,d,s,c,b. Neglecting isospin breaking, one may assume the light quarks to be degenerate and define $m_0^\mathrm{l} \equiv m_0^\mathrm{u} = m_0^\mathrm{d}$. Next, one calculates the masses of five different hadrons H containing quarks of all flavours that are to be renormalised, for example H=p,π,K,D,B. The hadron masses will, of course, depend on the bare parameters,

$$am_\mathrm{H} = am_\mathrm{H}(g_0, am_0^\mathrm{l}, am_0^\mathrm{s}, am_0^\mathrm{c}, am_0^\mathrm{b}). \tag{2.29}$$

To renormalise the theory, one first sets the proton mass m_p to its experimental value $m_\mathrm{p}^\mathrm{exp}$, determining the lattice spacing by

$$a = \frac{am_\mathrm{p}}{m_\mathrm{p}^\mathrm{exp}}, \tag{2.30}$$

Next, one has to choose the parameters am_0^{f} such that the hadrons get the masses known from experiment. Equivalently, one can fix the bare quark masses at a given value of g_0 from the condition

$$\frac{am_{\mathrm{H}}}{am_{\mathrm{p}}} = \frac{am_{\mathrm{H}}^{\mathrm{exp}}}{am_{\mathrm{p}}^{\mathrm{exp}}} \tag{2.31}$$

with H = π,K,D,B. The bare coupling then determines the lattice spacing via 2.30. Once having renormalised the masses this way and the coupling according to 2.22, the theory is completely defined in terms of physical observables.

Like the renormalised coupling, the renormalised masses are scale dependent. To describe their running, one may use the τ–function,

$$q\frac{\partial \overline{m}}{\partial q} = \tau(\bar{g})\overline{m}. \tag{2.32}$$

It has an asymptotic expansion

$$\tau(\bar{g}) \overset{\bar{g}\to 0}{\sim} -\bar{g}^2\left[d_0 + \bar{g}^2 d_1 + \mathrm{O}(\bar{g}^4)\right], \tag{2.33}$$

where all expansion coefficients are scheme dependent except the 1–loop anomalous dimension d_0. It is given by

$$d_0 = \frac{6C_{\mathrm{F}}}{(4\pi)^2}. \tag{2.34}$$

The 2–loop anomalous dimension d_1 is known in the $\overline{\mathrm{MS}}$ scheme. For the gauge group $SU(N)$ it is given by [35]

$$d_1^{\overline{\mathrm{MS}}} = \frac{C_{\mathrm{F}}}{(4\pi)^4}\left\{\frac{203}{6}N - \frac{3}{2}N^{-1} - \frac{10}{3}N_{\mathrm{f}}\right\}. \tag{2.35}$$

As an analogy to the Λ–parameter, one may introduce a *renormalisation group invariant quark mass* M, defined by

$$M = \lim_{q\to\infty} \overline{m}(2b_0\bar{g}^2)^{-d_0/2b_0^2}. \tag{2.36}$$

It can be shown to be independent of the renormalisation scheme. It can be used to obtain the running mass in any scheme by first computing it in one scheme and then inserting the proper β– and τ–functions of the other schemes into the renormalisation group equations [58].

Λ and M are fundamental parameters of QCD, which are not fixed by the theory, but have to be determined from experimental results.

2.4.3 Finite renormalisations

Having renormalised the coupling and the masses, the running parameters at the momentum scale q can be obtained by integrating (2.24) and (2.32) with the boundary conditions

$$\bar{g}(\mu) = g_{\rm R}, \qquad \overline{m}^f(\mu) = m_{\rm R}^f, \qquad f = 1, \ldots, N_{\rm f}. \tag{2.37}$$

Any two mass–independent renormalisation schemes are related by a finite renormalisation of the parameters,

$$\mu' = c\mu, \qquad c > 0, \tag{2.38}$$

$$g'_{\rm R} = g_{\rm R}\sqrt{\chi_{\rm g}(g_{\rm R})}, \tag{2.39}$$

$$m_{\rm R}^{f\,\prime} = m_{\rm R}^f\, \chi_{\rm m}(g_{\rm R}). \tag{2.40}$$

The finite renormalisation constants $\chi_{\rm g}$ and $\chi_{\rm m}$ may be expanded in perturbation theory,

$$\chi(g_{\rm R}) \stackrel{g_{\rm R}\to 0}{=\!\!\sim} 1 + \sum_{k=1}^{\infty} \chi^{(k)} g_{\rm R}^{2k}. \tag{2.41}$$

With this expansion, one finds that the 2–loop anomalous dimensions in both schemes are related by

$$d'_1 = d_1 + 2b_0\chi_{\rm m}^{(1)} - d_0\chi_{\rm g}^{(1)}. \tag{2.42}$$

The crucial point of this equation is that $\chi_{\rm m}^{(1)}$ and $\chi_{\rm g}^{(1)}$ are 1–loop coefficients. This means that, knowing the 2–loop anomalous dimension in one scheme, one may compute it in a different scheme by a 1–loop calculation. This will be used later in order to get the 2–loop anomalous dimension in the Schrödinger functional scheme from the 2–loop anomalous dimension in the $\overline{\rm MS}$–scheme.

Chapter 3

The Schrödinger functional

3.1 Motivation

In the last chapter, it was seen that one has two kinds of renormalised couplings: The perturbatively defined couplings like $\alpha_{\overline{\mathrm{MS}}}$ extracted from high energy experiments, and $\alpha_{q\bar{q}}$, defined non–perturbatively at the scale of hadron physics. Now, an obvious task for lattice QCD is to connect these couplings. This amounts to calculating the coupling non–perturbatively at low energy scales and then evolving it to high energies, where one may compare it with high energy experiments like the determination of jet cross sections. Thus one should be able to verify that the hadron spectrum and the properties of jets really are described by the same theory.

To do this calculation, one has to fulfil several requirements at the same time.

- One has to calculate $\alpha_{q\bar{q}}(q)$ at energy scales $q \sim 10\,\mathrm{GeV}$ or higher, in order to make the connection to other schemes with sufficiently small perturbative errors.
- One has to keep the renormalisation scale q sufficiently far from the cut-off a^{-1} in order to keep the discretisation errors small. Otherwise, a safe extrapolation to the continuum limit might not be possible.
- One has to keep the box size L large compared to the confinement scale in order to avoid large finite size effects.

These criteria can be summarised by

$$L \gg \frac{1}{0.4\,\mathrm{GeV}} \gg \frac{1}{q} \sim \frac{1}{10\,\mathrm{GeV}} \gg a. \tag{3.1}$$

This means that one has to perform a Monte Carlo simulation on a four dimensional lattice with a size of $L/a \gg 25$. Even with modern computer technique, lattices of this size are far from being accessible.

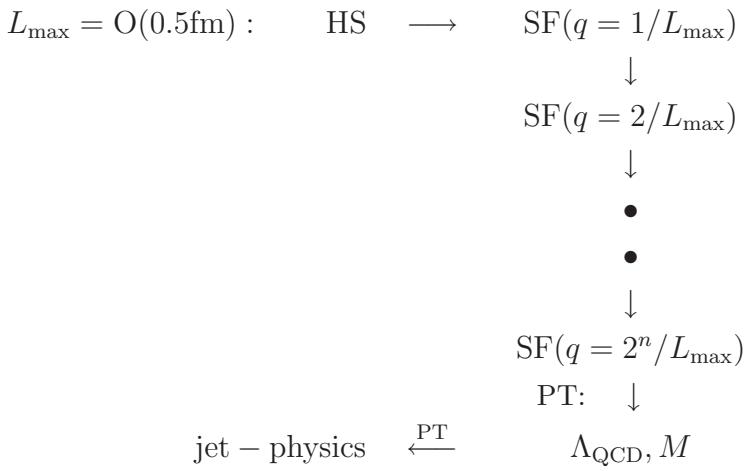

Figure 3.1: *Strategy for evolving the renormalised coupling to large energy scales*

However, there is a solution to this problem. The difficulties can be avoided by identifying the two physical scales [25],

$$q = \frac{1}{L}. \tag{3.2}$$

This means one takes a finite size effect as the physical observable. The strategy one may use now is presented in figure 3.1. First, the hadronic scheme HS can be related to a finite volume scheme denoted by SF at a low energy scale $q = 1/L_{\max}$. As a finite volume scheme, we will use the Schrödinger functional, which will be defined in the next section. Within this scheme, one may now compute the evolution up to the desired scale $q = 2^n/L_{\max}$ step by step. With this recursive procedure, one can thus avoid using quantities defined at energy scales very wide apart. At an energy scale large enough for perturbation theory, one can then compute the Λ–parameter and the renormalisation group invariant quark masses in order to make the connection to renormalisation schemes defined perturbatively.

3.2 Definition of the Schrödinger functional

The purpose of this section is to define the Schrödinger functional and introduce the basic notation. This will be done in the continuum. In the next section, these definitions will be carried over to the lattice.

3.2.1 Formal definition

We start with the definition of the Schrödinger functional in pure gauge theory and later add the fermions to this framework.

The Schrödinger functional is basically defined by the Hamiltonian evolution of the gauge fields. To this end, one has to specify the theory at $x_0 = 0$ (or any other fixed time) and write down the Hamiltonian of the theory.

Since the main purpose of the Schrödinger functional method is to study the scaling properties of QCD at a finite volume, the theory is set up in an $L \times L \times L$ box where L serves as the scale, and one assumes periodic boundary conditions for the gauge fields. The gauge fields are represented by vector potentials with values in the Lie algebra of $SU(N)$. The calculations in this thesis will be done for the case of $SU(3)$, but the definition is applicable for arbitrary N. In the temporal gauge, one is thus left with Lie algebra valued vector components $A_k(\mathbf{x})$ which have to be periodic.[1] Under gauge transformations $\Lambda(\mathbf{x})$, they transform like

$$A_k(\mathbf{x}) \to A_k^\Lambda(\mathbf{x}) = \Lambda(\mathbf{x}) A_k(\mathbf{x}) \Lambda(\mathbf{x})^{-1} + \Lambda(\mathbf{x}) \partial_k \Lambda(\mathbf{x})^{-1}. \tag{3.3}$$

In order to preserve the periodicity of the gauge fields, only periodic gauge functions $\Lambda(\mathbf{x})$ may be allowed, which can be regarded as continuous Lie group valued functions on a 3–dimensional torus. These functions are topologically non–trivial and fall into disconnected classes that are distinguished by an integer winding number. If one wrote down the Schrödinger functional in the functional integral representation, where one has to integrate over all gauge configurations, one would have to sum over all topological classes. However, since this difficulty does not occur on the lattice, it will not be studied in detail here.

Now, the quantum mechanical states may be defined as wave functionals $\psi[A]$ acting on the gauge fields. Then the quantity

$$\langle \psi | \chi \rangle = \int D[A] \psi[A]^* \chi[A] \tag{3.4}$$

defines a scalar product on these states. The measure $D[A]$ is meant to be

$$D[A] = \prod_{\mathbf{x},k,a} dA_k^a(\mathbf{x}), \tag{3.5}$$

where $A_k^a(\mathbf{x})$ are the components of $A_k(\mathbf{x})$ in a basis of the Lie algebra $su(n)$. The basis used in this thesis is explained in appendix A. However, not all states defined this way are physical. Physical states have to be gauge invariant, which means they have to satisfy

$$\psi[A^\Lambda] = \psi[A]. \tag{3.6}$$

[1] Here and in the following, bold letters like $\mathbf{x}$ denote vectors in the three dimensional space.

Obviously, these physical states form a subspace of the space of states. Any state can be projected onto this subspace by a projector $\mathbb{P}$, given by

$$\mathbb{P}\psi[A] = \int D[\Lambda]\psi[A^\Lambda], \tag{3.7}$$

where the measure $D[\Lambda]$ is defined by

$$D[\Lambda] = \prod_{\mathbf{x}} d\Lambda(\mathbf{x}). \tag{3.8}$$

The canonically conjugate field of the gauge field is the colour electric field

$$F^a_{0k}(\mathbf{x}) = -i\frac{\delta}{\delta A^a_k(\mathbf{x})}. \tag{3.9}$$

It is part of the colour field tensor, with the magnetic components given by

$$F^a_{kl}(\mathbf{x}) = \partial_k A^a_l(\mathbf{x}) - \partial_l A^a_k(\mathbf{x}) + f^{abc}A^b_k(\mathbf{x})A^c_l(\mathbf{x}), \tag{3.10}$$

where f^{abc} are the structure constants of $SU(N)$. Using this tensor, one can write down the Hamilton operator $\mathbb{H}$,

$$\mathbb{H} = \int_0^L d^3\mathbf{x}\left\{\frac{g_0^2}{2}F^a_{0k}(\mathbf{x})F^a_{0k}(\mathbf{x}) + \frac{1}{4g_0^2}F^a_{kl}(\mathbf{x})F^a_{kl}(\mathbf{x})\right\}. \tag{3.11}$$

Now, for any smooth gauge field C_k, a state $|C\rangle$ may be defined such that

$$\langle C|\psi\rangle = \psi[C] \tag{3.12}$$

holds for all wave functionals $\psi[A]$. This state is not necessarily physical, but of course it can be made so by projecting it onto the physical subspace using the projector $\mathbb{P}$. The Schrödinger functional $\mathcal{Z}[C', C]$ is then defined by

$$\mathcal{Z}[C', C] = \langle C'|e^{-\mathbb{H}T}\mathbb{P}|C\rangle. \tag{3.13}$$

The projector $\mathbb{P}$ makes sure that the Schrödinger functional is invariant under gauge transformations of C and C', since only gauge invariant intermediate states contribute.

An alternative way to write down the Schrödinger functional is to set up the theory on a 4–dimensional box $L \times L \times L \times T$ and express the time evolution operator $e^{-\mathbb{H}T}$ by a functional integral, using the action

$$S[A] = -\frac{1}{2g_0^2}\int_0^L d^4x\,\mathrm{tr}\{F_{\mu\nu}F_{\mu\nu}\}. \tag{3.14}$$

The fields C and C' then define the boundary conditions on the gauge field at $x_0 = 0$ and $x_0 = T$. This situation may be depicted by figure 3.2. On the lattice, this representation will be chosen.

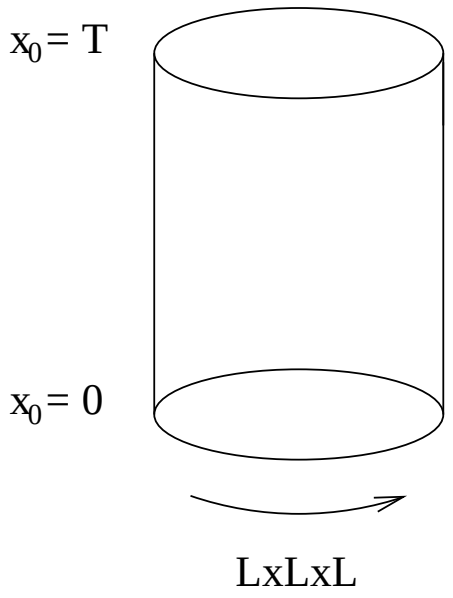

Figure 3.2: *The space time box of the Schrödinger functional*

3.2.2 Fermions in the Schrödinger functional

Though mostly used on a lattice, also the fermion part of the Schrödinger functional may formally be defined in the continuum [59, 32]. The easiest way to do this is in the functional integral representation with the action

$$\begin{aligned} S_{\mathrm{F}}[A,\bar{\psi},\psi] &= \int_0^T dx_0 \int_0^L d^3\mathbf{x}\, \bar{\psi}(x)\left(\gamma_\mu D_\mu + m_0\right)\psi(x) \\ &\quad - \int_0^L d^3\mathbf{x}\, \left[\bar{\psi}(x) P_- \psi(x)\right]_{x_0=0} \\ &\quad - \int_0^L d^3\mathbf{x}\, \left[\bar{\psi}(x) P_+ \psi(x)\right]_{x_0=T}, \end{aligned} \tag{3.15}$$

where $D_\mu = \partial_\mu + A_\mu$ is the covariant derivative of the fermion fields. The projectors P_+ and P_- are defined by

$$P_\pm = \frac{1}{2}\left(1 \pm \gamma_0\right). \tag{3.16}$$

In time direction, Dirichlet boundary conditions are imposed for the quark fields

$$P_+\psi(x)|_{x_0=0} = \rho(\mathbf{x}), \qquad P_-\psi(x)|_{x_0=T} = \rho'(\mathbf{x}), \tag{3.17}$$

and for the antiquark fields

$$\bar{\psi}(x)P_-|_{x_0=0} = \bar{\rho}(\mathbf{x}), \qquad \bar{\psi}(x)P_+|_{x_0=T} = \bar{\rho}'(\mathbf{x}). \tag{3.18}$$

In space direction, the quark fields are chosen to be periodic up to a phase factor,

$$\psi(x + L\hat{k}) = e^{i\theta}\psi(x), \quad \bar{\psi}(x + L\hat{k}) = e^{-i\theta}\bar{\psi}(x). \tag{3.19}$$

For the time being, θ will be left arbitrary. Later, several values for θ will be considered.

3.3 Lattice formulation

3.3.1 The Schrödinger functional action on the lattice

Since the Schrödinger functional is characterised by its boundary conditions, these boundary conditions have to be carried over to the lattice. This means that the link variables have to take fixed boundary values in the $x_0 = 0$ and $x_0 = T$ planes,

$$U(x, k)|_{x_0=0} = W(\mathbf{x}, k), \qquad U(x, k)|_{x_0=T} = W'(\mathbf{x}, k). \tag{3.20}$$

In order to make contact to the continuum definition of the Schrödinger functional, one has to relate the lattice boundary fields W and W' to the continuum boundary fields C and C'. This relationship is naturally established by recalling that the link variables are parallel transporters for colour vector fields. So it seems natural to define

$$W(\mathbf{x}, k) = \mathcal{P} \exp\left\{ a \int_0^1 dt\, C_k(\mathbf{x} + a\hat{k} - ta\hat{k}) \right\}, \tag{3.21}$$

and analogously for W' using the continuum field C' instead of C. Here, $\mathcal{P}$ denotes the path ordering along the link.

The gauge field action in the Schrödinger functional is given by the Wilson action

$$S_{\mathrm{G}}[U] = \frac{1}{g_0^2} \sum_p w(p) \mathrm{tr}\left\{1 - U(p)\right\}, \tag{3.22}$$

only modified by the weight factors $w(p)$. In the unimproved theory, one has $w(p) = 1/2$ for the spatial plaquettes at $x_0 = 0$ and $x_0 = T$ and $w(p) = 1$ in all other cases. In the improved theory, these weight factors will be modified at the boundaries. Here again, the sum in (3.22) is to be taken over all *oriented* plaquettes.

For the quarks, we take the usual Dirac–Wilson action,

$$S_{\mathrm{F}}[U, \bar{\psi}, \psi] = a^4 \sum_x \bar{\psi}(x)(D + m_0)\psi(x), \tag{3.23}$$

with the Dirac–Wilson operator (2.10)

$$D = \frac{1}{2}\left\{\gamma_\mu(\nabla_\mu^* + \nabla_\mu) - a\nabla_\mu^*\nabla_\mu\right\}. \tag{3.24}$$

The Schrödinger functional on the lattice is then given by

$$\mathcal{Z}[C', \bar{\rho}', \rho', C, \bar{\rho}, \rho] = \int D[\psi]D[\bar{\psi}]D[U]e^{-S[U,\bar{\psi},\psi]}, \tag{3.25}$$

where the action S is the sum of the gauge field action and the fermionic action, $S = S_{\mathrm{G}} + S_{\mathrm{F}}$. The expectation value of any product $\mathcal{O}$ of fields is now given by

$$\langle \mathcal{O} \rangle = \left\{ \frac{1}{\mathcal{Z}} \int D[U]D[\psi]D[\bar{\psi}]\mathcal{O}e^{-S[U,\bar{\psi},\psi]} \right\}_{\bar{\rho}'=\rho'=\bar{\rho}=\rho=0}. \tag{3.26}$$

Apart from the quark and gauge fields, the operator $\mathcal{O}$ may also contain the boundary fields

$$\zeta(\mathbf{x}) = \frac{\delta}{\delta\bar{\rho}(\mathbf{x})} \quad , \qquad \zeta'(\mathbf{x}) = \frac{\delta}{\delta\bar{\rho}'(\mathbf{x})}, \tag{3.27}$$

$$\bar{\zeta}(\mathbf{x}) = -\frac{\delta}{\delta\rho(\mathbf{x})} \quad , \qquad \bar{\zeta}'(\mathbf{x}) = -\frac{\delta}{\delta\rho'(\mathbf{x})}. \tag{3.28}$$

These derivatives have to be understood in the sense that they act on the Boltzmann factor in (3.26). They will be used to define correlation functions which play an important role in later chapters.

3.3.2 The background field

Unless they are zero, the boundary fields C and C' obviously impose a background field which is given by a solution of the field equations with the correct boundary values. It will be explained later that a non–zero background field is inevitably needed to define the renormalised coupling in the Schrödinger functional. Since only small lattices are accessible for numerical simulations, one cannot make the lattice spacing arbitrarily small. Thus one has to deal with considerable cutoff effects, which requires a strategy to keep the discretisation errors as small as possible. In particular, one has to look for a background field leading to minimal cutoff effects.

It can be shown that spatially constant Abelian boundary fields give good results [60]. So one may choose

$$C_k = \frac{i}{L} \begin{pmatrix} \phi_{k1} & 0 & 0 \\ 0 & \phi_{k2} & 0 \\ 0 & 0 & \phi_{k3} \end{pmatrix}, \tag{3.29}$$

and analogously for C'. In the following, C_k and C'_k will be chosen to be independent of k, i.e. $C_1 = C_2 = C_3$ and $C'_1 = C'_2 = C'_3$. An obvious solution of the field equations with these boundary conditions is

$$B_0 = 0, \quad B_k = \left[x_0 C'_k + (T - x_0)C_k\right]/T. \tag{3.30}$$

This solution is a constant colour electric field, which can easily be seen from the corresponding field tensor

$$G_{0k} = i\mathcal{E}, \quad G_{kl} = 0, \tag{3.31}$$

with

$$\mathcal{E} = -i[C'_k - C_k]/T. \tag{3.32}$$

On the lattice, the background field must of course be given in terms of the link variables. A good candidate for the lattice background field is

$$V(x,\mu) = \exp\{aB_\mu(x)\}, \tag{3.33}$$

which, after inserting (3.30), gives a field that only in the spatial directions is different from 1,

$$V(x,0) = 1, \quad V(x,k) = V(x_0), \tag{3.34}$$

with

$$V(x_0) = \exp\left\{i[\mathcal{E}x_0 - iC]\right\}. \tag{3.35}$$

This field trivially fulfils the boundary conditions and it can easily be shown to be a solution of the field equations. Yet, this field is still only a candidate for the background field. It has to be shown that V really is a configuration of least action and that the same action is only given by fields that are gauge equivalent to V. According to [60], this is the case for the gauge group $SU(N)$ if the $\phi_{k\alpha}$ and the $\phi'_{k\alpha}$ lie in the so called fundamental domain

$$\phi_{k1} < \phi_{k2} < \ldots < \phi_{kN}, \quad |\phi_{k\alpha} - \phi_{k\beta}| < 2\pi, \quad \sum_{\alpha=1}^{N} \phi_{k\alpha} = 0, \tag{3.36}$$

and the relation

$$TL/a^2 > (N-1)\pi^2 \max\{1, N/16\} \tag{3.37}$$

holds. This relation is only needed in the proof of the theorem for technical reasons, it is of no physical significance. For $N \leq 3$ and the lattices of interest, it is unimportant.

A convenient choice of boundary fields obeying the conditions mentioned above is

$$C_k = \frac{i}{L}\begin{pmatrix} \eta - \frac{\pi}{3} & 0 & 0 \\ 0 & \eta(-\frac{1}{2}+\nu) & 0 \\ 0 & 0 & -\eta(\frac{1}{2}+\nu) + \frac{\pi}{3} \end{pmatrix} \tag{3.38}$$

for the boundary field at $x_0 = 0$ and

$$C'_k = \frac{i}{L}\begin{pmatrix} -\eta - \pi & 0 & 0 \\ 0 & \eta(\frac{1}{2}+\nu) + \frac{\pi}{3} & 0 \\ 0 & 0 & \eta(\frac{1}{2}-\nu) + \frac{2\pi}{3} \end{pmatrix} \tag{3.39}$$

for the field at $x_0 = T$. Here, we will choose $\nu = 0$. Later, also η will be set to zero, but first it is needed as a variable in order to define the renormalised coupling in section 3.5.

3.4 O(a) improvement of the Schrödinger functional

In the Schrödinger functional, one has two kinds of counter-terms for O(a) improvement. The first one is the volume term, improving the fields in the interior of the lattice. The second kind are the boundary counter-terms arising from the Schrödinger functional boundary conditions in the time direction. The improved action thus becomes a sum

$$S_{\mathrm{impr}}[U,\bar{\psi},\psi] = S[U,\bar{\psi},\psi] + \delta S_{\mathrm{V}}[U,\bar{\psi},\psi] + \delta S_{\mathrm{G,b}}[U] + \delta S_{\mathrm{F,b}}[U,\bar{\psi},\psi], \qquad (3.40)$$

where the volume term δS_{V} is the Sheikholeslami–Wohlert term familiar from section 2.3.

On the boundaries at $x_0 = 0$ and $x_0 = T$, composite fields of dimension 4 have to be subtracted. There are contributions of order a both from the gauge fields and the quark fields [54]. The gauge field contribution is cancelled by the counter-term

$$\begin{aligned} \delta S_{\mathrm{G,b}}[U] &= \frac{1}{2g_0^2}(c_{\mathrm{s}}-1)\sum_{p_{\mathrm{s}}} \mathrm{tr}\{1-U(p_{\mathrm{s}})\} \\ &\quad + \frac{1}{g_0^2}(c_{\mathrm{t}}-1)\sum_{p_{\mathrm{t}}} \mathrm{tr}\{1-U(p_{\mathrm{t}})\}, \end{aligned} \qquad (3.41)$$

where the sum runs over all oriented plaquettes at the boundaries, both time-like (p_{t}) and space-like (p_{s}). This boundary improvement term simply amounts to changing the weights $w(p)$ in (3.22) to $w(p_{\mathrm{t}}) = c_{\mathrm{t}}$ and $w(p_{\mathrm{s}}) = c_{\mathrm{s}}/2$. The boundary improvement coefficients have perturbative expansions

$$c_{\mathrm{t}} = 1 + c_{\mathrm{t}}^{(1)} g_0^2 + c_{\mathrm{t}}^{(2)} g_0^4 + \mathrm{O}(g_0^6), \qquad (3.42)$$

$$c_{\mathrm{s}} = 1 + c_{\mathrm{s}}^{(1)} g_0^2 + c_{\mathrm{s}}^{(2)} g_0^4 + \mathrm{O}(g_0^6). \qquad (3.43)$$

The 1–loop coefficient for the time-like plaquettes can be decomposed into a part independent of the flavour number and a term linear in N_{f},

$$c_{\mathrm{t}}^{(1)} = c_{\mathrm{t}}^{(1,0)} + c_{\mathrm{t}}^{(1,1)} N_{\mathrm{f}}, \qquad (3.44)$$

where the coefficients are given by [26, 32]

$$c_{\mathrm{t}}^{(1,0)} = -0.08900(5), \qquad (3.45)$$

$$c_{\mathrm{t}}^{(1,1)} = 0.0191410(1). \qquad (3.46)$$

The 2–loop coefficient has a decomposition

$$c_{\mathrm{t}}^{(2)} = c_{\mathrm{t}}^{(2,0)} + c_{\mathrm{t}}^{(2,1)} N_{\mathrm{f}} + c_{\mathrm{t}}^{(2,2)} N_{\mathrm{f}}^2, \qquad (3.47)$$

with [61, 34]

$$c_{\rm t}^{(2,0)} = -0.0294(3), \tag{3.48}$$
$$c_{\rm t}^{(2,1)} = 0.002(1), \tag{3.49}$$
$$c_{\rm t}^{(2,2)} = 0.0000(1). \tag{3.50}$$

With the special choice of spatially constant Abelian boundary fields, the improvement term for the space-like plaquettes vanishes and $c_{\rm s}$ may be disregarded.

For the boundary counter-terms depending on the quark fields, all possible composite fields of dimension 4 and how most of them are eliminated are presented in [54]. It can be shown that one is left with four terms which, ensuring time reversal invariance, are given by

$$\begin{aligned}\delta S_{\rm F,b}[U,\bar\psi,\psi] &= a^4\sum_{\mathbf{x}}\Big\{(\tilde c_{\rm s}-1)[\hat{\mathcal{O}}_{\rm s}(\mathbf{x})+\hat{\mathcal{O}}'_{\rm s}(\mathbf{x})]\\ &\qquad (\tilde c_{\rm t}-1)[\hat{\mathcal{O}}_{\rm t}(\mathbf{x})+\hat{\mathcal{O}}'_{\rm t}(\mathbf{x})]\Big\},\end{aligned} \tag{3.51}$$

with the fields

$$\hat{\mathcal{O}}_{\rm s}(\mathbf{x}) = \frac{1}{2}\bar\rho(\mathbf{x})\gamma_k(\nabla_k^*+\nabla_k)\rho(\mathbf{x}), \tag{3.52}$$
$$\hat{\mathcal{O}}'_{\rm s}(\mathbf{x}) = \frac{1}{2}\bar\rho'(\mathbf{x})\gamma_k(\nabla_k^*+\nabla_k)\rho'(\mathbf{x}), \tag{3.53}$$
$$\hat{\mathcal{O}}_{\rm t}(\mathbf{x}) = \Big\{\bar\psi(y)P_+\nabla_0^*\psi(y)+\bar\psi(y)\overleftarrow{\nabla}_0^*P_-\psi(y)\Big\}_{y=(a,\mathbf{x})}, \tag{3.54}$$
$$\hat{\mathcal{O}}'_{\rm t}(\mathbf{x}) = \Big\{\bar\psi(y)P_-\nabla_0\psi(y)+\bar\psi(y)\overleftarrow{\nabla}_0P_+\psi(y)\Big\}_{y=(T-a,\mathbf{x})}. \tag{3.55}$$

Setting the boundary quark fields to zero, one is left only with $\hat{\mathcal{O}}_{\rm t}(\mathbf{x})$ and $\hat{\mathcal{O}}'_{\rm t}(\mathbf{x})$. The volume term and the quark boundary term may then be rewritten as a change in the Dirac–Wilson operator,

$$\delta D = \delta D_{\rm V} + \delta D_{\rm b}, \tag{3.56}$$

with the volume term

$$\delta D_{\rm V}\psi(x) = c_{\rm sw}\frac{i}{4}a\sigma_{\mu\nu}\hat F_{\mu\nu}(x)\psi(x), \tag{3.57}$$

and the boundary term

$$\begin{aligned}\delta D_{\rm b}\psi(x) &= (\tilde c_{\rm t}-1)\frac{1}{a}\Big\{\delta_{x_0,a}\Big[\psi(x)-U(x-a\hat 0,0)^{-1}P_+\psi(x-a\hat 0)\Big]\\ &\qquad +\delta_{x_0,T-a}\Big[\psi(x)-U(x,0)P_-\psi(x+a\hat 0)\Big]\Big\}.\end{aligned} \tag{3.58}$$

The improvement coefficient $\tilde{c}_{\rm t}$ can be computed in perturbation theory [50, 62] and is, up to 1–loop order, given by

$$\tilde{c}_{\rm t} = 1 - 0.01795(2)g_0^2 + {\rm O}(g_0^4). \tag{3.59}$$

Having improved the action, the expectation value of any improved field polynomial $\mathcal{O}$ converges to its continuum limit at a rate proportional to a^2. First integrating over the quark fields, this expectation value may be decomposed into a quark field average and a gauge field average,

$$\langle \mathcal{O} \rangle = \langle [\mathcal{O}]_{\rm F} \rangle_{\rm G}\,, \tag{3.60}$$

where $[\ldots]_{\rm F}$ is the quark field average at a given gauge field configuration U and $\langle \ldots \rangle_{\rm G}$ denotes the gauge field average with a probability density proportional to

$$\det(D + \delta D + m_0) \exp\left\{-S_{\rm G}[U] - \delta S_{\rm G,b}\right\}. \tag{3.61}$$

The quark field average $[\mathcal{O}]_{\rm F}$ can be defined by a generating functional,

$$\begin{aligned} \mathcal{Z}_{\rm F}[\bar{\rho}', \rho'; \bar{\rho}, \rho; \bar{\eta}, \eta; U] \;&=\; \int D[\psi] D[\bar{\psi}] \exp\Big\{ -S_{\rm F,impr}[U, \bar{\psi}, \psi] \\ &\quad + a^4 \sum_x \left[\bar{\psi}(x)\eta(x) + \bar{\eta}(x)\psi(x) \right] \Big\}, \end{aligned} \tag{3.62}$$

where $S_{\rm F,impr}$ is the improved fermion action and $\eta(x)$ and $\bar{\eta}(x)$, $0 < x_0 < T$, are source fields for the quark and antiquark fields in the interior of the space–time box. Substituting

$$\psi(x) \to \frac{\delta}{\delta \bar{\eta}(x)}, \qquad \bar{\psi}(x) \to -\frac{\delta}{\delta \eta(x)}, \tag{3.63}$$

one gets the quark field average by

$$[\mathcal{O}]_{\rm F} = \left\{ \frac{1}{\mathcal{Z}_{\rm F}} \mathcal{O} \mathcal{Z}_{\rm F} \right\}_{\bar{\rho}' = \ldots = \eta = 0}. \tag{3.64}$$

This decomposition into quark and gauge field averages will be used in later calculations.

3.5 The renormalised coupling in the Schrödinger functional

3.5.1 Definition of the coupling

Having introduced the Schrödinger functional, we can now turn to defining the renormalised coupling in this framework. In order to make practical use of this method, certain criteria have to be met by the coupling.

Since a central point in the Schrödinger functional method is the wish to compute a renormalised coupling non–perturbatively, the coupling should be easy to measure in Monte Carlo simulations. Furthermore, the results obtained in these simulations should be easy to extrapolate to the continuum limit without too large uncertainties. For this reason, discretisation errors should be small. And, last but not least, the coupling should have an easy perturbative expansion, such that the beta function can be computed to sufficient order and a matching can be done to perturbatively defined renormalisation schemes in the high energy regime.

Considering all these criteria leads to a definition based on the effective action

$$\Gamma[V] = -\ln \mathcal{Z}[C', C]. \tag{3.65}$$

Since the background field V depends on the parameter η in the boundary gauge fields (3.38) and (3.39), the effective action will be a function of η, too. So one may take the derivative

$$\Gamma'[V] = \frac{\partial}{\partial \eta}\Gamma[V], \tag{3.66}$$

and expand it in powers of the bare coupling g_0,

$$\Gamma'[V] = g_0^{-2}\Gamma'_0[V] + \Gamma'_1[V] + g_0^2\Gamma'_2[V] + \mathrm{O}(g_0^4). \tag{3.67}$$

Γ' can be shown to be finite when it is expressed in terms of a renormalised coupling like $\bar{g}_{\overline{\mathrm{MS}}}$. Properly normalised, it may itself serve as a renormalised coupling. Thus, the Schrödinger functional coupling is defined as

$$\bar{g}^2(L) = \left.\frac{\Gamma'_0[V]}{\Gamma'[V]}\right|_{\eta=0}. \tag{3.68}$$

The normalisation factor Γ'_0 makes sure that the coupling defined this way coincides with the bare coupling at tree level of perturbation theory. This coupling satisfies all requirements mentioned above. As the expectation value

$$\Gamma'[V] = \left\langle \frac{\partial S}{\partial \eta} \right\rangle, \tag{3.69}$$

it is easily accessible to Monte Carlo simulations. The discretisation errors turn out to be tolerable. And it is relatively easy to expand in perturbation theory. The problem of the perturbative expansion of the Schrödinger functional will be addressed in chapter 4.

3.5.2 The step scaling function and its lattice artefacts

By definition, the Schrödinger functional coupling defined in this chapter runs with the box size L. In order to study its scaling behaviour, one needs a recipe

for evolving the coupling from one length scale to another, which means that some kind of discrete β–function is required. An appropriate function in the Schrödinger functional is the step scaling function. First of all, one has to start from a given coupling $u = \bar{g}^2(L)$. Then the length scale is changed by a factor 2. (In principle, one may choose a different scale factor, but 2 is commonly used for obvious reasons. If one took a larger factor, one would have to perform simulations on larger lattices.) Then, keeping the bare coupling fixed, the coupling at the length scale $2L$ has a value $\bar{g}^2(2L) = u'$. The step scaling function σ is then defined as

$$\sigma(u) = u'. \tag{3.70}$$

Obviously, σ is an integral over the β–function. In fact, it has a perturbative expansion

$$\sigma(u) = u + 2b_0 \ln(2)\, u^2 + \ldots \tag{3.71}$$

However, this is only true in the continuum limit. On a lattice with finite lattice spacing a, the step scaling function will depend on the lattice resolution a/L. So, instead of (3.70), one has to define

$$\Sigma(u, a/L) = u'. \tag{3.72}$$

The continuum step scaling function σ is the continuum limit of Σ, i.e. $\sigma(u) = \lim_{a/L \to 0} \Sigma(u, a/L)$. In practice, the step scaling function is obtained by simulations on pairs of lattices to determine $\Sigma(u, a/L)$. One then gets $\sigma(u)$ by extrapolating these results to the continuum limit. The deviation of the step scaling function from its continuum limit,

$$\delta(u, a/L) = \frac{\Sigma(u, a/L) - \sigma(u)}{\sigma(u)}, \tag{3.73}$$

may be expanded in perturbation theory to give an idea of the size of the cutoff effects. Details of the perturbative expansion will be presented in chapter 4.

Chapter 4

Perturbation theory in the Schrödinger functional

4.1 The gauge fixed action

4.1.1 Preliminaries

It is a well known fact that, in order to set up perturbation theory, one has to fix the gauge. Otherwise, zero modes would occur, since the minimum of the action is degenerate in the directions of gauge transformations.

The Schrödinger functional on the lattice is invariant under all gauge transformations that leave the boundary fields unchanged. This condition is only satisfied by gauge functions $\Omega(x)$ that are constant and diagonal on the boundaries $x_0 = 0$ and $x_0 = T$. These gauge functions form a group $\hat{\mathcal{G}}$. However, not the whole group $\hat{\mathcal{G}}$ needs to be fixed. Those gauge functions $\Omega(x)$ which are constant and diagonal not only on the boundaries but on the whole lattice act trivially on the background field. They form a subgroup of $\hat{\mathcal{G}}$ isomorphic to the Cartan subgroup C_N of $SU(N)$, which may be factored out and then survives as a global symmetry of the theory. The gauge fixing has thus to be done on the group

$$\mathcal{G} = \hat{\mathcal{G}}/C_N. \tag{4.1}$$

$\mathcal{G}$ may be identified with the subgroup of transformations $\Omega \in \hat{\mathcal{G}}$ that are equal to a fixed constant diagonal matrix at $x_0 = T$. Here we choose $\Omega(x)|_{x_0=T} = 1$.

The Lie algebra $\mathcal{L}_\mathcal{G}$ of $\mathcal{G}$ consists of fields ω with $\omega(x) \in su(N)$. The gauge functions Ω may be parametrised as

$$\Omega(x) = \exp\{-g_0\omega(x)\} = 1 - g_0\omega(x) + \mathrm{O}(g_0^2). \tag{4.2}$$

Obviously, ω must obey the boundary conditions

$$\omega(0, \mathbf{x}) = \kappa, \qquad \omega(T, \mathbf{x}) = 0, \tag{4.3}$$

where κ is constant and diagonal.

Analogously, one may expand the gauge field U around the background field. Let $\mathcal{H}$ be the set of gauge fields satisfying the Schrödinger functional boundary conditions. In a neighbourhood of the background field, any gauge field U may be parametrised by

$$\begin{aligned} U(x,\mu) &= \exp\{g_0 a q_\mu(x)\} V(x,\mu) \\ &= \left\{1 + g_0 a q_\mu(x) + \frac{1}{2} g_0^2 a^2 q_\mu(x)^2 + \mathrm{O}(g_0^3)\right\} V(x,\mu), \end{aligned} \tag{4.4}$$

with $q_\mu(x) \in su(N)$. In perturbation theory, the vector fields q become the gluons. They form a linear space $\mathcal{L}_\mathcal{H}$ and obey the boundary conditions

$$q_k(0,\mathbf{x}) = 0, \qquad q_k(T,\mathbf{x}) = 0. \tag{4.5}$$

The time components $q_0(x)$ are unconstrained and defined for $0 \le x_0 < T$. We will however get boundary conditions for q_0 later by extending the lattice.

For later use, it is useful to define a scalar product on $\mathcal{L}_\mathcal{G}$ and $\mathcal{L}_\mathcal{H}$. For two vectors q and r in $\mathcal{L}_\mathcal{H}$, an obvious choice is

$$(q,r) = -2a^4 \sum_{x,\mu} \mathrm{tr}\{q_\mu(x) r_\mu(x)\}. \tag{4.6}$$

The scalar product on $\mathcal{L}_\mathcal{G}$ is defined similarly.

For the definition of a suitable gauge fixing function, we will need the covariant forward and backward derivatives on the lattice,

$$D_\mu f(x) = \frac{1}{a}\left[V(x,\mu) f(x+a\hat{\mu}) V(x,\mu)^{-1} - f(x)\right], \tag{4.7}$$

$$D_\mu^* f(x) = \frac{1}{a}\left[f(x) - V(x-a\hat{\mu},\mu)^{-1} f(x-a\hat{\mu}) V(x-a\hat{\mu},\mu)\right]. \tag{4.8}$$

Using the forward covariant derivative, one may define a linear operator $d : \mathcal{L}_\mathcal{G} \to \mathcal{L}_\mathcal{H}$ by

$$(d\omega)_\mu(x) = D_\mu \omega(x). \tag{4.9}$$

Another operator that will be used later is d^*. It is defined as minus the adjoint of d,

$$(d^* q, \omega) = -(q, d\omega) \tag{4.10}$$

for all $q \in \mathcal{L}_\mathcal{H}$ and $\omega \in \mathcal{L}_\mathcal{G}$. Starting from this definition, d^* is explicitly given by

$$(d^* q)_{\alpha\beta}(x) = \begin{cases} \sum_\mu (D_\mu^* q_\mu)_{\alpha\beta}(x) & \text{if} \quad 0 < x_0 < T, \\ (a^2/L^3) \sum_{\mathbf{y}} q_0(0,\mathbf{y})_{\alpha\beta} & \text{if} \quad \alpha = \beta \quad \text{and} \quad x_0 = 0, \\ 0 \quad \text{otherwise.} \end{cases} \tag{4.11}$$

This rather complicated formulation may be simplified to

$$d^* q(x) = D^*_\mu q_\mu(x) \tag{4.12}$$

for all x_0 by extending the field q to $x_0 = -1$ and $x_0 = T$ and imposing appropriate boundary conditions on the time component q_0. The new components are physically irrelevant and only used for technical reasons. Due to the special choice of background field used here, a complication does occur in this procedure. If one used, for example, the self dual background field considered in the continuum formulation in [60], one would get Neumann boundary conditions for all q_0. This is also the case with the Abelian background field used here, except for one case. If q_0 has got a part which is diagonal and spatially constant, this part satisfies Dirichlet boundary conditions at $x_0 = -1$. For this reason, the boundary conditions are easier to define in momentum space, where spatially constant fields q simply become gluons of zero momentum. So we switch to momentum space by taking the Fourier transform

$$q_0(\mathbf{p}, x_0) = \sum_{\mathbf{x}} e^{-i\mathbf{px}} q_0(x), \tag{4.13}$$

which may be decomposed in a basis of the Lie algebra of $SU(N)$,

$$q_0(\mathbf{p}, x_0) = \tilde{q}^a_0(\mathbf{p}, x_0) I^a. \tag{4.14}$$

The special choice of the basis I^a for the case of $SU(3)$ used in later calculations can be found in appendix A.

Now the boundary conditions are given by

$$\begin{aligned} \tilde{q}^a_0(\mathbf{p}, -1) &= 0 \quad \text{if} \quad I^a \in C_N \quad \text{and} \quad \mathbf{p} = \mathbf{0}, \\ \partial^*_0 \tilde{q}^a_0(\mathbf{p}, 0) &= 0 \quad \text{else}, \\ \partial^*_0 \tilde{q}^a_0(\mathbf{p}, T) &= 0. \end{aligned} \tag{4.15}$$

4.1.2 The gauge fixing procedure

In the following, we will use the gauge fixing procedure outlined in [63]. To this end, we will need a gauge fixing function $F(U)$, which is conveniently chosen to be a linear mapping from $\mathcal{H}$ to $\mathcal{L}_\mathcal{G}$. This function is defined in a neighbourhood $\mathcal{N}$ of the background field V and has to fulfil several conditions. First of all, it has to vanish on the background field,

$$F(V) = 0. \tag{4.16}$$

The first order variation of F under a gauge transformation generated by ω is a linear operator $L(U) : \mathcal{L}_\mathcal{G} \to \mathcal{L}_\mathcal{G}$,

$$L(U)\omega = \delta_\omega F(U). \tag{4.17}$$

For a gauge fixing function, the determinant of $L(U)$ is required not to vanish.

A suitable function that fulfils all conditions and is relatively easy to handle is

$$F(U) = d^* q. \tag{4.18}$$

Let now $f(U)$ be a function that is non–zero only in the neighbourhood $\mathcal{N}$. It can be shown [63] that

$$\int D[U] f(U) = k \int_{\mathcal{N}} D[U] f(U) \delta(F(U)) \det(L(U)). \tag{4.19}$$

This relation stays valid if one replaces the delta function by $\delta(F(U) - Z)$, where Z is an element of $\mathcal{L}_\mathcal{G}$ with $(Z, Z) < \epsilon$, where ϵ is chosen to be appropriately small. Since the left hand side of (4.19) is independent of Z, one can integrate over Z with a Gaussian measure, resulting in the gauge fixing term

$$S_{\mathrm{gf}}[V, q] = \frac{\lambda_0}{2}(d^* q, d^* q) \tag{4.20}$$

in the action.

In the usual way, the determinant in (4.19) may be rewritten in terms of Lie algebra valued Grassmann variables, the Faddeev–Popov ghost fields c and $\bar{c}$ with the action

$$S_{\mathrm{FP}}[V, q, \bar{c}, c] = -(\bar{c}, d^* \delta_c q). \tag{4.21}$$

Here, $\delta_c q$ denotes the first order variation of q under the gauge transformation generated by c. Expanding it to order g_0^2 yields

$$\begin{aligned} \delta_c q_\mu &= D_\mu c + g_0 \mathrm{Ad} q_\mu c \\ &\quad + \left[\frac{1}{2} g_0 a \mathrm{Ad} q_\mu + \frac{1}{12} (g_0 a \mathrm{Ad} q_\mu)^2 + \ldots \right] D_\mu c, \end{aligned} \tag{4.22}$$

with no sum over μ implied.

Also he ghost fields c and $\bar{c}$ have to satisfy certain boundary conditions. Like q, also the ghost field c may be Fourier transformed and decomposed in the basis I^a of the Lie algebra of $SU(N)$, resulting in the momentum dependent components $\tilde{c}^a(\mathbf{p}, x_0)$. By an analysis similar to the gluon case, one then gets the boundary conditions [64]

$$\begin{aligned} \partial_0^* \tilde{c}^a(\mathbf{p}, 0) &= 0 \quad \text{if} \quad I^a \in C_N \quad \text{and} \quad \mathbf{p} = \mathbf{0}, \\ \tilde{c}^a(\mathbf{p}, 0) &= 0 \quad \text{else}, \\ \tilde{c}^a(\mathbf{p}, T) &= 0. \end{aligned} \tag{4.23}$$

The same boundary conditions are valid for the ghost field $\bar{c}$.

4.1.3 The total action

Having fixed the gauge, we are now able to write down the action that will be used for perturbation theory in the Schrödinger functional.

The gluonic part of the action may be summarised as

$$S_{\mathrm{G}}[V,q] = \frac{1}{g_0^2}\sum_p w(p)\mathrm{tr}\left\{1-U(p)\right\} + S_{\mathrm{gf}}[V,q], \tag{4.24}$$

where the weights $w(p)$ are chosen such that the action is $\mathrm{O}(a)$ improved, i.e. $w(p_{\mathrm{t}}) = c_{\mathrm{t}}$ and $w(p_{\mathrm{s}}) = c_{\mathrm{s}}/2$ for the time-like and space-like plaquettes at the boundaries.
The ghosts contribute to the action with S_{FP} given in (4.21). The fermionic part of the total action is given by the Dirac–Wilson action including the volume and boundary improvement terms,

$$S_{\mathrm{F}}[V,q,\bar{\psi},\psi] = a^4\sum_x \bar{\psi}(x)(D+\delta D+m_0)\psi(x). \tag{4.25}$$

Apart from these contributions, there is an additional part of the action arising from the change of integration variables. Before, the gauge field integral was formulated using the measure $D[U]$. Now, we want to express the Schrödinger functional as an integral over the gluon fields q. For this purpose, it is useful to use

$$D[q] = \prod_{x,\mu,a} dq_\mu^a(x) \tag{4.26}$$

as a new measure. It may be obtained from the old measure by

$$D[U] = D[q]e^{-S_{\mathrm{m}}[q]}, \tag{4.27}$$

where, in the case of $SU(3)$, the measure part of the action is given by

$$S_{\mathrm{m}}[q] = \frac{g_0^2}{8}\sum_{x,\mu,a} q_\mu^a(x)q_\mu^{\bar{a}}(x) + \mathrm{O}(g_0^4). \tag{4.28}$$

In the case of $SU(2)$, one would have to replace the factor $\frac{1}{8}$ by $\frac{1}{12}$. So the additional contribution to the action due to the change of integration variables turns out to be of order g_0^2. For the later calculations in this thesis, the total action will only be needed up to order g_0, so S_{m} may be ignored here. It has, however, to be taken into account in the computation of the running coupling at 2–loop order.

The total action is the sum of all contributions,

$$S_{\mathrm{tot}}[V,q,\bar{c},c,\bar{\psi},\psi] = S_{\mathrm{G}}[V,q] + S_{\mathrm{FP}}[V,q,\bar{c},c] + S_{\mathrm{F}}[V,q,\bar{\psi},\psi] + S_{\mathrm{m}}[q]. \tag{4.29}$$

The Schrödinger functional now becomes

$$\mathcal{Z} = \int D[q]D[c]D[\bar{c}]D[\psi]D[\bar{\psi}]e^{-S_{\mathrm{tot}}}. \tag{4.30}$$

Let now $\mathcal{O}$ be a product of link variables. (We assume that $\mathcal{O}$ does not depend on the quark fields, which is the case after integrating over them.) The expectation value is then to be computed using the probability density (3.61). Writing the quark determinant as an integral over Grassmann variables, one gets

$$\langle \mathcal{O} \rangle_{\mathrm{G}} = \frac{1}{\mathcal{Z}} \int D[q]D[c]D[\bar{c}]D[\psi]D[\bar{\psi}]\mathcal{O}e^{-S_{\mathrm{tot}}}. \tag{4.31}$$

As a product of link variables, $\mathcal{O}$ may be written as a series in g_0,

$$\mathcal{O} = \mathcal{O}^{(0)} + g_0\mathcal{O}^{(1)} + g_0^2\mathcal{O}^{(2)} + \mathrm{O}(g_0^3), \tag{4.32}$$

where $\mathcal{O}^{(n)}$ contains products of n gluon fields q_μ. Since $\mathcal{O}^{(0)}$ is merely a constant, the functional integral becomes trivial,

$$\left\langle \mathcal{O}^{(0)} \right\rangle_{\mathrm{G}} = \mathcal{O}^{(0)}. \tag{4.33}$$

One thus gets the expansion

$$\langle \mathcal{O} \rangle_{\mathrm{G}} = \mathcal{O}^{(0)} + g_0 \left\langle \mathcal{O}^{(1)} \right\rangle_{\mathrm{G}} + g_0^2 \left\langle \mathcal{O}^{(2)} \right\rangle_{\mathrm{G}} + \mathrm{O}(g_0^3). \tag{4.34}$$

However, this is not yet the whole expansion, because the total action and thus the expectation value of $\mathcal{O}^{(n)}$ still depends on the bare coupling. In order to get the correct series, one has to expand the action too,

$$S_{\mathrm{tot}} = \frac{1}{g_0^2} S_{\mathrm{tot}}^{(-2)} + S_{\mathrm{tot}}^{(0)} + g_0 S_{\mathrm{tot}}^{(1)} + g_0^2 S_{\mathrm{tot}}^{(2)} + \mathrm{O}(g_0^3). \tag{4.35}$$

The term $S_{\mathrm{tot}}^{(-2)}$ comes from the gluon action and contains only the background field,

$$\begin{aligned} S_{\mathrm{tot}}^{(-2)} &= \sum_p \mathrm{tr}\left\{1 - V(p)\right\} \\ &= 12\frac{TL^3}{a^4}\left[\sin^2(\gamma) + 2\sin^2(\gamma/2)\right], \end{aligned} \tag{4.36}$$

with

$$\gamma = \frac{1}{LT}\left(\eta + \frac{\pi}{3}\right). \tag{4.37}$$

Since $S_{\mathrm{tot}}^{(-2)}$ does not depend on the variables integrated over in the functional integral, it cancels in all expectation values and may be neglected here. With this expansion, the exponential factor in the functional integral becomes

$$e^{-S_{\mathrm{tot}}} = \left[1 - g_0 S_{\mathrm{tot}}^{(1)} + g_0^2\left(\frac{1}{2}S_{\mathrm{tot}}^{(1)^2} - S_{\mathrm{tot}}^{(2)}\right)\right] e^{-S_{\mathrm{tot}}^{(0)}}. \tag{4.38}$$

Let now $\langle \ldots \rangle_0$ denote the gauge field average taken at zero bare coupling, which means that this average is computed using $S_{\mathrm{tot}}^{(0)}$ instead of the whole action. Inserting (4.38) into the functional integrals and integrating out the quark fields yields

$$\langle \mathcal{O} \rangle_{\mathrm{G}} = \mathcal{O}^{(0)} + g_0^2 \left[\left\langle \mathcal{O}^{(2)} \right\rangle_0 - \left\langle \mathcal{O}^{(1)} \left[S_{\mathrm{tot}}^{(1)} \right]_{\mathrm{F}} \right\rangle_0 \right] + \mathrm{O}(g_0^4). \tag{4.39}$$

Note that no terms proportional to g_0 or g_0^3 occur, because this would involve an integral over an odd number of gluon fields, giving zero. Another observation worth mentioning is that $S_{\mathrm{tot}}^{(1)}$ only is non–zero due the presence of the background field. Later, this term will lead to some Feynman diagrams that do not occur in the case of a vanishing background field.

4.2 Perturbative expansion of the coupling

4.2.1 The coupling at 1– and 2–loop order

The Schrödinger functional coupling $\bar{g}^2$ can be expanded in powers of the bare coupling g_0,

$$\bar{g}^2 = g_0^2 + p_1(L/a) g_0^4 + p_2(L/a) g_0^6 + \mathrm{O}(g_0^8). \tag{4.40}$$

At tree level, both couplings coincide due to the normalisation of $\bar{g}^2$. The 1–loop coefficient p_1 may be decomposed in an N_{f} dependent and an N_{f} independent part,

$$p_1 = p_{10} + p_{11} N_{\mathrm{f}}. \tag{4.41}$$

Both p_{10} and p_{11} are easy to calculate by expanding the total action. From the quadratic parts of the gluon, ghost, and quark actions one gets the inverse of the propagators. The coefficients p_{10} and p_{11} are obtained by differentiating the determinants of the inverse propagators with respect to the parameter η. The coefficient p_{10} has been computed in [26] (and in [60] for the case of $SU(2)$), the calculation of p_{11} can be found in [32].

At 2–loop level, one has a decomposition up to order N_{f}^2 [34, 65],

$$p_2 = p_{20} + p_{21} N_{\mathrm{f}} + p_{22} N_{\mathrm{f}}^2. \tag{4.42}$$

Here, the computation is more complicated and requires the calculation of Feynman diagrams. The coefficient p_{20} for the quenched case has been computed in [33], and in [64] for the case of $SU(2)$. The remaining coefficients p_{21} and p_{22} can be found in [34].

4.2.2 The step scaling function and its lattice artefacts at 1– and 2–loop order

Having expanded the coupling, one easily gets the expansion of the step scaling function, since it is given by the difference between the coupling at length scale

$2L$ and L at the required order of perturbation theory. This means one has to calculate the difference

$$\Delta p_{ij}(L/a) = p_{ij}(2L/a) - p_{ij}(L/a). \tag{4.43}$$

Also the deviation δ of the step scaling function from its continuum limit (3.73) can be expanded in perturbation theory,

$$\delta(u, a/L) = [\delta_{10} + \delta_{11} N_{\mathrm{f}}]\, u + \left[\delta_{20} + \delta_{21} N_{\mathrm{f}} + \delta_{22} N_{\mathrm{f}}^2\right] u^2 + \mathrm{O}(u^3). \tag{4.44}$$

The continuum limit of the step scaling function is determined by the beta function. In order to get the coefficients δ_{ij}, one has to decompose the coefficients of the beta function, (2.26) and (2.27), into the N_{f} independent parts b_{00} and b_{10} and the N_{f} dependent parts b_{01} and b_{11}. The coefficients δ_{ij} are then given by

$$\begin{aligned}
\delta_{10} &= \Delta p_{10} - 2b_{00}\ln(2), && (4.45)\\
\delta_{11} &= \Delta p_{11} - 2b_{01}\ln(2), && (4.46)\\
\delta_{20} &= \Delta p_{20} - 2b_{10}\ln(2) - 2\Delta p_{10}(p_{10} + b_{00}\ln(2)), && (4.47)\\
\delta_{21} &= \Delta p_{21} - 2b_{11}\ln(2) - 2\Delta p_{11}(p_{10} + b_{00}\ln(2)) \\
&\quad -2\Delta p_{10}(p_{11} + b_{01}\ln(2)), && (4.48)\\
\delta_{22} &= \Delta p_{22} - 2\Delta p_{11}(p_{11} + b_{01}\ln(2)). && (4.49)
\end{aligned}$$

The 1–loop coefficients δ_{1j} were first listed in [66], while the 2–loop coefficients δ_{2j} have been estimated in [34]. However, at vanishing renormalised quark mass, the two–loop coefficient δ_2 contains the critical quark mass at 1–loop order, which only in the continuum limit reaches the value used in [34]. In order to do a precise calculation, one has to specify the zero mass condition with the cutoff in place. So the results of [34] could only give a first idea of the size of the cutoff effects. For more accurate results, the critical quark mass has to be expanded up to 1–loop order at finite a/L and inserted in the formulae for δ_{2j} in [34]. This will happen in chapter 7.

According to the estimation in [34], the cutoff effects seem to be small. In order to compute the step scaling function non–perturbatively, one has to simulate a sequence of lattice pairs with decreasing lattice spacing and fixed coupling u and extrapolate the Monte Carlo data to the continuum limit. In this procedure, the perturbative expansion of $\delta(u, a/L)$ may be used to remove the cutoff effects up to 2–loop order from the non–perturbative values of the step scaling function $\Sigma(u, a/L)$ [31].

Chapter 5

The current quark mass

5.1 The PCAC relation

Several ways to define a renormalised quark mass have been sketched in chapter 2. For the Schrödinger functional, a suitable definition has been given in [54], using the partial conservation of the isovector axial current. The axial current and density are defined by

$$A_\mu^a(x) = \bar{\psi}(x)\gamma_\mu\gamma_5\frac{1}{2}\tau^a\psi(x), \tag{5.1}$$

$$P^a(x) = \bar{\psi}(x)\gamma_5\frac{1}{2}\tau^a\psi(x). \tag{5.2}$$

As already mentioned in chapter 2, a deficit of Wilson fermions is that the chiral symmetry of the theory is explicitly broken and only restored in the continuum limit. Thus only in the continuum limit, the isovector axial current $A_\mu^a(x)$ will satisfy the PCAC relation

$$\partial_\mu A_\mu^a(x) = 2mP^a(x), \tag{5.3}$$

while at finite lattice spacing, this relation will be violated by terms of order a.

In order to make the axial current converge faster towards its continuum limit, one may apply Symanzik's improvement programme by adding an appropriate improvement term

$$(A_\mathrm{I})_\mu^a(x) = A_\mu^a(x) + a\delta A_\mu^a(x). \tag{5.4}$$

The improvement term δA_μ^a turns out to be [54]

$$\delta A_\mu^a(x) = c_\mathrm{A}\frac{1}{2}(\partial_\mu + \partial_\mu^*)P^a(x). \tag{5.5}$$

This $\mathrm{O}(a)$ correction is proportional to the improvement coefficient c_A, which is

$$c_\mathrm{A}(g_0) = -0.00756(1)g_0^2 + \mathrm{O}(g_0^4) \tag{5.6}$$

to 1–loop order of perturbation theory [50]. The axial density P^a can be shown to converge to its continuum limit with a rate proportional to a^2, hence it does not need to be improved.

In the case of a non–vanishing physical quark mass, the quantities defined this way are still not fully improved. In order to improve A^a_μ and P^a completely, one still has to subtract a mass dependent counter-term. However, this amounts to a mass dependent multiplicative renormalisation, so it seems more natural to include this factor in the definition of the renormalised quantities.

In general, the quark mass will get an additive renormalisation, which means that, in the plane of bare parameters, there will be a critical line

$$m_0 = m_{\rm c}(g_0), \tag{5.7}$$

where the renormalised quark mass vanishes. For convenience, one may define the subtracted mass

$$m_{\rm q} = m_0 - m_{\rm c}. \tag{5.8}$$

Then this mass will only have to be renormalised multiplicatively.
Including the already mentioned mass dependent factors needed for improvement, the renormalised axial current and density may now be written as

$$(A_{\rm R})^a_\mu = Z_{\rm A}(1 + b_{\rm A} a m_{\rm q})\{A^a_\mu + a c_{\rm A}\frac{1}{2}(\partial_\mu + \partial^*_\mu)P^a\}, \tag{5.9}$$

$$(P_{\rm R})^a = Z_{\rm P}(1 + b_{\rm P} a m_{\rm q})P^a. \tag{5.10}$$

Here, $b_{\rm A}$ and $b_{\rm P}$ cancel mass dependent cutoff effects. At tree level one has [67, 50]

$$b^{(0)}_{\rm A} = b^{(0)}_{\rm P} = 1. \tag{5.11}$$

Since all calculations in this thesis are done at vanishing renormalised mass, which is equivalent to setting $m_{\rm q} = 0$, these coefficients are not needed here. In the following, they are therefore ignored.

The renormalisation constant $Z_{\rm A}$ would be equal to one in the continuum. This is a consequence of the $SU(N_{\rm f})_{\rm L} \times SU(N_{\rm f})_{\rm R}$ symmetry, leading to chiral ward identities, which may be used to normalise the currents [68, 69]. In the regularised theory, this symmetry is violated by terms of order a. This means that the PCAC relation and the chiral ward identities are only valid up to $\mathrm{O}(a)$ corrections, resulting in a renormalisation of the axial current. It stays, however, finite and scale independent. Up to 1–loop order of perturbation theory, one gets [70, 71]

$$Z_{\rm A}(g_0) = 1 + Z^{(1)}_{\rm A} g_0^2 + \mathrm{O}(g_0^4), \tag{5.12}$$

with

$$Z^{(1)}_{\rm A} = -0.087344(1) \times C_{\rm F}. \tag{5.13}$$

In contrast to Z_{A}, the renormalisation constant Z_{P} is scale dependent and thus responsible for the running of the renormalised mass. This issue will be addressed in chapter 6.

A renormalised quark mass m_{R} may now be defined as the proportionality constant in

$$\left\langle \frac{1}{2}(\partial_\mu^* + \partial_\mu)(A_{\mathrm{R}})_\mu^a(x)\mathcal{O} \right\rangle = 2m_{\mathrm{R}} \left\langle (P_{\mathrm{R}})^a(x)\mathcal{O} \right\rangle + \mathrm{O}(a^2) \tag{5.14}$$

for any product $\mathcal{O}$ of renormalised improved fields located at a non–zero distance from each other and from x. The lattice artefacts of order a^2 depend on the choice of $\mathcal{O}$.

5.2 The current mass and its lattice artefacts

In order to compute the renormalised mass, one needs to choose an operator $\mathcal{O}$. Using this operator, one then has to construct bare correlation functions containing the axial current and density and then renormalise both these quantities and the operator $\mathcal{O}$.

One possible choice is to introduce the bare correlation functions

$$f_{\mathrm{A}}(x_0) = -a^6 \sum_{\mathbf{y},\mathbf{z}} \frac{1}{3} \left\langle A_0^a(x)\bar{\zeta}(\mathbf{y})\gamma_5 \frac{1}{2}\tau^a \zeta(\mathbf{z}) \right\rangle, \tag{5.15}$$

$$f_{\mathrm{P}}(x_0) = -a^6 \sum_{\mathbf{y},\mathbf{z}} \frac{1}{3} \left\langle P^a(x)\bar{\zeta}(\mathbf{y})\gamma_5 \frac{1}{2}\tau^a \zeta(\mathbf{z}) \right\rangle, \tag{5.16}$$

where $\zeta(\mathbf{x})$ is the functional derivative with respect to the boundary quark fields at $x_0 = 0$ defined in (3.27) and (3.28). These correlation functions are proportional to the probability amplitude that a quark antiquark pair created at $x_0 = 0$ propagates into the interior of the lattice and annihilates at the point x. This situation may be depicted by figure 5.1.

Now one can define the x_0 dependent current quark mass

$$m(x_0) = \frac{\frac{1}{2}(\partial_0^* + \partial_0) f_{\mathrm{A}}(x_0) + c_{\mathrm{A}} a \partial_0^* \partial_0 f_{\mathrm{P}}(x_0)}{2 f_{\mathrm{P}}(x_0)}, \tag{5.17}$$

which, taken at a certain x_0, may serve as an unrenormalised quark mass. A convenient choice is to take m in the centre of the lattice, i.e.

$$m_1 = \begin{cases} m\left(\frac{T}{2}\right) & \text{for even } T/a, \\ \frac{1}{2}\left(m\left(\frac{T-a}{2}\right) + m\left(\frac{T+a}{2}\right)\right) & \text{for odd } T/a. \end{cases} \tag{5.18}$$

This current quark mass will, of course, depend on the lattice size L/a. It is then straightforward to show that the renormalised quark mass defined as the

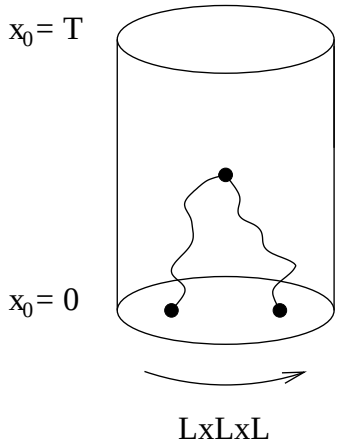

Figure 5.1: *The correlation functions $f_{\rm A}$ and $f_{\rm P}$*

proportionality factor in the PCAC relation is given by

$$m_{\rm R} = \frac{Z_{\rm A}(1 + b_{\rm A} a m_{\rm q})}{Z_{\rm P}(1 + b_{\rm A} a m_{\rm q})} m_1 + {\rm O}(a^2). \tag{5.19}$$

One may of course take different operators $\mathcal{O}$ which will give quark masses differing from m_1 by terms that are expected to be of order a^2. These ${\rm O}(a^2)$–terms may serve as a direct check of the size of the lattice effects.

A possible choice is to take the boundary quark fields at $x_0 = T$ instead of $x_0 = 0$, i.e. to use the correlation functions

$$f'_{\rm A}(T - x_0) = -a^6 \sum_{\mathbf{y},\mathbf{z}} \frac{1}{3} \left\langle A_0^a(x) \bar{\zeta}'(\mathbf{y}) \gamma_5 \frac{1}{2} \tau^a \zeta'(\mathbf{z}) \right\rangle, \tag{5.20}$$

$$f'_{\rm P}(T - x_0) = -a^6 \sum_{\mathbf{y},\mathbf{z}} \frac{1}{3} \left\langle P^a(x) \bar{\zeta}'(\mathbf{y}) \gamma_5 \frac{1}{2} \tau^a \zeta'(\mathbf{z}) \right\rangle \tag{5.21}$$

instead of $f_{\rm A}$ and $f_{\rm P}$. Let m' be defined in the same way as m_1, but with $f'_{\rm A}$ and $f'_{\rm P}$ instead of $f_{\rm A}$ and $f_{\rm P}$. Now, a new unrenormalised mass may be defined by

$$m_2 = \frac{1}{2}(m_1 + m'). \tag{5.22}$$

Then the lattice artefact

$$d(L/a) = m_2(L/a) - m_1(L/a) \tag{5.23}$$

should be of order a^2.

A different possibility to estimate the size of the lattice effects is to take the difference

$$e(L/a) = m_1(2L/a) - m_1(L/a). \tag{5.24}$$

One aim of this work is to compute these lattice artefacts up to 1–loop order of perturbation theory. To this end, the 1–loop expansion of the correlation functions f_{A} and f_{P} is needed.

5.3 1–loop expansion of f_{A} and f_{P}

For convenience, the calculation in this section is done in lattice units, i.e. $a = 1$.

The principle ideas of the expansion of f_{A} and f_{P} have been outlined in [50], a more detailed discussion has been given in [51] (and in [72] for the case of a vanishing background field). In this section, the details of the calculation shall be presented following the lines of [51].

5.3.1 Preliminaries

In order to expand f_{A} and f_{P}, they have to be brought into a form more suitable for perturbation theory. Applying Wick's theorem on (5.15) and (5.16), one gets

$$f_{\mathrm{A}}(x_0) = \sum_{\mathbf{y},\mathbf{z}} \frac{1}{2} \Big\langle \mathrm{Tr}\Big\{ [\zeta(\mathbf{z})\bar{\psi}(x)]_{\mathrm{F}} \gamma_0\gamma_5 [\psi(x)\bar{\zeta}(\mathbf{y})]_{\mathrm{F}} \gamma_5 \Big\} \Big\rangle_{\mathrm{G}}, \tag{5.25}$$

$$f_{\mathrm{P}}(x_0) = \sum_{\mathbf{y},\mathbf{z}} \frac{1}{2} \Big\langle \mathrm{Tr}\Big\{ [\zeta(\mathbf{z})\bar{\psi}(x)]_{\mathrm{F}} \gamma_5 [\psi(x)\bar{\zeta}(\mathbf{y})]_{\mathrm{F}} \gamma_5 \Big\} \Big\rangle_{\mathrm{G}}, \tag{5.26}$$

where the trace is to be taken over Dirac and colour indices only.
Let ψ_{cl} be a solution of the Dirac equation,

$$(D + \delta D + m_0)\psi_{\mathrm{cl}}(x) = 0. \tag{5.27}$$

Then it can be shown [50] that

$$[\psi(x)\bar{\zeta}(\mathbf{y})]_{\mathrm{F}} = \frac{\delta\psi_{\mathrm{cl}}(x)}{\delta\rho(\mathbf{y})}. \tag{5.28}$$

So using the matrix

$$H(x) = \sum_{\mathbf{y}} \frac{\delta\psi_{\mathrm{cl}}(x)}{\delta\rho(\mathbf{y})}, \tag{5.29}$$

f_{A} and f_{P} may be written as

$$f_{\mathrm{A}}(x_0) = -\frac{1}{2} \left\langle \mathrm{Tr}\{H(x)^\dagger \gamma_0 H(x)\} \right\rangle_{\mathrm{G}}, \tag{5.30}$$

$$f_{\mathrm{P}}(x_0) = \frac{1}{2} \left\langle \mathrm{Tr}\{H(x)^\dagger H(x)\} \right\rangle_{\mathrm{G}}. \tag{5.31}$$

The matrix H has an expansion

$$H(x) = H^{(0)}(x) + g_0 H^{(1)}(x) + g_0^2 H^{(2)}(x) + \mathrm{O}(g_0^3), \tag{5.32}$$

resulting in the 1–loop expansion of $f_{\rm A}$,

$$\begin{aligned} f_{\rm A}(x_0) &= -\frac{1}{2}\mathrm{Tr}\Big\{H^{(0)}(x)^\dagger\gamma_0 H^{(0)}(x)\Big\} - g_0^2\frac{1}{2}\Big[\Big\langle \mathrm{Tr}\Big\{H^{(0)}(x)^\dagger\gamma_0 H^{(2)}(x)\Big\}\Big\rangle_0 \\ &\quad + \Big\langle \mathrm{Tr}\Big\{H^{(1)}(x)^\dagger\gamma_0 H^{(1)}(x)\Big\}\Big\rangle_0 + \Big\langle \mathrm{Tr}\Big\{H^{(2)}(x)^\dagger\gamma_0 H^{(0)}(x)\Big\}\Big\rangle_0 \\ &\quad - \Big\langle \mathrm{Tr}\Big\{H^{(0)}(x)^\dagger\gamma_0 H^{(1)}(x)\Big\}\Big[S^{(1)}_{\rm tot}\Big]_{\rm F}\Big\rangle_0 \\ &\quad - \Big\langle \mathrm{Tr}\Big\{H^{(1)}(x)^\dagger\gamma_0 H^{(0)}(x)\Big\}\Big[S^{(1)}_{\rm tot}\Big]_{\rm F}\Big\rangle_0\Big], \end{aligned} \tag{5.33}$$

and analogously for $f_{\rm P}$ with -1 instead of γ_0. So, in order to compute the 1–loop coefficients of $f_{\rm A}$ and $f_{\rm P}$, one has to expand $S_{\rm tot}$ up to order g_0 and

$$H(x) = \tilde{c}_{\rm t}\sum_{\mathbf{y}} S(x,y)U(y-\hat{0},0)^{-1}P_+|_{y_0=1} \tag{5.34}$$

up to order g_0^2. Here, $S(x,y)$ denotes the quark propagator, which is the inverse of the Dirac–Wilson operator $(D+\delta D+m_0)$. So one has to expand the propagator $S(x,y)$ and the link variables. Since the overall factor $\tilde{c}_{\rm t}$ cancels in the definition of the current mass, it may be ignored here. There will however be a contribution proportional to $\tilde{c}_{\rm t}^{(1)}$ due to the boundary counter-term in the quark action, leading to a corresponding term in the g_0^2 coefficient in the expansion of the propagator.

Following the lines of [51], the calculation is done in momentum space. First, the gluon fields have to be decomposed in a basis of the Lie–algebra of $SU(3)$

$$q(x) = \sum_a \tilde{q}^a(x)I^a, \tag{5.35}$$

with the basis I^a chosen such that the star operation defined in appendix A and the covariant derivative act diagonally:

$$\cosh G_{0k}\star I^a = C_a I^a, \tag{5.36}$$

$$\sinh G_{0k}\star I^a = S_a I^a, \tag{5.37}$$

$$(D_k f)(x) = \sum_a\Big[\Omega_a(x_0)f^a(x+\hat{k}) - f^a(x)\Big]I^a, \tag{5.38}$$

$$(D_k^* f)(x) = \sum_a\Big[f^a(x) - \Omega_a(x_0)^* f^a(x-\hat{k})\Big]I^a. \tag{5.39}$$

The I^a are explicitly given in appendix A. The coefficients $\Omega_a(x_0)$ can be parametrised as

$$\Omega_a(x_0) = e^{i\phi_a(x_0)}, \tag{5.40}$$

with the $\phi_a(x_0)$ given in appendix A. Then one may introduce the Fourier transformed fields

$$\tilde{q}_0^a(x) = \frac{1}{L^3}\sum_{\mathbf{p}} e^{i\mathbf{p}\mathbf{x}}\tilde{q}_0^a(\mathbf{p},x_0), \tag{5.41}$$

$$\tilde{q}^a_k(x) \;=\; \frac{1}{L^3}\sum_{\mathbf{p}} e^{i\mathbf{px}} e^{(p_k+\phi_a(x_0))/2}\tilde{q}^a_k(\mathbf{p},x_0). \tag{5.42}$$

Furthermore, the ϕ_a may be used to define the quantities

$$s^a_k(\mathbf{p},x_0) \;=\; 2\sin\left[\frac{1}{2}\Big(p_k+\phi_a(x_0)\Big)\right], \tag{5.43}$$

$$c^a_k(\mathbf{p},x_0) \;=\; 2\cos\left[\frac{1}{2}\Big(p_k+\phi_a(x_0)\Big)\right], \tag{5.44}$$

and

$$R_a = (C_a - S_a)e^{i\partial_0\phi_a(x_0)/2}, \tag{5.45}$$

which will be used to make the expressions for the propagators and vertices more compact. Here, C_a and S_a are the components of $\cosh G_{0k}$ and $\sinh G_{0k}$ according to (5.36) and (5.37). They and the R_a are explicitly given in appendix A.

The same is done for the ghost fields

$$c(x) \;=\; \frac{1}{L^3}\sum_{\mathbf{p}} e^{i\mathbf{px}}c(\mathbf{p},x_0) = \frac{1}{L^3}\sum_{\mathbf{p}} e^{i\mathbf{px}}\sum_a \tilde{c}^a(\mathbf{p},x_0)I^a, \tag{5.46}$$

$$\bar{c}(x) \;=\; \frac{1}{L^3}\sum_{\mathbf{p}} e^{i\mathbf{px}}\bar{c}(\mathbf{p},x_0) = \frac{1}{L^3}\sum_{\mathbf{p}} e^{i\mathbf{px}}\sum_a \tilde{\bar{c}}^a(\mathbf{p},x_0)I^a, \tag{5.47}$$

and also the quark fields are Fourier transformed

$$\psi(x) \;=\; \frac{1}{L^3}\sum_{\mathbf{p}} e^{i\mathbf{px}}\psi(\mathbf{p},x_0), \tag{5.48}$$

$$\bar{\psi}(x) \;=\; \frac{1}{L^3}\sum_{\mathbf{p}} e^{i\mathbf{px}}\bar{\psi}(\mathbf{p},x_0). \tag{5.49}$$

5.3.2 The propagators

In momentum space, the quadratic part of the pure gluonic action takes the form

$$S^{(0)}_{\rm G} = \frac{1}{2}\frac{1}{L^3}\sum_{\mathbf{p}}\sum_{x_0,y_0=0}^{T-1}\sum_a \tilde{q}^{\bar{a}}_\mu(-\mathbf{p},x_0)K^a_{\mu\nu}(\mathbf{p};x_0,y_0)\tilde{q}^a_\nu(\mathbf{p},y_0), \tag{5.50}$$

where

$$\begin{aligned} K^a_{kl}(\mathbf{p};x_0,y_0) \;=\;& \delta_{x_0,y_0}\Big[\delta_{kl}\mathbf{s}^a(\mathbf{p},x_0)^2 - s^a_k(\mathbf{p},x_0)s^a_l(\mathbf{p},x_0)(1-\lambda_0)\Big] \\ & +\delta_{kl}\Big[2C_a\delta_{x_0,y_0} - R_a(\delta_{x_0+1,y_0}+\delta_{x_0-1,y_0})\Big], \end{aligned} \tag{5.51}$$

$$
\begin{aligned}
K^a_{k0}(\mathbf{p};x_0,y_0) &= iR_a\Big[\delta_{x_0,y_0}s^a_k(\mathbf{p},x_0+1)-\delta_{x_0-1,y_0}s^a_k(\mathbf{p},y_0)\Big] \\
&\quad -i\lambda_0 s^a_k(\mathbf{p},x_0)\Big[\delta_{x_0,y_0}-\delta_{x_0-1,y_0}\Big], \qquad (5.52)\\
K^a_{0k}(\mathbf{p};x_0,y_0) &= -K^a_{k0}(\mathbf{p};y_0,x_0), \qquad (5.53)\\
K^a_{00}(\mathbf{p};x_0,y_0) &= R_a\delta_{x_0,y_0}\mathbf{s}^a(\mathbf{p},x_0)\cdot\mathbf{s}^a(\mathbf{p},x_0+1) \\
&\quad +\lambda_0\Big[2\delta_{x_0,y_0}-\delta_{x_0+1,y_0}-\delta_{x_0-1,y_0}\Big] \\
&\quad -\lambda_0\delta_{x_0,y_0}\Big[\delta_{x_0,0}(1-\chi_a\delta_{\mathbf{p},\mathbf{0}})+\delta_{x_0,T-1}\Big], \qquad (5.54)
\end{aligned}
$$

where $\chi_a = 1$ for $a = 3, 8$ and $\chi_a = 0$ otherwise. Then the free gluon propagator is given by

$$\langle\tilde{q}^a_\mu(\mathbf{p},x_0)\tilde{q}^b_\nu(\mathbf{p}',y_0)\rangle_0 = \delta_{b\bar{a}}L^3\delta_{\mathbf{p}+\mathbf{p}'}D^a_{\mu\nu}(\mathbf{p};x_0,y_0), \qquad (5.55)$$

where D^a is the inverse of K^a.

The ghost action takes the form

$$S_{\rm gh} = \sum_{n=0}^{\infty}\frac{1}{n!}g_0^n S^{(n)}_{\rm gh}, \qquad (5.56)$$

where the quadratic part is given by

$$S^{(0)}_{\rm gh} = \frac{1}{L^3}\sum_{\mathbf{p}}\sum_{s_0,t_0}\sum_a \tilde{\bar{c}}^{\bar{a}}(-\mathbf{p},s_0)F^a(\mathbf{p};s_0,t_0)\tilde{c}^a(\mathbf{p},t_0). \qquad (5.57)$$

For $a \neq 3, 8$ one has

$$F^a(\mathbf{p};s_0,t_0) = \delta_{s_0,t_0}\left[2+\mathbf{s}^a(\mathbf{p},s_0)^2\right]-\delta_{s_0+1,t_0}-\delta_{s_0-1,t_0}. \qquad (5.58)$$

The computation aimed at here only involves closed loops of charged ghost fields coupled to a neutral gluon. Hence the quadratic ghost action for $a = 3, 8$ is not needed here. Now we get the free ghost propagator

$$\langle\tilde{c}^a(\mathbf{p},s_0)\tilde{\bar{c}}^b(\mathbf{p}',t_0)\rangle_0 = \delta_{b\bar{a}}L^3\delta_{\mathbf{p}+\mathbf{p}'}D^a(\mathbf{p};s_0,t_0), \qquad (5.59)$$

where D^a is the inverse of F^a.

The free part of the quark action is given by

$$S^{(0)}_{\rm F} = \frac{1}{L^3}\sum_{\mathbf{p}}\sum_{x_0,y_0}\bar{\psi}(-\mathbf{p},x_0)\tilde{D}(\mathbf{p};x_0,y_0)\psi(\mathbf{p},y_0), \qquad (5.60)$$

where $\tilde{D}$ is the improved Dirac–Wilson operator $(D + \delta D + m_0)$ at lowest order of g_0, namely

$$\tilde{D}(\mathbf{p};x_0,y_0) = -P_-\delta_{x_0+1,y_0}+B(\mathbf{p}^+,x_0)\delta_{x_0,y_0}-P_+\delta_{x_0-1,y_0}, \qquad (5.61)$$

with $p_k^+ = p_k + \theta/L$ and

$$\begin{aligned} B(\mathbf{p}, x_0) &= 4 + m_0 - \sum_k \left[\frac{1}{2}(1+\gamma_k)e^{-ip_k}V(x_0)^\dagger + \frac{1}{2}(1-\gamma_k)e^{ip_k}V(x_0)\right] \\ &\quad + iH\gamma_0 \sum_k \gamma_k. \end{aligned} \tag{5.62}$$

Here H is a diagonal matrix in colour space with the elements

$$H_{\alpha\alpha} = -\frac{1}{2}c_{\rm sw}^{(0)} \sin \mathcal{E}_\alpha. \tag{5.63}$$

The quark propagator S is now defined as the inverse of the operator $\tilde{D}$.

5.3.3 The vertices

The expansion of the pure gluonic action gives the triple gluon vertex. At 1–loop order we have

$$\begin{aligned} S_{\rm G}^{(1)} &= \frac{1}{3!} g_0 \frac{1}{L^6} \sum_{\mathbf{q}_1,\mathbf{q}_2,\mathbf{q}_3} \delta_{\rm P}(\mathbf{q}_1+\mathbf{q}_2+\mathbf{q}_3) \\ &\quad \cdot \sum_{\mu_1,\mu_2,\mu_3} \sum_{t_1,t_2,t_3} \sum_{a_1,a_2,a_3} V_{\mu_1\mu_2\mu_3}^{a_1a_2a_3}(\mathbf{q}_1,\mathbf{q}_2,\mathbf{q}_3;t_1,t_2,t_3) \\ &\quad \cdot \prod_j \tilde{q}_{\mu_j}^{a_j}(-\mathbf{q}_j, t_j), \end{aligned} \tag{5.64}$$

where $\delta_{\rm P}$ denotes the periodic delta function, i.e. the delta function modulo 2π. In this expression, a term proportional to $c_{\rm t}^{(1)}$ is missing, which will be treated later. In order to make the somewhat complicated expressions for the vertex V slightly more compact, we introduce the following notations for traces and permutations of the basis of the Lie algebra and the background field:

$$c_{abc} = -2i \ {\rm tr} I^a [I^b, I^c], \tag{5.65}$$

$$e_{abc} = -2i \ {\rm tr}\Big(e^{i\mathcal{E}} I^a I^b I^c - e^{-i\mathcal{E}} I^c I^b I^a\Big). \tag{5.66}$$

Furthermore, we use the shorthand notations

$$E_k = e^{\frac{i}{2}(p_k+q_k+r_k)} \tag{5.67}$$

and $\phi_c' = \partial_0 \phi_c(x_0)$. Since all non–zero ϕ_c are linear in x_0, ϕ_c' does not depend on x_0.

Using these notations, one gets for the vertex

$$V^{abc}_{klm}(\mathbf{p},\mathbf{q},\mathbf{r};s_0,t_0,u_0) = c_{abc}\delta_{s_0,t_0}\delta_{s_0,u_0}\Big\{\delta_{kl}E_kE_m$$
$$\cdot\sin\frac{1}{2}[p_m-\phi_a(s_0)-q_m+\phi_b(s_0)]c^c_k(-\mathbf{r},s_0)+2\text{ permutations}\Big\}$$
$$-\frac{i}{4}\exp\frac{i}{2}[\phi_a(s_0)+\phi_b(t_0)+\phi_c(u_0)]\delta_{klm}E_k\Big\{\delta_{s_0,t_0}[(e_{abc}+e_{bac})\delta_{s_0+1,u_0}$$
$$-(e_{cab}+e_{cba})\delta_{s_0-1,u_0}]+2\text{ permutations}\Big\}. \tag{5.68}$$

Here, "2 permutations" is meant such that one has to take cyclic permutations of k,l,m and a,b,c, respectively. The vertex is thus made totally symmetric under interchange of labels. Then the other parts of the vertex become

$$V^{abc}_{000}(\mathbf{p},\mathbf{q},\mathbf{r};s_0,t_0,u_0) = -\frac{i}{4}\delta_{s_0,t_0}\delta_{s_0,u_0}\sum_k\Big\{(e_{abc}+e_{bac})e^{i[r_k-\phi_c(s_0)]}$$
$$-(e_{cab}+e_{cba})e^{-i[r_k-\phi_c(s_0)]}+2\text{ permutations}\Big\}, \tag{5.69}$$

$$V^{abc}_{kl0}(\mathbf{p},\mathbf{q},\mathbf{r};s_0,t_0,u_0) = -\frac{i}{2}\delta_{kl}E_k$$
$$\cdot\Big(\frac{1}{2}\delta_{s_0,t_0}\delta_{s_0,u_0}\Big\{(e_{abc}+e_{bac})e^{\frac{i}{2}[r_k-\phi_c(u_0)]}-(e_{cab}+e_{cba})e^{-\frac{i}{2}[r_k-\phi_c(u_0)]}\Big\}$$
$$-\frac{i}{2}\delta_{s_0,t_0}\delta_{s_0-1,u_0}(e_{cab}+e_{cba})e^{-\frac{i}{2}\phi'_c}s^c_k(-\mathbf{r},u_0)$$
$$+\Big\{e^{\frac{i}{2}\phi'_b}\Big[e_{cab}e^{-\frac{i}{2}[r_k-\phi_c(u_0)]}-e_{acb}e^{\frac{i}{2}[r_k-\phi_c(u_0)]}\Big]\delta_{s_0,t_0-1}\delta_{s_0,u_0}$$
$$+1\text{ permutation}\Big\}\Big), \tag{5.70}$$

$$V^{abc}_{00k}(\mathbf{p},\mathbf{q},\mathbf{r};s_0,t_0,u_0) = -\frac{i}{2}\delta_{s_0,t_0}$$
$$\cdot\Big(-\frac{1}{2}\delta_{s_0,u_0}\Big\{(e_{cab}+e_{cba})e^{-\frac{i}{2}[r_k-\phi_c(u_0)]}+(e_{abc}+e_{bac})e^{\frac{i}{2}[r_k-\phi_c(u_0)]}\Big\}$$
$$+\frac{1}{2}\delta_{s_0,u_0-1}e^{\frac{i}{2}\phi'_c}(e_{abc}+e_{bac})c^c_k(-\mathbf{r},s_0)$$
$$+\Big\{e^{\frac{i}{2}[-r_k-2p_k+2\phi_a(s_0)+\phi_c(u_0)]}[e_{acb}\delta_{s_0,u_0}-e_{abc}\delta_{s_0,u_0-1}]$$
$$+1\text{ permutation}\Big\}\Big). \tag{5.71}$$

The gluon–ghost vertex is given by the 1–loop expansion of the ghost action. Here one gets

$$S^{(1)}_{\rm gh} = \frac{1}{L^6}\sum_{\mathbf{p},\mathbf{p}',\mathbf{q}}\delta_{\rm P}(\mathbf{p}+\mathbf{p}'+\mathbf{q})\sum_{s_0,t_0,u_0}\sum_\mu$$
$$\sum_{a,b,c}\tilde{\bar{c}}^a(-\mathbf{p}',s_0)F^{abc}_\mu(\mathbf{p}',\mathbf{p},\mathbf{q};s_0,t_0,u_0)\tilde{c}^b(-\mathbf{p},t_0)\tilde{q}^c_\mu(-\mathbf{q},u_0). \tag{5.72}$$

As already mentioned, only the vertex of a neutral gluon (i.e. $c = 3, 8$) and charged ghosts is needed here. In this case, the vertex becomes

$$\begin{aligned} F_0^{abc}(\mathbf{p}', \mathbf{p}, \mathbf{q}; s_0, t_0, u_0) &= -\frac{i}{2} c_{abc} \Big\{ \delta_{s_0,u_0} [\delta_{s_0+1,t_0} + \delta_{s_0,t_0}] \\ &\quad - \delta_{s_0-1,u_0} [\delta_{s_0,t_0} + \delta_{s_0-1,t_0}] \Big\}, \end{aligned} \tag{5.73}$$

$$\begin{aligned} F_k^{abc}(\mathbf{p}', \mathbf{p}, \mathbf{q}; s_0, t_0, u_0) &= c_{abc} \delta_{s_0,t_0} \delta_{s_0,u_0} c_k^b(-\mathbf{p}, s_0) \\ &\quad \cdot \sin \frac{1}{2} [-p_k - q_k + \phi_b(s_0) + \phi_c(s_0)]. \end{aligned} \tag{5.74}$$

The quark action has to be expanded up to order g_0^2 to get the quark–quark–gluon and the 2 quark – 2 gluon vertices. Both vertices have two terms, one coming from the Wilson part and one coming from the Sheikholeslami–Wohlert part of the action.

The Wilson part of the action has the expansion

$$S_{\rm F,Wilson} = S_{\rm F,Wilson}^{(0)} + \sum_{n=1}^{\infty} \frac{1}{n!} g_0^n S_{\rm F,Wilson}^{(n)}, \tag{5.75}$$

where $S_{\rm F,Wilson}^{(0)}$ has been given in (5.60) and the n-th order expansion coefficient may be written as

$$\begin{aligned} S_{\rm F,Wilson}^{(n)} &= \left(\frac{1}{L^3} \right)^{n+1} \sum_{\mathbf{p},\mathbf{p}',\mathbf{q}_1,\ldots,\mathbf{q}_n} \delta_{\rm P} \left(\mathbf{p} + \mathbf{p}' + \sum_{j=1}^{n} \mathbf{q}_j \right) \sum_{\mu} \sum_{x_0,y_0,z_0} \sum_{a_1,\ldots,a_n} \\ &\quad \bar{\psi}(-\mathbf{p}', x_0) V_\mu^{a_1 \ldots a_n}(\mathbf{s}; x_0, y_0, z_0) \psi(-\mathbf{p}, y_0) \prod_{j=1}^{n} \tilde{q}_\mu^{a_j}(-\mathbf{q}_j, z_0), \end{aligned} \tag{5.76}$$

with $\mathbf{s} = \frac{1}{2}(\mathbf{p}' - \mathbf{p})$. Using the notation

$$I^{a_1 \ldots a_n} = \frac{1}{n!} \sum_{\text{perms } \sigma} I^{\sigma(a_1)} \ldots I^{\sigma(a_n)}, \tag{5.77}$$

the time components of the vertex V become

$$\begin{aligned} V_0^{a_1 \ldots a_n}(\mathbf{s}; x_0, y_0, z_0) &= -I^{a_1 \ldots a_n} \Big\{ P_- \delta_{x_0+1,y_0} \delta_{x_0,z_0} \\ &\quad + (-1)^n P_+ \delta_{x_0-1,y_0} \delta_{y_0,z_0} \Big\}. \end{aligned} \tag{5.78}$$

In contrast to the time components, the space components

$$\begin{aligned} V_k^{a_1 \ldots a_n}(\mathbf{s}; x_0, y_0, z_0) &= -I^{a_1 \ldots a_n} \frac{1}{2} \delta_{x_0,y_0} \delta_{x_0,z_0} \Big\{ W_k^{a_1 \ldots a_n}(\mathbf{s}, x_0)(1 - \gamma_k) \\ &\quad + (-1)^n W_k^{a_1 \ldots a_n}(\mathbf{s}, x_0)^{-1}(1 + \gamma_k) \Big\} \end{aligned} \tag{5.79}$$

depend on the background field via

$$W_k^{a_1\ldots a_n}(\mathbf{s},x_0) = V(x_0)\exp\Big(i[s_k^+ + \frac{1}{2}\sum_j \phi_{a_j}(x_0)]\Big). \tag{5.80}$$

While the Sheikholeslami–Wohlert term (2.14) does not contribute to the free action (5.60), it has to be taken into account for higher orders,

$$\delta S_{\mathrm{V}} = c_{\mathrm{sw}}(g_0)\sum_{n=1}^{\infty}\frac{1}{n!}g_0^n\delta S_{\mathrm{V}}^{(n)}, \tag{5.81}$$

where the n-th order expansion coefficient is given by

$$\begin{aligned}\delta S_{\mathrm{V}}^{(n)} &= \left(\frac{1}{L^3}\right)^{n+1}\sum_{\mathbf{p},\mathbf{p}',\mathbf{q}_1,\ldots,\mathbf{q}_n}\delta_{\mathrm{P}}\left(\mathbf{p}+\mathbf{p}'+\sum_{j=1}^{n}\mathbf{q}_j\right)\sum_{x_0,z_{10},\ldots,z_{n0}}\sum_{\mu_1,\ldots,\mu_n}\sum_{a_1,\ldots,a_n}\\ &\quad \bar\psi(-\mathbf{p}',x_0)S_{\mu_1\ldots\mu_n}^{a_1\ldots a_n}(\mathbf{q}_1,\ldots,\mathbf{q}_n;x_0,z_{10},\ldots,z_{n0})\psi(-\mathbf{p},x_0)\\ &\quad \cdot\prod_{j=1}^{n}\tilde q_{\mu_j}^{a_j}(-\mathbf{q}_j,z_{j0}).\end{aligned} \tag{5.82}$$

For $n=1$, the vertex S may easily be written down as

$$\begin{aligned}S_0^a(\mathbf{q};x_0,z_0) &= \frac{1}{16}\sum_j\sigma_{0j}c_j^a(-\mathbf{q},x_0)\\ &\quad\cdot\Big((\delta_{x_0,z_0}+\delta_{x_0-1,z_0})\{I^a,\cos\mathcal{E}\}s_j^a(-\mathbf{q},x_0)\\ &\quad-(\delta_{x_0,z_0}-\delta_{x_0-1,z_0})[I^a,\sin\mathcal{E}]c_j^a(-\mathbf{q},x_0)\Big),\end{aligned} \tag{5.83}$$

$$\begin{aligned}S_k^a(\mathbf{q};x_0,z_0) &= \frac{i}{16}\sigma_{0k}\Big((\delta_{x_0+1,z_0}-\delta_{x_0-1,z_0})\{I^a,\cos\mathcal{E}\}c_k^a(-\mathbf{q},z_0)\\ &\quad-(\delta_{x_0+1,z_0}+2\delta_{x_0,z_0}+\delta_{x_0-1,z_0})[I^a,\sin\mathcal{E}]s_k^a(-\mathbf{q},z_0)\Big)\\ &\quad-\frac{1}{8}I^a\delta_{x_0,z_0}c_k^a(-\mathbf{q},z_0)\sum_j\sigma_{jk}s_j^a(-\mathbf{q},z_0)c_j^a(-\mathbf{q},z_0).\end{aligned} \tag{5.84}$$

For $n=2$, the vertex is much more complicated. Fortunately, it is not needed completely for the calculation of f_{A} and f_{P} at one loop order. The only thing which really is needed is $\langle\mathcal{F}_{\mu\nu}(x)\rangle$ at order g_0^2, which is given by

$$\langle\mathcal{F}_{jk}(x)\rangle = \mathrm{O}(g_0^3), \tag{5.85}$$

and

$$\begin{aligned}
\langle \mathcal{F}_{0k}(x)\rangle = g_0^2 \frac{1}{4}\frac{1}{L^3}\sum_{\mathbf{q}}\sum_c I^c I^{\bar{c}}\Big\{ \\
2i\cos[\mathcal{E}-\frac{1}{2}(q_k+\phi_c(x_0+1))]\Big(D^c_{00}(\mathbf{q};x_0,x_0)s^c_k(\mathbf{q},x_0+1) \\
+2iD^c_{k0}(\mathbf{q};x_0+1,x_0)\Big) \\
-2i\cos[\mathcal{E}+\frac{1}{2}(q_k+\phi_c(x_0-1))]\Big(D^c_{00}(\mathbf{q};x_0-1,x_0-1)s^c_k(\mathbf{q},x_0-1) \\
-2iD^c_{k0}(\mathbf{q};x_0-1,x_0-1)\Big) \\
+i\sin\mathcal{E}\Big(D^c_{kk}(\mathbf{q};x_0+1,x_0+1)+2D^c_{kk}(\mathbf{q};x_0,x_0) \\
+D^c_{kk}(\mathbf{q};x_0-1,x_0-1)\Big) \\
-2i\sin[\mathcal{E}-\frac{1}{2}\phi'_c]\Big(D^c_{kk}(\mathbf{q};x_0+1,x_0)+D^c_{kk}(\mathbf{q};x_0-1,x_0) \\
+is^c_k(\mathbf{q},x_0+1)D^c_{k0}(\mathbf{q};x_0,x_0)-is^c_k(\mathbf{q},x_0-1)D^c_{k0}(\mathbf{q};x_0,x_0-1)\Big)\Big\} \\
+\mathrm{O}(g_0^3). \qquad (5.86)
\end{aligned}$$

The complete vertices may now be computed by combining the Wilson and Sheikholeslami–Wohlert parts. The quark–quark–gluon vertex is then given by

$$V^a_\mu(\mathbf{p}',\mathbf{p},\mathbf{q};s_0,t_0,u_0) = V^a_\mu(\mathbf{s};s_0,t_0,u_0)+c^{(0)}_{\rm sw}S^a_\mu(\mathbf{q};s_0,u_0)\delta_{s_0,t_0}, \qquad (5.87)$$

and the 2 quark – 2 gluon vertex by

$$\begin{aligned}
V^{ab}_{\mu\nu}(\mathbf{p}',\mathbf{p},\mathbf{q},\mathbf{q}';s_0,t_0,u_0,u'_0) &= V^{ab}_\mu(\mathbf{s};s_0,t_0,u_0)\delta_{\mu\nu}\delta_{u_0,u'_0} \\
&\quad +c^{(0)}_{\rm sw}S^{ab}_{\mu\nu}(\mathbf{q},\mathbf{q}';s_0,u_0,u'_0)\delta_{s_0,t_0}. \qquad (5.88)
\end{aligned}$$

5.3.4 The diagrams

Having calculated the propagators and vertices, one may now expand $f_{\rm A}$ and $f_{\rm P}$. The calculation can be made slightly more general by defining the function

$$\begin{aligned}
f(\Gamma;\mathbf{p},x_0) &= \sum_{\mathbf{y},\mathbf{z}} e^{i\mathbf{p}(\mathbf{y}-\mathbf{z})}\frac{1}{2}\Big\langle \mathrm{Tr}\{P_+\Gamma P_- U(z-\hat{0},0)S(z,x) \\
&\qquad \cdot\Gamma S(x,y)U(y-\hat{0},0)^{-1}\}\Big\rangle_{\rm G}\Big|_{y_0=z_0=1}. \qquad (5.89)
\end{aligned}$$

According to (5.30),(5.31), and (5.34), one has

$$\begin{aligned}
f_{\rm A}(x_0) &= \tilde{c}_{\rm t}^2 f(\gamma_0\gamma_5;\mathbf{0},x_0), \qquad (5.90)\\
f_{\rm P}(x_0) &= \tilde{c}_{\rm t}^2 f(\gamma_5;\mathbf{0},x_0). \qquad (5.91)
\end{aligned}$$

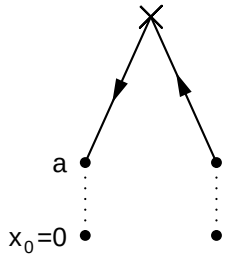

Figure 5.2: *Diagram for $f_{\rm A}$ and $f_{\rm P}$ at tree level. The dotted lines denote the link variables between $x_0 = 0$ and $x_0 = a$, and the cross represents the insertion of the axial current or density.*

Calculating the function f at tree level only amounts to taking the tree level values of the quark propagators and Fourier transforming everything, leading to

$$f(\Gamma;\mathbf{p},x_0)^{(0)} = \frac{1}{2}\mathrm{Tr}\Big\{P_+\Gamma P_- S(\mathbf{p};1,x_0)\Gamma S(\mathbf{p};x_0,1)\Big\}. \tag{5.92}$$

Since the quark propagator is diagonal in colour space, $f(\Gamma;\mathbf{p},x_0)^{(0)}$ may be decomposed into colour components

$$f(\Gamma;\mathbf{p},x_0)^{(0)} = \sum_{\alpha=1}^{N} f(\Gamma;\mathbf{p},x_0)^{(0)}_\alpha, \tag{5.93}$$

with the colour components given by

$$f(\Gamma;\mathbf{p},x_0)^{(0)}_\alpha = \frac{1}{2}\mathrm{tr}\Big\{P_+\Gamma P_- S(\mathbf{p};1,x_0)_\alpha\Gamma S(\mathbf{p};x_0,1)_\alpha\Big\}, \tag{5.94}$$

where tr denotes the trace over the Dirac indices only. Thus one gets a tree level coefficient which can be depicted by the diagram in figure 5.2.

For the 1–loop expansion, the propagators and link variables in (5.89) have to be expanded according to

$$S(x,y) = S^{(0)}(x,y) + g_0 S^{(1)}(x,y) + g_0^2 S^{(2)}(x,y) + \mathrm{O}(g_0^3), \tag{5.95}$$

and

$$\begin{aligned} U(x,\mu) &= \exp\{g_0 q_\mu(x)\}V(x,\mu) \\ &= \left\{1 + g_0 q_\mu(x) + \frac{1}{2}g_0^2 q_\mu(x)^2 + \mathrm{O}(g_0^3)\right\}V(x,\mu). \end{aligned} \tag{5.96}$$

In order to compute f at 1–loop order, one has to insert these expansions, gather all contributions of order g_0^2 and contract the gluon fields to gluon propagators. Apart from these contributions, there are improvement terms proportional to the 1–loop improvement coefficients. In order to compute f at $m_1 = 0$, one has to do the calculation at the critical quark mass $m_{\rm c}$, which has an expansion

$$m_{\rm c} = m_{\rm c}^{(0)} + g_0^2 m_{\rm c}^{(1)} + {\rm O}(g_0^4). \tag{5.97}$$

The 1–loop coefficient of f then gets a contribution proportional to $m_{\rm c}^{(1)}$. Thus we get the sum

$$\begin{aligned} f(\Gamma;\mathbf{p},x_0)^{(1)} &= \sum_n f(\Gamma;\mathbf{p},x_0)_n^{(1)} + c_{\rm sw}^{(1)} f(\Gamma;\mathbf{p},x_0)_{\rm V}^{(1)} \\ &\quad + \tilde{c}_{\rm t}^{(1)} f(\Gamma;\mathbf{p},x_0)_{\rm Fb}^{(1)} + c_{\rm t}^{(1)} f(\Gamma;\mathbf{p},x_0)_{\rm Gb}^{(1)} \\ &\quad + m_{\rm c}^{(1)} \frac{\partial}{\partial m_0} f(\Gamma;\mathbf{p},x_0)^{(0)}. \end{aligned} \tag{5.98}$$

Here, all expansion coefficients have to be calculated at $m_0 = m_{\rm c}^{(0)}$, which will be obtained by a tree level calculation explained in section 5.4. For $f_{\rm A}$, one gets the additional contribution $f_{\delta A}^{(1)}$ proportional to $c_{\rm A}^{(1)}$.

The contributions $f(\Gamma;\mathbf{p},x_0)_n^{(1)}$ may be depicted by the diagrams in figure 5.3. The second order contributions of the link variables give diagrams 1a and 1b,

$$f(\Gamma;\mathbf{p},x_0)_{1a}^{(1)} = -\frac{1}{2}\frac{1}{L^3}\sum_\alpha f(\Gamma;\mathbf{p},x_0)_\alpha^{(0)} \sum_{\mathbf{q}} \sum_a D_{00}^a(\mathbf{q};0,0)\mathcal{C}_\alpha^a, \tag{5.99}$$

where

$$\mathcal{C}_\alpha^a = -\left(I^a I^{\bar{a}}\right)_{\alpha\alpha}. \tag{5.100}$$

Diagram 1b is simply given by

$$f(\Gamma;\mathbf{p},x_0)_{1b}^{(1)} = f(\Gamma;\mathbf{p},x_0)_{1a}^{(1)}. \tag{5.101}$$

In the following, we define $\mathbf{r} = \mathbf{p} + \mathbf{q}$ for convenience. Then the contraction of the first order terms of both link variables yields diagram 2,

$$f(\Gamma;\mathbf{p},x_0)_2^{(1)} = \frac{1}{L^3}\sum_\alpha \sum_{\mathbf{q}} f(\Gamma;\mathbf{r},x_0)_\alpha^{(0)} \sum_a D_{00}^a(\mathbf{q};0,0)\mathcal{C}_\alpha^a. \tag{5.102}$$

Obviously, there are four different ways to combine the first order terms of the link variables with the first order terms of the propagators. Contracting the first order term of the link variables with the first order terms of the propagators on the same side gives diagrams 3a and 3b,

$$\begin{aligned} f(\Gamma;\mathbf{p},x_0)_{3a}^{(1)} &= \frac{1}{2}\frac{1}{L^3}\sum_{\mathbf{q}}\sum_\mu \sum_{s_0,t_0,u_0}\sum_a D_{0\mu}^a(\mathbf{q};0,u_0)\mathrm{Tr}\Big\{ I^a P_+ \Gamma P_- S(\mathbf{p};1,x_0) \\ &\quad \cdot\Gamma S(\mathbf{p};x_0,s_0) V_\mu^{\bar{a}}(\mathbf{p},-\mathbf{r},\mathbf{q};s_0,t_0,u_0) S(\mathbf{r};t_0,1)\Big\}, \end{aligned} \tag{5.103}$$

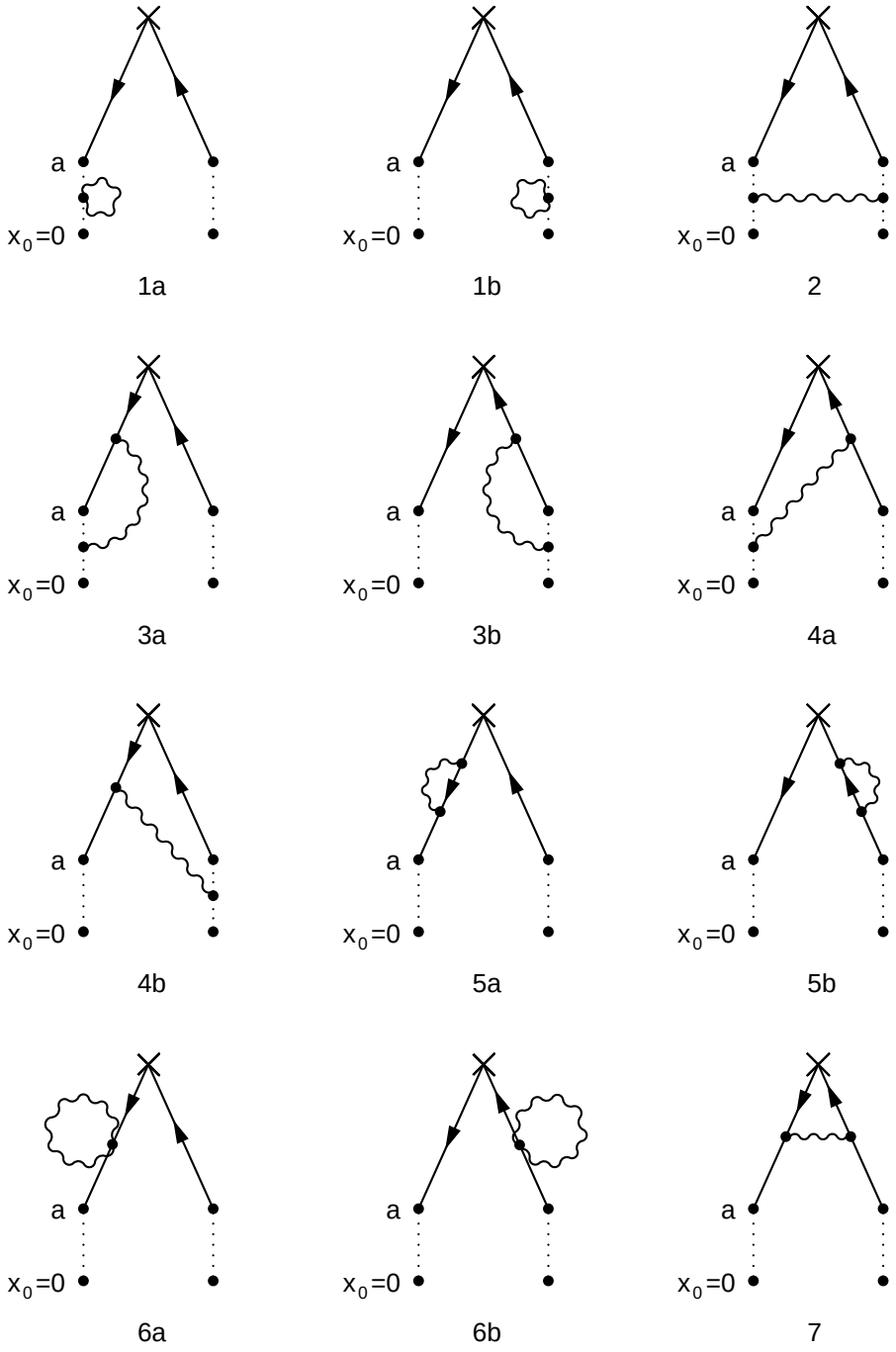

Figure 5.3: *Diagrams contributing to $f_{\mathrm{A}}(x_0)$ and $f_{\mathrm{P}}(x_0)$ at 1–loop order of perturbation theory both at vanishing and non–vanishing background field.*

$$f(\Gamma;\mathbf{p},x_0)^{(1)}_{3b} = -\frac{1}{2}\frac{1}{L^3}\sum_{\mathbf{q}}\sum_{\mu}\sum_{s_0,t_0,u_0}\sum_{a} D^a_{\mu 0}(\mathbf{q};u_0,0)\mathrm{Tr}\Big\{I^{\bar a}P_+\Gamma P_- S(\mathbf{r};1,s_0) \cdot V^a_\mu(\mathbf{r},-\mathbf{p},-\mathbf{q};s_0,t_0,u_0)S(\mathbf{p};t_0,x_0)\Gamma S(\mathbf{p};x_0,1)\Big\}, \quad (5.104)$$

while combining them with the first order terms of the propagators on the opposite side results in diagrams 4a and 4b,

$$f(\Gamma;\mathbf{p},x_0)^{(1)}_{4a} = \frac{1}{2}\frac{1}{L^3}\sum_{\mathbf{q}}\sum_{\mu}\sum_{s_0,t_0,u_0}\sum_{a} D^a_{0\mu}(\mathbf{q};0,u_0)\mathrm{Tr}\Big\{I^{a}P_+\Gamma P_- S(\mathbf{p};1,s_0) \cdot V^{\bar a}_\mu(\mathbf{p},-\mathbf{r},\mathbf{q};s_0,t_0,u_0)S(\mathbf{r};t_0,x_0)\Gamma S(\mathbf{r};x_0,1)\Big\}, \quad (5.105)$$

$$f(\Gamma;\mathbf{p},x_0)^{(1)}_{4b} = -\frac{1}{2}\frac{1}{L^3}\sum_{\mathbf{q}}\sum_{\mu}\sum_{s_0,t_0,u_0}\sum_{a} D^a_{\mu 0}(\mathbf{q};u_0,0)\mathrm{Tr}\Big\{I^{\bar a}P_+\Gamma P_- S(\mathbf{r};1,x_0) \cdot \Gamma S(\mathbf{r};x_0,s_0)V^a_\mu(\mathbf{r},-\mathbf{p},-\mathbf{q};s_0,t_0,u_0)S(\mathbf{p};t_0,1)\Big\}. \quad (5.106)$$

The second order terms of the quark propagators consist of two parts: One containing two quark–quark–gluon vertices with a quark line in between, and one containing a 2 quark–2 gluon vertex. The part with the two vertices leads to diagrams 5a and 5b,

$$f(\Gamma;\mathbf{p},x_0)^{(1)}_{5a} = \frac{1}{2}\frac{1}{L^3}\sum_{\mathbf{q}}\sum_{\mu,\nu}\sum_{s_0,t_0,u_0}\sum_{s_0',t_0',u_0'}\sum_{a} D^a_{\nu\mu}(\mathbf{q};u_0',u_0)\mathrm{Tr}\Big\{P_+\Gamma P_- \cdot S(\mathbf{p};1,x_0)\Gamma S(\mathbf{p};x_0,s_0)V^{\bar a}_\mu(\mathbf{p},-\mathbf{r},\mathbf{q};s_0,t_0,u_0)S(\mathbf{r};t_0,s_0') \cdot V^a_\nu(\mathbf{r},-\mathbf{p},-\mathbf{q};s_0',t_0',u_0')S(\mathbf{p};t_0',1)\Big\}, \quad (5.107)$$

$$f(\Gamma;\mathbf{p},x_0)^{(1)}_{5b} = \frac{1}{2}\frac{1}{L^3}\sum_{\mathbf{q}}\sum_{\mu,\nu}\sum_{s_0,t_0,u_0}\sum_{s_0',t_0',u_0'}\sum_{a} D^a_{\nu\mu}(\mathbf{q};u_0',u_0)\mathrm{Tr}\Big\{P_+\Gamma P_- \cdot S(\mathbf{p};1,s_0)V^{\bar a}_\mu(\mathbf{p},-\mathbf{r},\mathbf{q};s_0,t_0,u_0)S(\mathbf{r};t_0,s_0') \cdot V^a_\nu(\mathbf{r},-\mathbf{p},-\mathbf{q};s_0',t_0',u_0')S(\mathbf{p};t_0',x_0)\Gamma S(\mathbf{p};x_0,1)\Big\}, \quad (5.108)$$

while the part containing the 2 quark–2 gluon vertex gives diagrams 6a and 6b,

$$f(\Gamma;\mathbf{p},x_0)^{(1)}_{6a} = -\frac{1}{4}\frac{1}{L^3}\sum_{\mathbf{q}}\sum_{\mu,\nu}\sum_{s_0,t_0}\sum_{u_0,u_0'}\sum_{a} D^a_{\nu\mu}(\mathbf{q};u_0',u_0)\mathrm{Tr}\Big\{P_+\Gamma P_- \cdot S(\mathbf{p};1,x_0)\Gamma S(\mathbf{p};x_0,s_0)V^{\bar a a}_{\mu\nu}(\mathbf{p},-\mathbf{p},\mathbf{q},-\mathbf{q};s_0,t_0,u_0,u_0') \cdot S(\mathbf{p};t_0,1)\Big\}, \quad (5.109)$$

$$
\begin{aligned}
f(\Gamma;\mathbf{p},x_0)^{(1)}_{6b} &= -\frac{1}{4}\frac{1}{L^3}\sum_{\mathbf{q}}\sum_{\mu,\nu}\sum_{s_0,t_0}\sum_{u_0,u_0'}\sum_{a} D^a_{\nu\mu}(\mathbf{q};u_0',u_0)\mathrm{Tr}\Big\{P_+\Gamma P_- \\
&\quad\cdot S(\mathbf{p};1,s_0)V^{\bar{a}a}_{\mu\nu}(\mathbf{p},-\mathbf{p},\mathbf{q},-\mathbf{q};s_0,t_0,u_0,u_0')S(\mathbf{p};t_0,x_0) \\
&\quad\cdot\Gamma S(\mathbf{p};x_0,1)\Big\}. \qquad (5.110)
\end{aligned}
$$

In the improved theory, these diagrams do not give the total contribution of the second order terms of the quark propagators. There are two more parts, one proportional to $\tilde{c}_{\mathrm{t}}^{(1)}$ and one proportional to $c_{\mathrm{sw}}^{(1)}$. These contributions will be dealt with separately. Finally, the combination of the first order terms of both propagators results in diagram 7,

$$
\begin{aligned}
f(\Gamma;\mathbf{p},x_0)^{(1)}_{7} &= \frac{1}{2}\frac{1}{L^3}\sum_{\mathbf{q}}\sum_{\mu,\nu}\sum_{s_0,t_0,u_0}\sum_{s_0',t_0',u_0'}\sum_{a} D^a_{\nu\mu}(\mathbf{q};u_0',u_0)\mathrm{Tr}\Big\{P_+\Gamma P_- \\
&\quad\cdot S(\mathbf{p};1,s_0)V^{\bar{a}}_{\mu}(\mathbf{p},-\mathbf{r},\mathbf{q};s_0,t_0,u_0)S(\mathbf{r};t_0,x_0) \\
&\quad\cdot\Gamma S(\mathbf{r};x_0,s_0')V^{a}_{\nu}(\mathbf{r},-\mathbf{p},-\mathbf{q};s_0',t_0',u_0')S(\mathbf{p};t_0',1)\Big\}. \qquad (5.111)
\end{aligned}
$$

So far, the calculation has been completely analogous to the case of a vanishing background field. However, with the non–zero background field considered here, one has to take the terms in (5.33) containing $S^{(1)}_{\mathrm{tot}}$ into account. This means one has to contract the first order terms of the link variables and the propagators with the first order terms of the total action, leading to the diagrams in figure 5.4. Starting with the first order term of a propagator, we get

$$
\begin{aligned}
f(\Gamma;\mathbf{p},x_0)^{(1)}_{8a} &= -\frac{1}{2}\sum_{\mu,\nu}\sum_{s_0,t_0}\sum_{u_0,u_0'}\sum_{a} D^a_{\nu\mu}(\mathbf{0};u_0',u_0)\mathrm{Tr}\Big\{P_+\Gamma P_- \\
&\quad\cdot S(\mathbf{p};1,x_0)\Gamma S(\mathbf{p};x_0,s_0)V^{a}_{\nu}(\mathbf{p},-\mathbf{p},\mathbf{0};s_0,t_0,u_0') \\
&\quad\cdot S(\mathbf{p};t_0,1)\Big\}T^{\bar{a}}_{\mu}(u_0), \qquad (5.112)
\end{aligned}
$$

where T^a_μ denotes the sum of the closed gluon, ghost, and quark loops,

$$
T^a_\mu(u_0) = T^a_{\mu,\mathrm{gluon}}(u_0) + T^a_{\mu,\mathrm{ghost}}(u_0) + N_{\mathrm{f}}T^a_{\mu,\mathrm{quark}}(u_0). \qquad (5.113)
$$

Note that the time component T^a_0 vanishes due to CP invariance. The gluon loop is given by

$$
T^a_{\mu,\mathrm{gluon}}(u_0) = -\frac{1}{2}\frac{1}{L^3}\sum_{\mathbf{q}}\sum_{\nu,\rho}\sum_{s_0,t_0}\sum_{c} V^{\bar{c}ca}_{\nu\rho\mu}(\mathbf{q},-\mathbf{q},\mathbf{0};s_0,t_0,u_0)D^c_{\rho\nu}(\mathbf{q};t_0,s_0), \qquad (5.114)
$$

the ghost loop by

$$
T^a_{\mu,\mathrm{ghost}}(u_0) = \frac{1}{L^3}\sum_{\mathbf{q}}\sum_{s_0,t_0}\sum_{c} F^{\bar{c}ca}_{\mu}(\mathbf{q},-\mathbf{q},\mathbf{0};s_0,t_0,u_0)D^c(\mathbf{q};t_0,s_0), \qquad (5.115)
$$

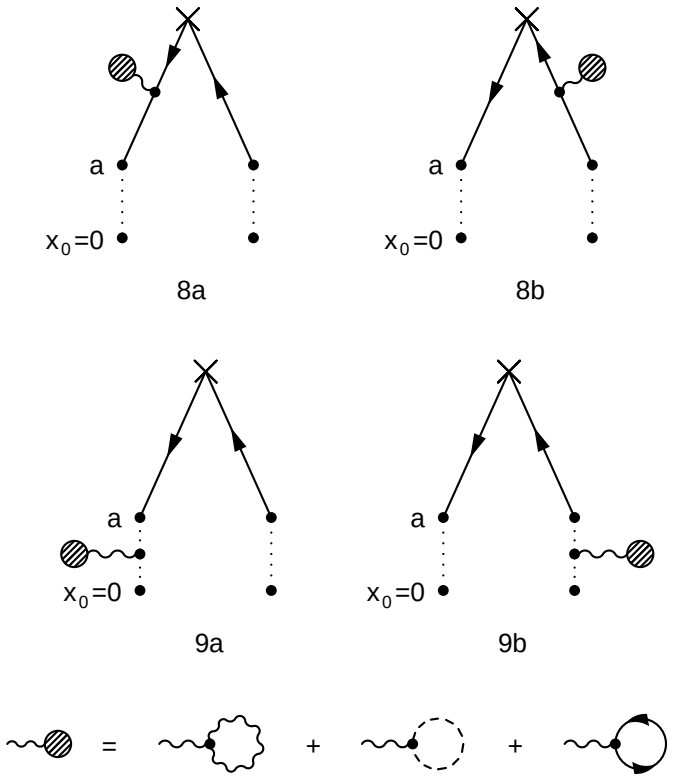

Figure 5.4: *Tadpole diagrams contributing to $f_{\mathrm{A}}(x_0)$ and $f_{\mathrm{P}}(x_0)$ at 1–loop order of perturbation theory. These terms are only present with a non–vanishing background field.*

and the quark loop by

$$T^a_{\mu,\mathrm{quark}}(u_0) = \frac{1}{L^3}\sum_{\mathbf{q}}\sum_{s_0,t_0}\mathrm{Tr}\Big\{V^a_\mu(\mathbf{q},-\mathbf{q},\mathbf{0};s_0,t_0,u_0)S(\mathbf{q};t_0,s_0)\Big\}. \tag{5.116}$$

Analogously, one gets diagram 8b,

$$\begin{aligned} f(\Gamma;\mathbf{p},x_0)^{(1)}_{8b} &= -\frac{1}{2}\sum_{\mu,\nu}\sum_{s_0,t_0}\sum_{u_0,u_0'}\sum_a D^a_{\nu\mu}(\mathbf{0};u_0',u_0)\mathrm{Tr}\Big\{P_+\Gamma P_- \\ &\quad \cdot S(\mathbf{p};1,s_0)V^a_\nu(\mathbf{p},-\mathbf{p},\mathbf{0};s_0,t_0,u_0')S(\mathbf{p};t_0,x_0) \\ &\quad \cdot\Gamma S(\mathbf{p};x_0,1)\Big\}T^{\bar a}_\mu(u_0). \end{aligned} \tag{5.117}$$

The combination of $S^{(1)}_{\mathrm{tot}}$ and the first order terms of the link variables yields diagrams 9a and 9b, which are given by

$$\begin{aligned} f(\Gamma;\mathbf{p},x_0)^{(1)}_{9a} &= -\frac{1}{2}\sum_{\mu}\sum_{u_0}\sum_a D^a_{0\mu}(\mathbf{0};0,u_0)\mathrm{Tr}\Big\{I^aP_+\Gamma P_-S(\mathbf{p};1,x_0) \\ &\quad \cdot\Gamma S(\mathbf{p};x_0,1)\Big\}T^{\bar a}_\mu(u_0) \end{aligned} \tag{5.118}$$

and

$$f(\Gamma;\mathbf{p},x_0)^{(1)}_{9b} = -f(\Gamma;\mathbf{p},x_0)^{(1)}_{9a}. \tag{5.119}$$

Since they are of opposite sign, they cancel in the sum and may be ignored. This leaves diagrams 8a and 8b as the only diagrams depending on the number of flavours. Note that these terms are not present in the case of a vanishing background field. This means that with a non–vanishing background field, the critical quark mass is dependent on N_{f} at 1–loop order, while with a vanishing background field it is not.

5.3.5 The improvement terms

It was already mentioned that diagrams 6a and 6b get additional contributions from the volume and boundary counter-terms in the quark action.
The volume term gives corrections proportional to $c^{(0)}_{\mathrm{sw}}$,which have already been taken into account in the vertices, and corrections proportional to $c^{(1)}_{\mathrm{sw}}$ which still have to be computed. These corrections to the propagator at order g_0^2 are imposed by the Sheikholeslami–Wohlert part of the Dirac operator, which at this order is

$$\delta D^{(2)}_{\mathrm{V}} = -\frac{i}{2}c^{(1)}_{\mathrm{sw}}\gamma_0\sum_k\gamma_k\sin\mathcal{E}. \tag{5.120}$$

In diagram 6a, this leads to the correction

$$f(\Gamma;\mathbf{p},x_0)^{(1)}_{6a,\rm V} = \frac{i}{4}c^{(1)}_{\rm sw}\sum_{\alpha}\sum_{s_0=1}^{T-1}\mathrm{tr}\Big\{P_+\Gamma P_- S(\mathbf{p};1,x_0)_\alpha\Gamma S(\mathbf{p};x_0,s_0)_\alpha \cdot\gamma_0\sum_k\gamma_k S(\mathbf{p};x_0,1)_\alpha\Big\}\sin\mathcal{E}_\alpha. \tag{5.121}$$

Using the symmetry of the quark propagator

$$S(\mathbf{p};x_0,y_0) = \gamma_5 S(\mathbf{p};y_0,x_0)^\dagger\gamma_5, \tag{5.122}$$

one can show that the contribution to diagram 6b is the same. Thus, the total contribution proportional to $c^{(1)}_{\rm sw}$ becomes

$$f(\Gamma;\mathbf{p},x_0)^{(1)}_{\rm V} = 2f(\Gamma;\mathbf{p},x_0)^{(1)}_{6a,\rm V}. \tag{5.123}$$

Another way to get this improvement term is by Taylor expansion,

$$f(\Gamma;\mathbf{p},x_0)^{(1)}_{\rm V} = \frac{\partial}{\partial c_{\rm sw}} f(\Gamma;\mathbf{p},x_0)^{(0)}\Big|_{c_{\rm sw}=1}. \tag{5.124}$$

So, the volume term could, in principle, also be obtained from the tree level result by numerical differentiation. While this procedure turned out not to be suitable for the calculation, since it gives the result with less accuracy, it was successfully used to check the result obtained according to (5.123).

Apart from the volume term, diagrams 6a and 6b get a contribution from the boundary counter-term of the quark action, which acts on the propagator as

$$\delta D^{(2)}_{\rm b} S(x,y) = \tilde{c}^{(1)}_{\rm t}\left\{\delta_{x_0,1}S(x,y) + \delta_{x_0,T-1}S(x,y)\right\}. \tag{5.125}$$

In diagram 6a, this leads to the contribution

$$f(\Gamma;\mathbf{p},x_0)^{(1)}_{6a,\rm b} = -\frac{1}{2}\tilde{c}^{(1)}_{\rm t}\mathrm{Tr}\Big\{P_+\Gamma P_- S(\mathbf{p};1,x_0)\Gamma\Big[S(\mathbf{p};x_0,1)S(\mathbf{p};1,1) + S(\mathbf{p};x_0,T-1)S(\mathbf{p};T-1,1)\Big]\Big\}. \tag{5.126}$$

Here again, the corresponding contribution to diagram 6b can be shown to be the same. One thus gets

$$f(\Gamma;\mathbf{p},x_0)^{(1)}_{\rm Fb} = 2f(\Gamma;\mathbf{p},x_0)^{(1)}_{6a,\rm b}. \tag{5.127}$$

Strictly speaking, this does not give the whole term of $f_{\rm A}$ and $f_{\rm P}$ proportional to $\tilde{c}_{\rm t}$, because there is still the overall factor of $\tilde{c}^2_{\rm t}$ in (5.90) and (5.91) to be taken into account. As stated before, this factor cancels in the current quark mass and may be neglected in this calculation. It may, however, be used as a consistency

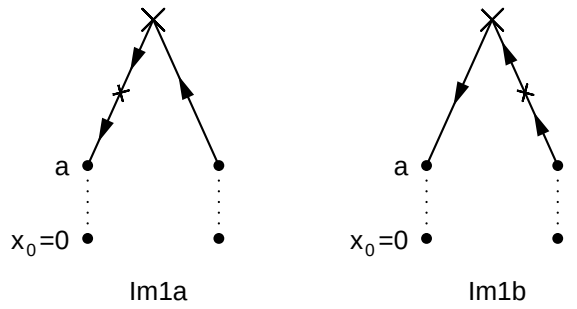

Figure 5.5: *Diagrams for* $f(\Gamma;\mathbf{p},x_0)^{(1)}_{\mathrm{V}}$, $f(\Gamma;\mathbf{p},x_0)^{(1)}_{\mathrm{Fb}}$, *and* $\frac{\partial}{\partial m_0}f(\Gamma;\mathbf{p},x_0)^{(0)}$

check, since, as an improvement term, $(f^{(1)}_{\mathrm{A/P,Fb}}+2f^{(0)}_{\mathrm{A/P}})$ has to approach zero in the continuum limit, which $f^{(1)}_{\mathrm{A/P,Fb}}$ and $f^{(0)}_{\mathrm{A/P}}$ do not do separately.

Both improvement terms calculated so far come from the insertion of $\delta D^{(2)}$ into the quark line and may thus be depicted by the diagrams in figure 5.5.

Another term that may be depicted by the same diagrams is the derivative of f at tree level with respect to the bare mass. To this end, one has to take the derivative

$$\frac{\partial}{\partial m_0}S(\mathbf{p};x_0,y_0)=-\sum_{s_0}S(\mathbf{p};x_0,s_0)S(\mathbf{p};s_0,y_0) \tag{5.128}$$

of the quark propagators in (5.92). The two contributions coming from differentiating the two propagators can be shown to be the same, leading to

$$\frac{\partial}{\partial m_0}f(\Gamma;\mathbf{p},x_0)^{(0)}=-\sum_{s_0}\mathrm{Tr}\left\{P_+\Gamma P_-S(\mathbf{p};1,x_0)\Gamma S(\mathbf{p};x_0,s_0)S(\mathbf{p};s_0,1)\right\}. \tag{5.129}$$

With a non–vanishing background field, there is also an improvement term proportional to $c_{\mathrm{t}}^{(1)}$, giving an additional contribution to diagram 8a and 8b. This term arises from a contribution proportional to $c_{\mathrm{t}}^{(1)}$ in the total action, contributing to f_{A} and f_{P} via (5.33). Apart from the gluon tadpole, the gluon part (4.24) of the total action yields the boundary counter-term

$$S^{(1)}_{\mathrm{tot,b}}=\frac{2}{\sqrt{3}}c_{\mathrm{t}}^{(1)}\sum_k\left[\tilde{q}^8_k(\mathbf{0},1)-\tilde{q}^8_k(\mathbf{0},T-1)\right]\left[\sin(2\gamma)+\sin\gamma\right], \tag{5.130}$$

where the parameter γ is given by

$$\gamma=\frac{1}{LT}\left(\eta+\frac{\pi}{3}\right). \tag{5.131}$$

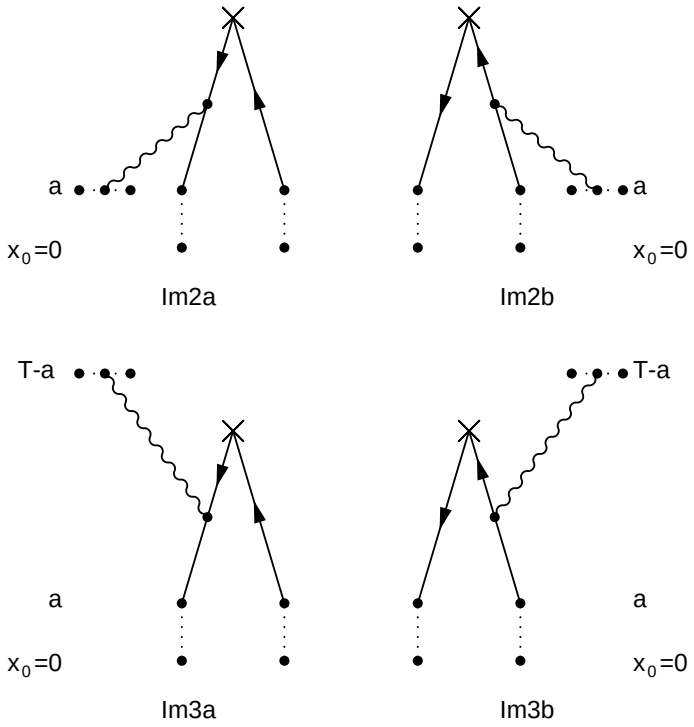

Figure 5.6: *Diagrams contributing to the improvement term proportional to* $c_{\mathrm{t}}^{(1)}$ *for* f_{A} *and* f_{P} *at 1–loop order*

Contracting this part of the total action with the first order term of the quark line gives the contribution

$$\begin{aligned} f(\Gamma;\mathbf{p},x_0)^{(1)}_{\mathrm{Im2a/Im3a}} &= \frac{c_{\mathrm{t}}^{(1)}}{\sqrt{3}} \sum_{s_0,t_0,u_0} \sum_{\mu} \sum_{k} \mathrm{Tr}\Big\{ P_+ \Gamma P_- S(\mathbf{p};1,x_0) \Gamma S(\mathbf{p};x_0,s_0) \\ &\quad \cdot V_\mu^8(\mathbf{p},-\mathbf{p},\mathbf{0};s_0,t_0,u_0) S(\mathbf{p};t_0,1) \Big\} \Big[D^8_{\mu k}(\mathbf{0};u_0,1) \\ &\quad - D^8_{\mu k}(\mathbf{0};u_0,T-1) \Big] \left[\sin(2\gamma) + \sin\gamma \right], \end{aligned} \tag{5.132}$$

which may be depicted by diagrams Im2a and Im3a in figure 5.6. The corresponding correction depicted by diagrams Im2b and Im3b can be shown to be the same, such that the total contribution proportional to $c_{\mathrm{t}}^{(1)}$ becomes

$$f(\Gamma;\mathbf{p},x_0)^{(1)}_{\mathrm{Gb}} = 2 f(\Gamma;\mathbf{p},x_0)^{(1)}_{\mathrm{Im2a/Im3a}}. \tag{5.133}$$

Strictly speaking, there are also contributions proportional to $c_{\mathrm{t}}^{(1)}$ from the contractions of the time–like link variables at the boundary with the gluons in (5.130),

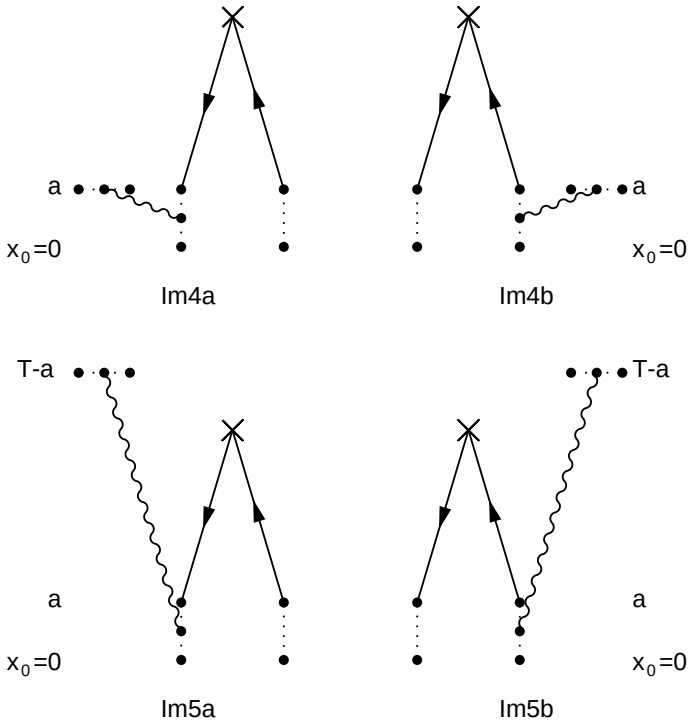

Figure 5.7: *Further diagrams contributing to the improvement term proportional to* $c_{\rm t}^{(1)}$ *for* $f_{\rm A}$ *and* $f_{\rm P}$ *at 1–loop order*

depicted by diagrams Im4a, Im4b, Im5a, and Im5b in figure 5.7. But, like the diagrams 9a and 9b, these contributions are of opposite sign and thus cancel in the sum.

The $c_{\mathrm{t}}^{(1)}$–term was neglected in the computation of $c_{\mathrm{sw}}^{(1)}$ in [51]. This is permissible, because in the current mass, the boundary counter-terms only contribute at order a^2. This is due to the fact that (5.14) remains valid even if the boundary counter-terms $\delta S_{\mathrm{G,b}}$ and $\delta S_{\mathrm{F,b}}$ are dropped. Further explanations concerning this matter can be found in [54]. Furthermore, this term was missing in the perturbative results for the discretisation errors in [27]. To which extent this term changes the results published there will be discussed in chapter 7.

A further improvement term only present in f_{A} arises from the $\mathrm{O}(a)$ correction of the axial current (5.4). Insertion of (5.5) into the correlation function yields

$$f_{\delta A}^{(1)}(x_0) = \frac{1}{2} c_{\mathrm{A}}^{(1)} (\partial_0^* + \partial_0) f_{\mathrm{P}}^{(0)}(x_0). \tag{5.134}$$

5.4 Calculation of the critical quark mass and the lattice artefacts

With the one loop expansion of f_{A} and f_{P}, one is now able to compute the critical quark mass at 1–loop order. To this end, the tree level and 1–loop coefficients of m_1 have to be computed at a given m_0. From (5.17) one gets the x_0 dependent mass $m(x_0)$ at tree level by

$$m^{(0)}(x_0) = \frac{(\partial_0^* + \partial_0) f_{\mathrm{A}}^{(0)}(x_0)}{4 f_{\mathrm{P}}^{(0)}(x_0)}, \tag{5.135}$$

while at 1–loop level it is given by

$$\begin{aligned} m^{(1)}(x_0) &= \frac{(\partial_0^* + \partial_0) f_{\mathrm{A}}^{(1)}(x_0)}{4 f_{\mathrm{P}}^{(0)}(x_0)} - f_{\mathrm{P}}^{(1)}(x_0) \frac{(\partial_0^* + \partial_0) f_{\mathrm{A}}^{(0)}(x_0)}{4 f_{\mathrm{P}}^{(0)2}(x_0)} \\ &\quad + c_{\mathrm{A}}^{(1)} \frac{\partial_0^* \partial_0 f_{\mathrm{P}}^{(0)}(x_0)}{2 f_{\mathrm{P}}^{(0)}(x_0)}, \end{aligned} \tag{5.136}$$

with $f_{\mathrm{A}}^{(1)}$ and $f_{\mathrm{P}}^{(1)}$ including the volume and boundary improvement terms (5.123), (5.127), and (5.133). The current quark mass m_1 is then computed at tree and 1–loop level by taking $m^{(0)}$ and $m^{(1)}$ in the centre of the lattice according to (5.18). Of course, the expansion coefficients of f_{A} and f_{P} depend on the bare quark mass at which they are computed. Thus one gets an expansion

$$m_1 = m_1^{(0)}(m_0) + m_1^{(1)}(m_0) g_0^2 + \mathrm{O}(g_0^4), \tag{5.137}$$

where the expansion coefficients depend on the bare quark mass m_0. To set up perturbation theory for the critical mass, we consider m_0 also to be a series,

$$m_0 = m_0^{(0)} + m_0^{(1)} g_0^2 + \mathrm{O}(g_0^4), \tag{5.138}$$

and expand m_1 further as

$$m_1 = m_1^{(0)}\left(m_0^{(0)}\right) + \left[m_1^{(1)}\left(m_0^{(0)}\right) + m_0^{(1)}\frac{\partial}{\partial m_0} m_1^{(0)}\left(m_0^{(0)}\right)\right] g_0^2 + \mathrm{O}(g_0^4). \tag{5.139}$$

Therefore, the computation of $m_\mathrm{c}^{(1)}$ has to be done in two steps. First we compute $m_\mathrm{c}^{(0)}$ by requiring

$$m_1^{(0)}\left(m_\mathrm{c}^{(0)}\right) = 0, \tag{5.140}$$

then we can determine $m_\mathrm{c}^{(1)}$ from

$$m_1^{(1)}\left(m_\mathrm{c}^{(0)}\right) + m_\mathrm{c}^{(1)}\frac{\partial}{\partial m_0} m_1^{(0)}\left(m_\mathrm{c}^{(0)}\right) = 0. \tag{5.141}$$

The first step is easily done numerically using a discretised version of the Newton–Raphson method. The second step mainly amounts to expanding f_A and f_P up to 1–loop order as described in the previous subsection. Results for $m_\mathrm{c}^{(0)}$ and $m_\mathrm{c}^{(1)}$ can be found in chapter 7.

The lattice artefact e may now be computed at tree and 1–loop level. In lattice units, e is given by

$$e(L) = m_1(2L) - m_1(L), \tag{5.142}$$

where m_1 is to be taken at the critical bare mass at lattice size L, which means that the bare mass is chosen such that $m_1(L) = 0$. So, in order to get $e(L)$, one first has to compute the critical mass at lattice size L and then, using this bare mass, compute m_1 on a lattice twice as large. The results for e are shown in chapter 7.

The lattice artefact

$$d(L) = m_2(L) - m_1(L) \tag{5.143}$$

remains to be computed. To this end, one has to expand the functions f'_A and f'_P up to 1–loop order. However, this turns out to be an easy task. It is straightforward to show that f'_A and f'_P are the same as f_A and f_P with inverted background field. This means, in order to compute $m_2(L)$, one only has to compute m_1 and then repeat the computation after exchanging the boundary values C and C'. (One has of course to take care of the $\phi_a(x_0)$ in the propagators and vertices, which depend crucially on the background field.) The results for d can be found in chapter 7.

5.5 Numerical computation of $f_{\mathrm{A}}^{(1)}$ and $f_{\mathrm{P}}^{(1)}$

Since most of the computation merely consists of matrix multiplications, the structure of the program is rather simple. However, due to the complicated formulae for the propagators and vertices, there is a big risk of errors. For this reason, a careful check of the results is necessary. To this end, the gauge parameter λ_0 was left arbitrary, and it was checked that the results do not depend on λ_0. While this only gives a check on the total result, there is a possibility to check at least those diagrams separately that come in two types, labelled a and b here. Due to the symmetries of the propagators and vertices, these two types have to give the same results. The results using the tree level improvement coefficients as well as the gluon boundary term have been compared to Monte Carlo results obtained by Juri Rolf. Finally, two sets of programs have been written independently, one by Peter Weisz and one by the author of this thesis, and the results have been compared.

While the general structure of the program is relatively simple, the computation of the propagators is technically somewhat more involved. In contrast to the case of a vanishing background field, the propagators for the gluon, ghost, and fermion fields cannot be computed analytically. For this reason, a numerical calculation is required. Of course it would be possible to invert the operators K^a, F^a, and D by a simple inversion routine. However, on large lattices, this would mean inverting very large matrices, which would take a large amount of computer time. A more convenient way to compute the propagators is a procedure using Wronskian forms described in [64] for the gluon and ghost propagators and in [34] for the fermions. This method, which is briefly outlined in appendix B, was used in the computation of f_{A} and f_{P} at 1–loop order. However, even with this method, computer time is far from being negligible. On a 200 MHz Pentium PC, the computation at $L = 16$ took 16 hours of CPU time. Even on a 900 MHz PC, lattices with $L > 32$ could not be computed in reasonable time. Since one has to sum over three momentum components and two vertex times in the diagrams, the time needed scales asymptotically with L^5. This means that larger lattices up to $L = 64$ seem to be beyond reach.

Chapter 6

The renormalised quark mass

6.1 The renormalisation constant Z_{P} and its step scaling function

6.1.1 The renormalisation constant Z_{P}

In chapter 5, the renormalised quark mass defined by the PCAC relation was found to be related to the current quark mass via (5.19). The actual renormalisation is done by renormalising the axial current and density, leading to a running mass, since the renormalisation constants depend on the renormalisation scale. This is, however, not true for Z_{A}, which is only present due to the violation of the chiral symmetry and can be shown to be finite and scale independent. Thus the renormalisation constant that actually makes the running is Z_{P}. In order to compute Z_{P}, one may use the correlation function f_{P}. However, in f_{P}, one does not only have to renormalise the pseudo scalar density, but also the boundary fields ζ and $\bar{\zeta}$, such that the renormalised correlation function becomes

$$(f_{\mathrm{P}})_{\mathrm{R}}(x_0) = Z_{\mathrm{P}} Z_\zeta^2 f_{\mathrm{P}}(x_0). \tag{6.1}$$

In order to cancel the unwelcome renormalisation factor Z_ζ^2, one may use the correlation function f_1, defined by

$$f_1 = -\frac{a^{12}}{L^6} \sum_{\mathbf{u},\mathbf{v},\mathbf{y},\mathbf{z}} \frac{1}{3} \left\langle \bar{\zeta}'(\mathbf{u})\gamma_5 \frac{1}{2}\tau^a \zeta'(\mathbf{v}) \bar{\zeta}(\mathbf{y})\gamma_5 \frac{1}{2}\tau^a \zeta(\mathbf{z}) \right\rangle, \tag{6.2}$$

which is renormalised by Z_ζ only,

$$(f_1)_{\mathrm{R}} = Z_\zeta^4 f_1. \tag{6.3}$$

This correlation function is proportional to the probability amplitude that a quark antiquark pair created at $x_0 = 0$ propagates to $x_0 = T$, a situation which may

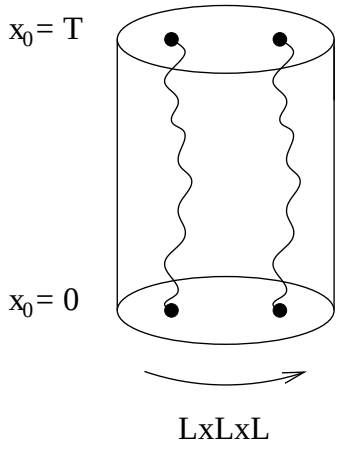

Figure 6.1: *The correlation function* f_1

be depicted by figure 6.1. Like f_A and f_P, f_1 may be expanded in powers of the bare coupling,

$$f_1 = f_1^{(0)} + g_0^2 f_1^{(1)} + \mathrm{O}(g_0^4). \tag{6.4}$$

Now, Z_P^2 can be computed as

$$Z_\mathrm{P}^2 = \frac{\left[f_\mathrm{P}^{(0)}(T/2)\right]^2}{f_1^{(0)}} \frac{f_1}{\left[f_\mathrm{P}(T/2)\right]^2}, \tag{6.5}$$

where the normalisation is chosen such that Z_P is 1 at tree level.

The renormalisation constant Z_P may be expanded in powers of the bare coupling,

$$Z_\mathrm{P}(g_0, L/a) = 1 + \sum_{k=1}^{\infty} Z_\mathrm{P}^{(k)}(L/a) g_0^{2k}. \tag{6.6}$$

The 1–loop coefficient $Z_\mathrm{P}^{(1)}$ contains a logarithmic divergence. It may hence be decomposed into a logarithmic term, a constant term, and terms that vanish in the continuum limit,

$$Z_\mathrm{P}^{(1)} = C_\mathrm{F} z_\mathrm{p}(\theta, \rho) - d_0 \ln(L/a) + \mathrm{O}(a/L). \tag{6.7}$$

Here, z_p denotes the term independent of L/a. It only depends on the phase θ and on the ratio of the lattice extensions in time and space directions, $\rho = T/L$.

6.1.2 The step scaling function of the running mass

In analogy to the coupling, the running of the mass may be described by a step scaling function, giving the change of the running mass when changing the scale

L by a certain scale factor. In the following, this scale factor is chosen to be 2, which is a convention widely used in numerical computations. Since the running of the renormalised mass is completely described by the running of Z_{P}, a suitable definition of the step scaling function at vanishing renormalised quark mass is [73]

$$\Sigma_{\mathrm{P}}(g_{\mathrm{R}}^2, a/L) = \left.\frac{Z_{\mathrm{P}}(g_0, 2L/a)}{Z_{\mathrm{P}}(g_0, L/a)}\right|_{g_0=g_0(g_{\mathrm{R}},L/a)}, \tag{6.8}$$

with the continuum limit

$$\lim_{a/L\to 0} \Sigma_{\mathrm{P}}(g_{\mathrm{R}}^2, a/L) = \sigma_{\mathrm{P}}(g_{\mathrm{R}}^2). \tag{6.9}$$

As the renormalised coupling, one here has to take the Schrödinger functional coupling at length scale L, i.e. $g_{\mathrm{R}} = \bar{g}(L)$. Like the step scaling function σ is used as a discretised version of the β–function, the step scaling function σ_{P} serves as a discretised τ–function.

The step scaling function may be expanded in perturbation theory,

$$\Sigma_{\mathrm{P}}(g_{\mathrm{R}}^2, a/L) = 1 + k(L/a)g_{\mathrm{R}}^2 + \mathrm{O}(g_{\mathrm{R}}^4). \tag{6.10}$$

Since the tree level value of Z_{P} is 1 at all scales, the 1–loop coefficient $k(L/a)$ is simply given by

$$k(L/a) = Z_{\mathrm{P}}^{(1)}(2L/a) - Z_{\mathrm{P}}^{(1)}(L/a), \tag{6.11}$$

where $Z_{\mathrm{P}}^{(1)}(L/a)$ and $Z_{\mathrm{P}}^{(1)}(2L/a)$ have to be taken at the same bare quark mass. In the case of a vanishing physical quark mass, this is the critical mass at length scale L. For the continuum limit, one gets from (6.7)

$$k(\infty) = -d_0 \ln(2). \tag{6.12}$$

Like in the case of the renormalised coupling, one has lattice artefacts making the step scaling function deviate from its continuum limit. These lattice artefacts can be estimated at 1–loop order by

$$\delta_k(L/a) = \frac{k(L/a)}{k(\infty)} - 1. \tag{6.13}$$

In [35], these lattice artefacts have been computed for several choices of θ and ρ in the case of a vanishing background field. To do this calculation with a non vanishing background field is one of the main aims of this thesis. The size of the lattice artefacts is also important for the question whether it makes sense to compute the renormalised quark mass non–perturbatively with a non–vanishing background field. So far, this calculation has only be done at zero background field [74].

6.1.3 The 2–loop anomalous dimension

It was already shown in subsection 2.4.3 that one may obtain the 2–loop anomalous dimension d_1 in the Schrödinger functional scheme from a 1–loop computation by using (2.42) to convert the known anomalous dimension in the $\overline{\mathrm{MS}}$–scheme to the Schrödinger functional scheme. In order to do this, one has to convert the coupling and the masses. For the coupling, one has

$$\bar{g}^2_{\mathrm{SF}}(L) = \bar{g}^2_{\overline{\mathrm{MS}}}(q)\chi_{\mathrm{g}}(\bar{g}_{\overline{\mathrm{MS}}}(q), qL), \tag{6.14}$$

where the 1–loop coefficient of χ_{g} is given by

$$\chi^{(1)}_{\mathrm{g}} = 2b_0 \ln(qL) - \frac{1}{4\pi}(c_{1,0} + c_{1,1}N_{\mathrm{f}}). \tag{6.15}$$

The coefficient $c_{1,0}$ has been computed in [26] and $c_{1,1}$ in [32]. For $\theta = \pi/5$ and $\rho = 1$, one obtains

$$c_{1,0} = 1.25563(4), \qquad c_{1,1} = 0.039863(2). \tag{6.16}$$

In order to get the conversion of the renormalised mass from the $\overline{\mathrm{MS}}$–scheme to the Schrödinger functional scheme, one has to use the relation between the renormalised mass and the subtracted bare mass. In the $\overline{\mathrm{MS}}$–scheme, it has been computed in [70] and since then been verified numerous times. It turns out to be

$$\overline{m}_{\overline{\mathrm{MS}}}(q) = m_{\mathrm{q}}\left\{1 + g_0^2\Big[-d_0 \ln(aq) + 0.122282(1)C_{\mathrm{F}}\Big] + \mathrm{O}(g_0^4)\right\}. \tag{6.17}$$

By calculating the renormalised mass in the Schrödinger functional at a non–vanishing mass, one gets [62]

$$\overline{m}_{\mathrm{SF}}(L) = m_{\mathrm{q}}\left\{1 + g_0^2\Big[Z^{(1)}_{\mathrm{A}} - Z^{(1)}_{\mathrm{P}}(L/a) + 0.067886(1)C_{\mathrm{F}}\Big] + \mathrm{O}(g_0^4)\right\}. \tag{6.18}$$

Inserting the results for $Z^{(1)}_{\mathrm{A}}$ from (5.13) and $Z^{(1)}_{\mathrm{P}}$ from (6.7) then yields

$$\overline{m}_{\mathrm{SF}}(L) = m_{\mathrm{q}}\left\{1 + g_0^2\Big[d_0 \ln(L/a) - (z_{\mathrm{p}} + 0.019458(1))C_{\mathrm{F}}\Big] + \mathrm{O}(g_0^4)\right\}. \tag{6.19}$$

Using these results for the masses in the $\overline{\mathrm{MS}}$ scheme and in the Schrödinger functional scheme, one finds the relation between both schemes,

$$\overline{m}_{\mathrm{SF}}(L) = \overline{m}_{\overline{\mathrm{MS}}}(q)\left\{1 + g_0^2\Big[d_0 \ln(qL) - (z_{\mathrm{p}} + 0.141740(2))C_{\mathrm{F}}\Big] + \mathrm{O}(g_0^4)\right\}. \tag{6.20}$$

From this relation, one may easily read off the 1–loop coefficient $\chi^{(1)}_{\mathrm{m}}$,

$$\chi^{(1)}_{\mathrm{m}} = d_0 \ln(qL) - (z_{\mathrm{p}} + 0.141740(2))C_{\mathrm{F}}. \tag{6.21}$$

Now, one can compute the 2–loop anomalous dimension in the Schrödinger functional scheme. From (2.42), one has

$$d_1^{\mathrm{SF}} = d_1^{\overline{\mathrm{MS}}} - d_0\chi^{(1)}_{\mathrm{g}} + 2b_0\chi^{(1)}_{\mathrm{m}}, \tag{6.22}$$

with b_0, d_0, and $d_1^{\overline{\mathrm{MS}}}$ from (2.26), (2.34), and (2.35), and $\chi^{(1)}_{\mathrm{g}}$ and $\chi^{(1)}_{\mathrm{m}}$ from (6.15) and (6.21).

6.2 The renormalisation constant Z_{P} at 1–loop order

6.2.1 Preliminaries

The expansion of f_1 at 1–loop order has been outlined in [62] for the case of a vanishing background field. In the following, the calculation will be done for the non–zero background field used to define the coupling.

In order to make contact to the calculation of f_{A} and f_{P} and thus simplify the computation, it is useful to rewrite f_1 in a slightly different form. To this end, we define

$$K = \tilde{c}_{\mathrm{t}} \frac{a^3}{L^3} \sum_{\mathbf{x}} \Big\{ P_+ U(x,0)^{-1} H(x) \Big\} \Big|_{x_0 = T-a} . \tag{6.23}$$

Using this notation, f_1 may be written as

$$f_1 = \frac{1}{2} \left\langle \mathrm{Tr}\{K^\dagger K\} \right\rangle_{\mathrm{G}} . \tag{6.24}$$

The expansion of f_1 thus amounts to expanding K. This makes part of the calculation exceptionally easy, because all contributions in which the link variables only appear at tree level may be reduced to f_{A} and f_{P}, so these diagrams may be computed using the results of chapter 5. This is easily seen at tree level, where one has

$$K^{(0)} = \frac{a^3}{L^3} \sum_{\mathbf{x}} \Big\{ P_+ H^{(0)}(x) \Big\} \Big|_{x_0 = T-a} . \tag{6.25}$$

The clou to reducing f_1 to f_{A} and f_{P} lies in the fact that $H^{(0)}(x)$ does not depend on the spatial position $\mathbf{x}$. This means that the sum over $\mathbf{x}$ is trivial, giving

$$K^{(0)} = P_+ \, H^{(0)}(x) \big|_{x_0 = T-a} , \tag{6.26}$$

or, inserted in (6.24)

$$f_1^{(0)} = \frac{1}{2} \, \mathrm{Tr} \Big\{ H^{(0)\dagger}(x) P_+ H^{(0)}(x) \Big\} \Big|_{x_0 = T-a} . \tag{6.27}$$

Comparing this expression to (5.30) and (5.31) then yields

$$f_1^{(0)} = \frac{1}{2} \left[f_{\mathrm{P}}^{(0)}(T-a) - f_{\mathrm{A}}^{(0)}(T-a) \right] , \tag{6.28}$$

which may be decomposed into colour components,

$$f_{1\alpha}^{(0)} = \frac{1}{2} \left[f_{\mathrm{P}\alpha}^{(0)}(T-a) - f_{\mathrm{A}\alpha}^{(0)}(T-a) \right] . \tag{6.29}$$

The same will apply for several diagrams at 1–loop order. At tree level, f_1 may be visualised by the diagram in figure 6.2.

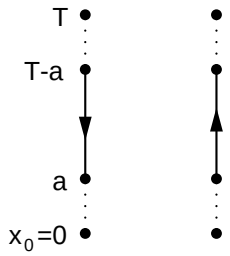

Figure 6.2: *Diagram for f_1 at tree level*

6.2.2 The correlation function f_1 at 1–loop order

For simplicity, we return to lattice units and take $a = 1$ for the rest of this chapter.

At 1–loop order, f_1 can, just like f_A and f_P, be written as a sum over diagrams, improvement terms, and the mass derivative,

$$\begin{aligned} f_1^{(1)} &= \sum_n f_{1,n}^{(1)} + c_\mathrm{sw}^{(1)} f_{1,\mathrm{V}}^{(1)} \\ &\quad + \tilde{c}_\mathrm{t}^{(1)} \left(f_{1,\mathrm{Fb}}^{(1)} + 4 f_1^{(0)} \right) + c_\mathrm{t}^{(1)} f_{1,\mathrm{Gb}}^{(1)} \\ &\quad + m_\mathrm{c}^{(1)} \frac{\partial}{\partial m_0} f_1^{(0)}. \end{aligned} \tag{6.30}$$

The term $4 f_1^{(0)}$ is there because f_1 gets an overall factor $\tilde{c}_\mathrm{t}^4$ from K and H. However, this term may be neglected, since it is cancelled by the overall factor $\tilde{c}_\mathrm{t}^2$ of f_P.

For the 1–loop diagrams, one has to expand the link variables and H in (6.23) up to order g_0^2. It was already stated that the diagrams containing the tree level values of the link variables are obviously related to the corresponding diagrams for f_A and f_P. These diagrams either contain a combination of $H^{(0)}$ and $H^{(2)}$ or of $H^{(1)}$ and $H^{(1)}$. The expression becomes particularly simple for the first case since $H^{(0)}$ is spatially constant and does not depend on the gluon fields. The gluonic expectation value is thus only to be taken over $H^{(2)}$. This expectation value $\langle H^{(2)}(x) \rangle_0$ is again spatially constant, which means that the same argument may be used as in the tree level case. One thus gets for $n = 1a, 1b, 3a, 3b, 5a, 5b, 6a, 6b$

$$f_{1,n}^{(1)} = \frac{1}{2} \Big[f_{\mathrm{P},n}^{(1)}(T-1) - f_{\mathrm{A},n}^{(1)}(T-1) \Big]. \tag{6.31}$$

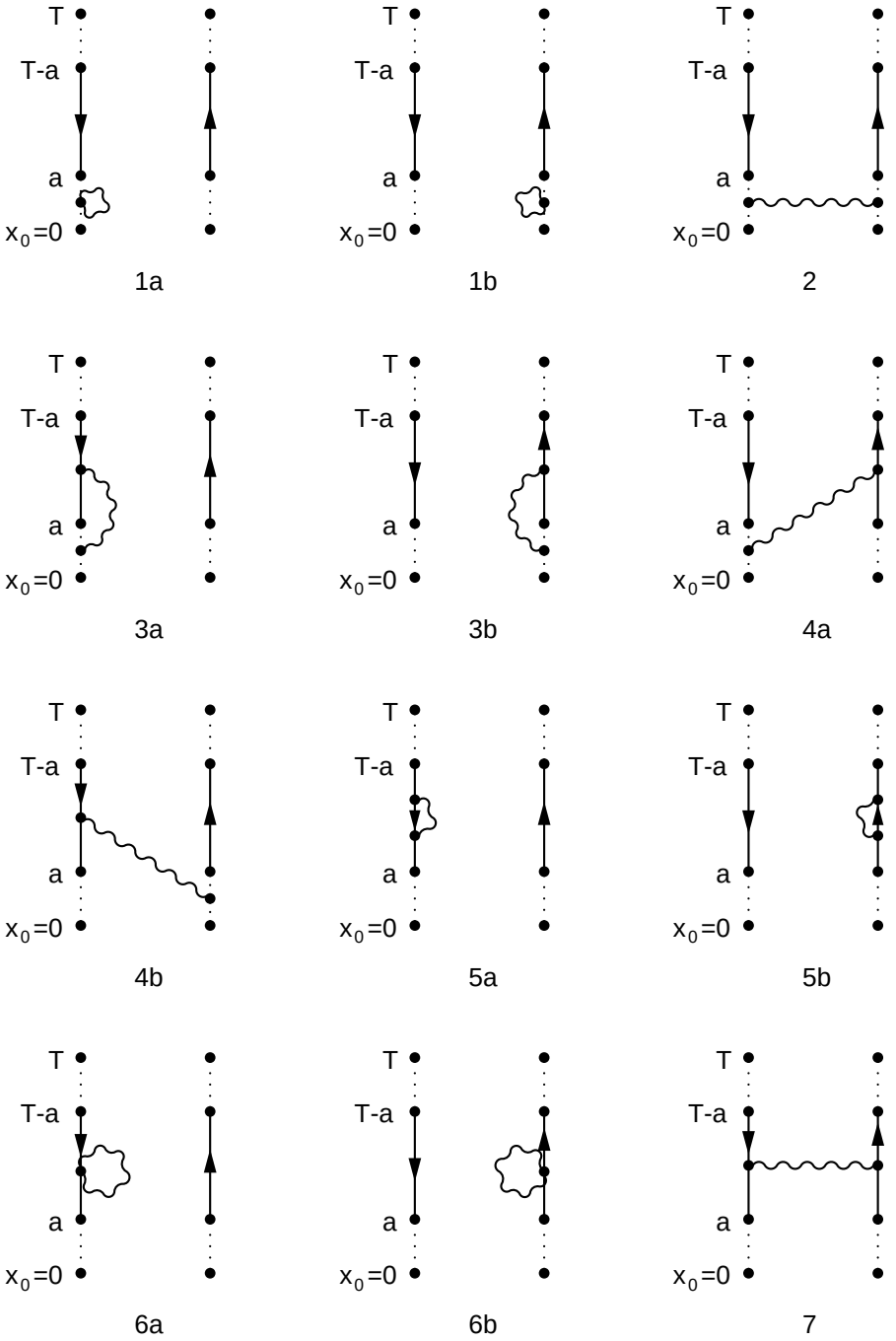

Figure 6.3: *Diagrams contributing to f_1 at 1–loop order of perturbation theory.*

For the combination of $H^{(1)}$ with $H^{(1)}$, the situation is slightly more complicated. Here, the expectation value $\langle H^{(1)}(x)^\dagger H^{(1)}(x)\rangle_0$ does depend on $\mathbf{x}$ and the sum has a non trivial effect. When transforming the expectation value to the momentum representation, the sum together with the exponential factor acts as a delta function, leaving only the contribution with zero loop momentum. One thus gets for $n = 2, 4a, 4b, 7$

$$f^{(1)}_{1,n} = \frac{1}{2}\Big[f^{(1)}_{\mathrm{P},n}(T-1) - f^{(1)}_{\mathrm{A},n}(T-1)\Big]_{\mathbf{q}=\mathbf{0}}, \tag{6.32}$$

where $[\ldots]_{\mathbf{q}=\mathbf{0}}$ means that, instead of the sum over $\mathbf{q}$ in (5.102), (5.105), (5.106), and (5.111), one has to take the term with $\mathbf{q} = \mathbf{0}$ only. The 1–loop terms covered so far are represented by the diagrams in figure 6.3.

For the tadpole diagrams, one finds that $\langle H^{(1)}(x)[S^{(1)}_{\mathrm{tot}}]_{\mathrm{F}}\rangle_0$ is independent of $\mathbf{x}$. One thus gets

$$f^{(1)}_{1,n} = \frac{1}{2}\Big[f^{(1)}_{\mathrm{P},n}(T-1) - f^{(1)}_{\mathrm{A},n}(T-1)\Big] \tag{6.33}$$

for $n = 8a, 8b, 9a, 9b$.

Now one is left with the diagrams containing the link variables at the upper boundary of the box, i.e. the link variables in (6.23), at order g_0 and g_0^2. The g_0^2 terms can be treated in total analogy to diagrams 1a and 1b, resulting in diagrams 10a and 10b of figure 6.4. They are given by

$$f^{(1)}_{1,10a} = -\frac{1}{2}\frac{1}{L^3}\sum_\alpha f^{(0)}_{1\alpha}\sum_{\mathbf{q}}\sum_a D^a_{00}(\mathbf{q}; T-1, T-1)\mathcal{C}^a_\alpha, \tag{6.34}$$

and

$$f^{(1)}_{1,10b} = f^{(1)}_{1,10a}. \tag{6.35}$$

Contracting the terms of both link variables proportional to g_0 yields diagram 11,

$$f^{(1)}_{1,11} = \frac{1}{L^3}\sum_\alpha f^{(0)}_{1\alpha}\sum_a D^a_{00}(\mathbf{0}; T-1, T-1)\mathcal{C}^a_\alpha. \tag{6.36}$$

Next, one has to contract the link variables at the upper boundary with $H^{(1)}$ or, to be more precise, with the first order terms of the propagators and link variables contained in $H^{(1)}$. Combining them with the quark lines on the same side gives diagrams 12a and 12b,

$$\begin{aligned} f^{(1)}_{1,12a} \;=\; & \frac{1}{2}\frac{1}{L^3}\sum_{\mathbf{q}}\sum_\mu\sum_{s_0,t_0,u_0}\sum_a D^a_{\mu 0}(\mathbf{q}; u_0, T-1)\mathrm{Tr}\Big\{P_+\gamma_5 S(\mathbf{0}; 1, T-1)\gamma_5 P_+ \\ & \cdot I^{\bar a} S(\mathbf{q}; T-1, s_0) V^a_\mu(\mathbf{q}, \mathbf{0}, -\mathbf{q}; s_0, t_0, u_0) S(\mathbf{0}; t_0, 1)\Big\}, \end{aligned} \tag{6.37}$$

$$\begin{aligned} f^{(1)}_{1,12b} \;=\; & -\frac{1}{2}\frac{1}{L^3}\sum_{\mathbf{q}}\sum_\mu\sum_{s_0,t_0,u_0}\sum_a D^a_{0\mu}(\mathbf{q}; T-1, u_0)\mathrm{Tr}\Big\{P_+\gamma_5 S(\mathbf{0}; 1, s_0) \\ & \cdot V^{\bar a}_\mu(\mathbf{0}, -\mathbf{q}, \mathbf{q}; s_0, t_0, u_0) S(\mathbf{q}; t_0, T-1) I^a \gamma_5 P_+ S(\mathbf{0}; T-1, 1)\Big\}, \end{aligned} \tag{6.38}$$

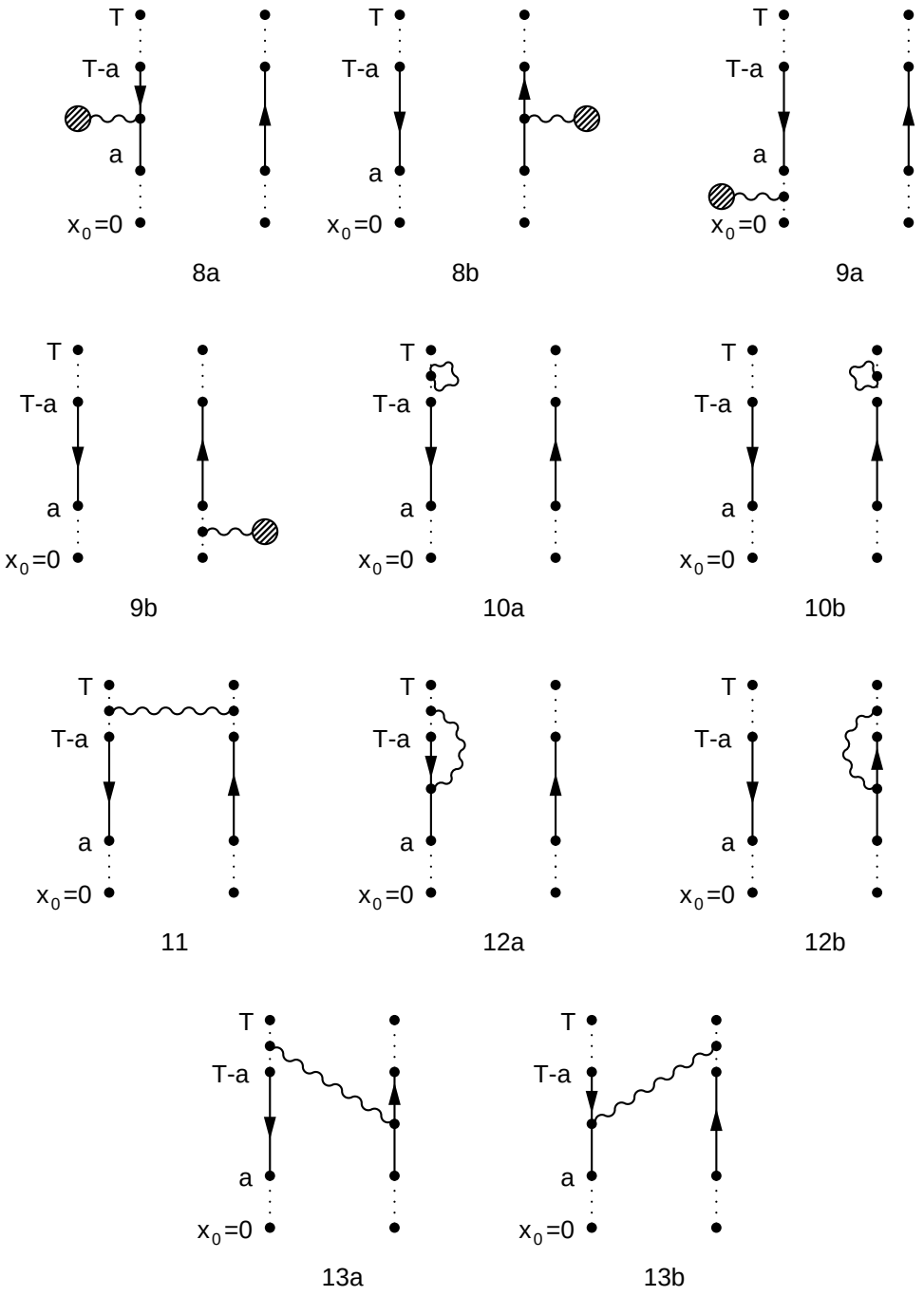

Figure 6.4: *Further diagrams contributing to f_1 at 1–loop order of perturbation theory.*

while the combination with the quarks on the opposite side result in diagrams 13a and 13b,

$$f^{(1)}_{1,13a} = \frac{1}{2}\frac{1}{L^3}\sum_{\mu}\sum_{s_0,t_0,u_0}\sum_{a} D^a_{0\mu}(\mathbf{0};T-1,u_0)\mathrm{Tr}\Big\{P_+\gamma_5 S(\mathbf{0};1,s_0) \cdot V^{\bar{a}}_{\mu}(\mathbf{0},\mathbf{0},\mathbf{0};s_0,t_0,u_0)S(\mathbf{0};t_0,T-1)I^a\gamma_5 P_+ S(\mathbf{0};T-1,1)\Big\}, \quad (6.39)$$

$$f^{(1)}_{1,13b} = -\frac{1}{2}\frac{1}{L^3}\sum_{\mu}\sum_{s_0,t_0,u_0}\sum_{a} D^a_{0\mu}(\mathbf{0};T-1,u_0)\mathrm{Tr}\Big\{P_+\gamma_5 S(\mathbf{0};1,T-1)\gamma_5 P_+ \cdot I^a S(\mathbf{0};T-1,s_0)V^{\bar{a}}_{\mu}(\mathbf{0},\mathbf{0},\mathbf{0};s_0,t_0,u_0)S(\mathbf{0};t_0,1)\Big\}. \quad (6.40)$$

The remaining combinations are those of the link variables at the upper boundary with the link variables at the lower boundary. They are depicted by the diagrams in figure 6.5 and can be computed via

$$f^{(1)}_{1,14a} = \frac{1}{2}\frac{1}{L^3}\sum_{\mathbf{q}}\sum_{a} D^a_{00}(\mathbf{q};0,T-1)\mathrm{Tr}\Big\{P_+\gamma_5 S(\mathbf{0};1,T-1) \cdot\gamma_5 P_+ I^{\bar{a}} S(\mathbf{q};T-1,1)I^a\Big\}, \quad (6.41)$$

$$f^{(1)}_{1,14b} = \frac{1}{2}\frac{1}{L^3}\sum_{\mathbf{q}}\sum_{a} D^a_{00}(\mathbf{q};T-1,0)\mathrm{Tr}\Big\{P_+\gamma_5 S(\mathbf{q};1,T-1) \cdot\gamma_5 P_+ I^a S(\mathbf{0};T-1,1)I^{\bar{a}}\Big\}, \quad (6.42)$$

$$f^{(1)}_{1,15a} = -\frac{1}{2}\frac{1}{L^3}\sum_{a} D^a_{00}(\mathbf{0};T-1,0)\mathrm{Tr}\Big\{P_+\gamma_5 S(\mathbf{0};1,T-1) \cdot\gamma_5 P_+ I^a S(\mathbf{0};T-1,1)I^{\bar{a}}\Big\}, \quad (6.43)$$

and

$$f^{(1)}_{1,15b} = f^{(1)}_{1,15a}. \quad (6.44)$$

The only remaining diagrams are now the contractions of the first order terms of the link variables at the upper boundary with the first order term of the total action. In complete analogy to diagrams 9a and 9b one gets

$$f^{(1)}_{1,16a} = -\frac{1}{2}\sum_{\mu}\sum_{u_0}\sum_{a} D^a_{00}(\mathbf{0};T-1,u_0)\mathrm{Tr}\Big\{P_+\gamma_5 S(\mathbf{0};1,T-1) \cdot\gamma_5 P_+ I^a S(\mathbf{0};T-1,1)\Big\}T^{\bar{a}}_{\mu}(u_0), \quad (6.45)$$

and

$$f^{(1)}_{1,16b} = -f^{(1)}_{1,16a}. \quad (6.46)$$

So these diagrams cancel in the sum and leave diagrams 8a and 8b as the only N_f dependent contributions to f_1.

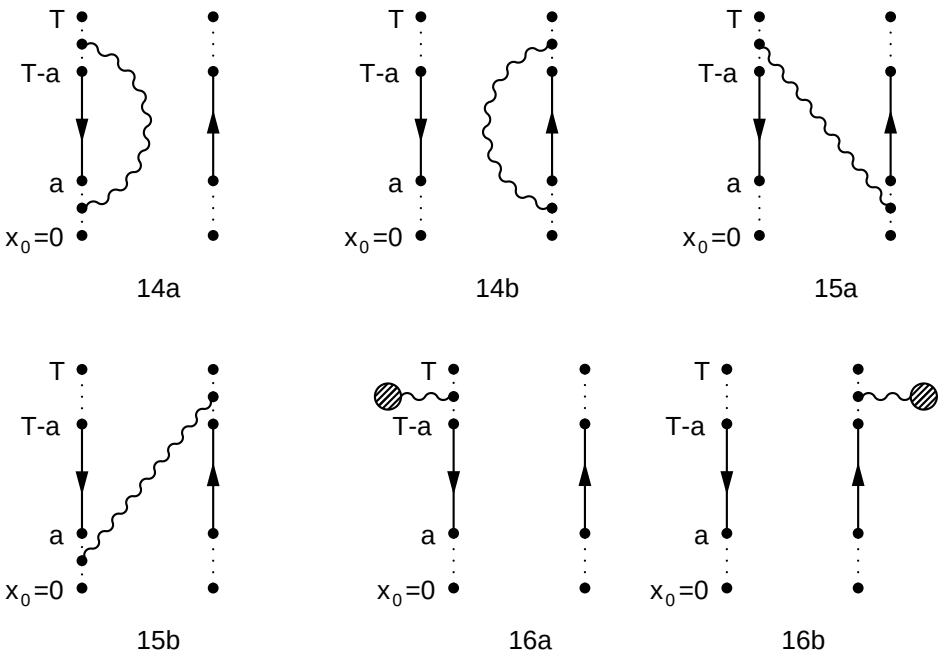

Figure 6.5: *More diagrams contributing to f_1 at 1–loop order of perturbation theory.*

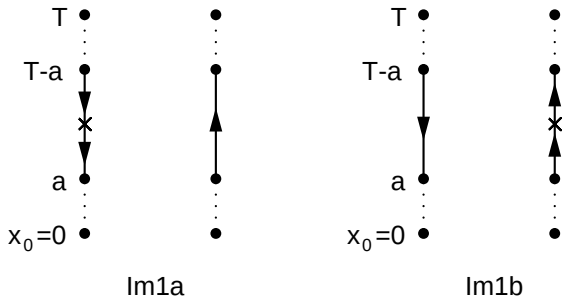

Figure 6.6: *Diagrams for* $f^{(1)}_{1,\mathrm{V}}$ *and* $f^{(1)}_{1,\mathrm{Fb}}$

6.2.3 The improvement terms

In the computation of f_1, all improvement terms can be reduced to the corresponding terms of f_A and f_P. For the terms proportional to $c^{(1)}_\mathrm{sw}$ and $\tilde{c}^{(1)}_\mathrm{t}$, which are additional contributions to diagrams 6a and 6b, one may use the same argument applied there, namely the independence of $H^{(0)}(x)$ and $\langle H^{(2)}(x)\rangle_0$ of the spatial position $\mathbf{x}$. One thus gets

$$f_{1,\mathrm{V}} = \frac{1}{2}\left[f_{\mathrm{P},\mathrm{V}}(T-1) - f_{\mathrm{A},\mathrm{V}}(T-1)\right] \tag{6.47}$$

for the volume term and

$$f_{1,\mathrm{Fb}} = \frac{1}{2}\left[f_{\mathrm{P},\mathrm{Fb}}(T-1) - f_{\mathrm{A},\mathrm{Fb}}(T-1)\right] \tag{6.48}$$

for the quark boundary term. These terms can be depicted by the diagrams in figure 6.6.

For the boundary counter-term proportional to $c^{(1)}_\mathrm{t}$, one gets several diagrams in total analogy to the calculation for f_A and f_P. For the diagrams shown in figure 6.7, the same argument applies as above, yielding

$$f_{1,\mathrm{Gb}} = \frac{1}{2}\left[f_{\mathrm{P},\mathrm{Gb}}(T-1) - f_{\mathrm{A},\mathrm{Gb}}(T-1)\right]. \tag{6.49}$$

Apart from these diagrams, one gets the contributions shown in figure 6.8. However, like for f_A and f_P, these contributions cancel pairwise in the sum and may thus be ignored. So the improvement terms for f_1 can easily be computed using (5.123), (5.127), and (5.133).

Also for f_1, we will need the derivative of the tree level coefficient with respect to the bare mass. Differentiating (6.28) gives

$$\frac{\partial}{\partial m_0} f_1^{(0)} = \frac{1}{2}\frac{\partial}{\partial m_0}\left[f_\mathrm{P}^{(0)}(T-1) - f_\mathrm{A}^{(0)}(T-1)\right], \tag{6.50}$$

where $f_\mathrm{P}^{(0)}$ and $f_\mathrm{A}^{(0)}$ can be taken from (5.92).

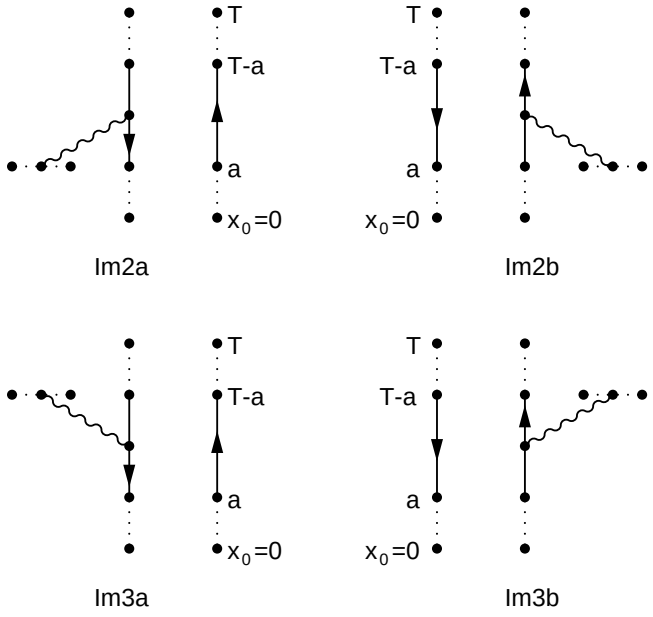

Figure 6.7: Diagrams contributing to $f^{(1)}_{1,\rm Gb}$

6.2.4 Computation of $Z_{\rm P}$ at 1–loop order

The renormalisation constant $Z_{\rm P}$ at 1–loop order is obtained by expanding f_1 and $f_{\rm P}$ in (6.5). One thus gets

$$Z^{(1)}_{\rm P} = \frac{f^{(1)}_1}{2f^{(0)}_1} - \frac{f^{(1)}_{\rm P}(T/2)}{f^{(0)}_{\rm P}(T/2)}. \tag{6.51}$$

In order to get $Z_{\rm P}$ at vanishing renormalised quark mass, f_1 and $f_{\rm P}$, which depend on the bare quark mass, have to be computed at the critical quark mass $m_{\rm c}$. In perturbation theory, one has to use the expansion

$$m_{\rm c} = m^{(0)}_{\rm c} + m^{(1)}_{\rm c} g_0^2 + {\rm O}(g_0^4), \tag{6.52}$$

where the computation of $m^{(0)}_{\rm c}$ and $m^{(1)}_{\rm c}$ has been outlined in chapter 5. Taylor expansion then yields

$$f_1(m_{\rm c}) = f_1(m^{(0)}_{\rm c}) + g_0^2 m^{(1)}_{\rm c} \frac{\partial}{\partial m_0} f_1(m^{(0)}_{\rm c}) + {\rm O}(g_0^4), \tag{6.53}$$

which leads to the 1–loop coefficient

$$f^{(1)}_1(m_{\rm c}) = f^{(1)}_1(m^{(0)}_{\rm c}) + m^{(1)}_{\rm c} \frac{\partial}{\partial m_0} f^{(0)}_1(m^{(0)}_{\rm c}), \tag{6.54}$$

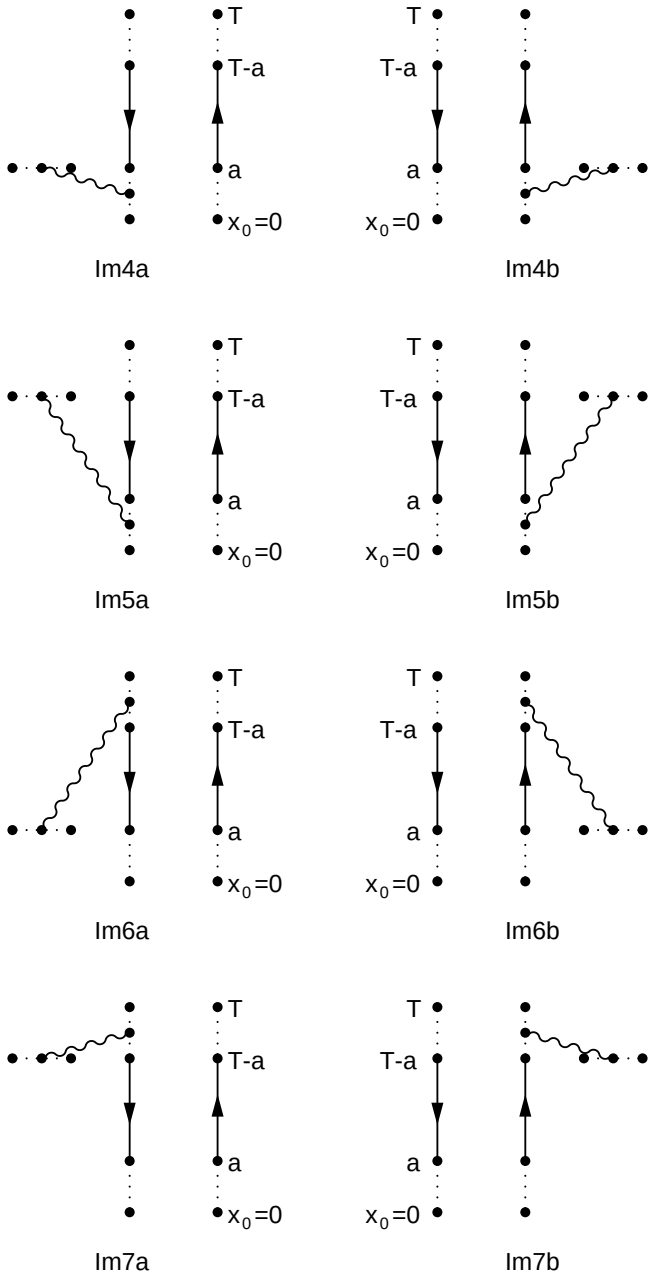

Figure 6.8: More diagrams for $f^{(1)}_{1,\mathrm{Gb}}$. These contributions cancel in the sum.

and analogously for f_{P}.

Furthermore, $f_1^{(1)}$ and $f_{\mathrm{P}}^{(1)}$ are meant to include all improvement terms. Then the results obtained in the calculation should converge to their continuum limits at a rate proportional to a^2.

By calculating all the diagrams, one is now able to compute the renormalisation constant Z_{P} at different lattice sizes. In the case of $\theta = \pi/5$ and $\rho = 1$, the coefficient z_{p} defined in (6.7) could be obtained by extrapolation to the continuum limit, using the extrapolation procedure described in appendix C. From this calculation, one automatically gets the 2–loop anomalous dimension in the Schrödinger functional scheme by (6.22). This means that the 2–loop anomalous dimension could be obtained by a 1–loop calculation, since the 2–loop anomalous dimension in the $\overline{\mathrm{MS}}$–scheme is already known.

Setting $m_1(L) = 0$ and computing $Z_{\mathrm{P}}(L)$ and $Z_{\mathrm{P}}(2L)$ at this mass gives the 1–loop coefficient $k(L)$ of the step scaling function. One is thus able to compute the size of the discretisation error (6.13). This computation was done in the case of $\theta = \pi/5$ and $\rho = 1$. For some smaller lattices, we did the calculation also at $\theta = 0$ and $\theta = 0.5$ and at $\rho = 2$, in order to get a better comparison with the results obtained in [35], which were computed at these values of θ and ρ.

Since $f_1^{(1)}$ has not been computed with a non–vanishing background field before, there are no results to compare the results obtained in this calculation to. For this reason, careful checks of the results are necessary. For f_1, all checks described for f_{A} and f_{P} are applicable. Moreover, it was checked that the results both for the sum of the diagrams and for the improvement terms are invariant when interchanging the boundary conditions in time direction, as they should be.

All results can be found in chapter 7.

Chapter 7

Results

The following results have been computed at vanishing renormalised mass, which means setting $m_1 = 0$ or $m_0 = m_c$. The results depend, of course, on the phase angle θ and the ratio $\rho = T/L$. Unless stated otherwise, all results presented here are for $\theta = \pi/5$ and $\rho = 1$.

7.1 The current quark mass

7.1.1 The critical quark mass

At tree level, the critical quark mass is independent of the flavour number, while at 1–loop level, there is a linear dependence on N_f due to the closed quark loops in diagrams 8a and 8b in figure 5.4. The 1–loop coefficient may hence be written as

$$m_c^{(1)} = m_{c0}^{(1)} + m_{c1}^{(1)} N_f. \tag{7.1}$$

The results for the tree level coefficient $m_c^{(0)}$ and the 1–loop coefficients $m_{c0}^{(1)}$ and $m_{c1}^{(1)}$ can be found in table 7.1. The critical mass at 1–loop level is also shown in figure 7.1 for different flavour numbers. The unusual case $N_f = -2$ refers to so called bermions, which were invented because Monte Carlo simulations are considerably cheaper in this model than in full QCD. The original idea was to extrapolate from negative values to $N_f = 2$ [29, 28], which is, however, problematical. Nowadays, bermions are more used as a toy model [30, 31].

A clear dependence of the 1–loop critical quark mass on the flavour number can only be seen on very small lattices. For larger L/a, the 1–loop coefficient can be seen to be practically constant at its continuum limit value, which is [49, 50]

$$am_c^{(1)} = -0.2700753495(2). \tag{7.2}$$

L/a	$am_{\mathrm{c}}^{(0)}$	$am_{\mathrm{c0}}^{(1)}$	$am_{\mathrm{c1}}^{(1)}$
4	-0.0015131	-0.2653473	0.0024231
5	-0.0016969	-0.2675073	0.0006225
6	-0.0006384	-0.2699739	0.0002269
7	-0.0005761	-0.2700126	0.0000978
8	-0.0003209	-0.2700683	0.0000522
9	-0.0002753	-0.2700656	0.0000300
10	-0.0001835	-0.2700733	0.0000192
11	-0.0001561	-0.2700708	0.0000129
12	-0.0001145	-0.2700730	0.0000091
13	-0.0000979	-0.2700720	0.0000066
14	-0.0000761	-0.2700731	0.0000050
15	-0.0000657	-0.2700729	0.0000039
16	-0.0000531	-0.2700736	0.0000030
17	-0.0000463	-0.2700736	0.0000024
18	-0.0000385	-0.2700741	0.0000020
19	-0.0000339	-0.2700742	0.0000016
20	-0.0000288	-0.2700745	0.0000013
21	-0.0000256	-0.2700746	0.0000011
22	-0.0000221	-0.2700749	0.0000009
23	-0.0000198	-0.2700750	0.0000008
24	-0.0000173	-0.2700751	0.0000007
25	-0.0000156	-0.2700752	0.0000006
26	-0.0000138	-0.2700753	0.0000005
27	-0.0000125	-0.2700754	0.0000005
28	-0.0000112	-0.2700755	0.0000004
29	-0.0000102	-0.2700755	0.0000004
30	-0.0000092	-0.2700756	0.0000003
31	-0.0000084	-0.2700756	0.0000003
32	-0.0000076	-0.2700756	0.0000003

Table 7.1: *Perturbative results for the critical quark mass m_{c} up to 1–loop order*

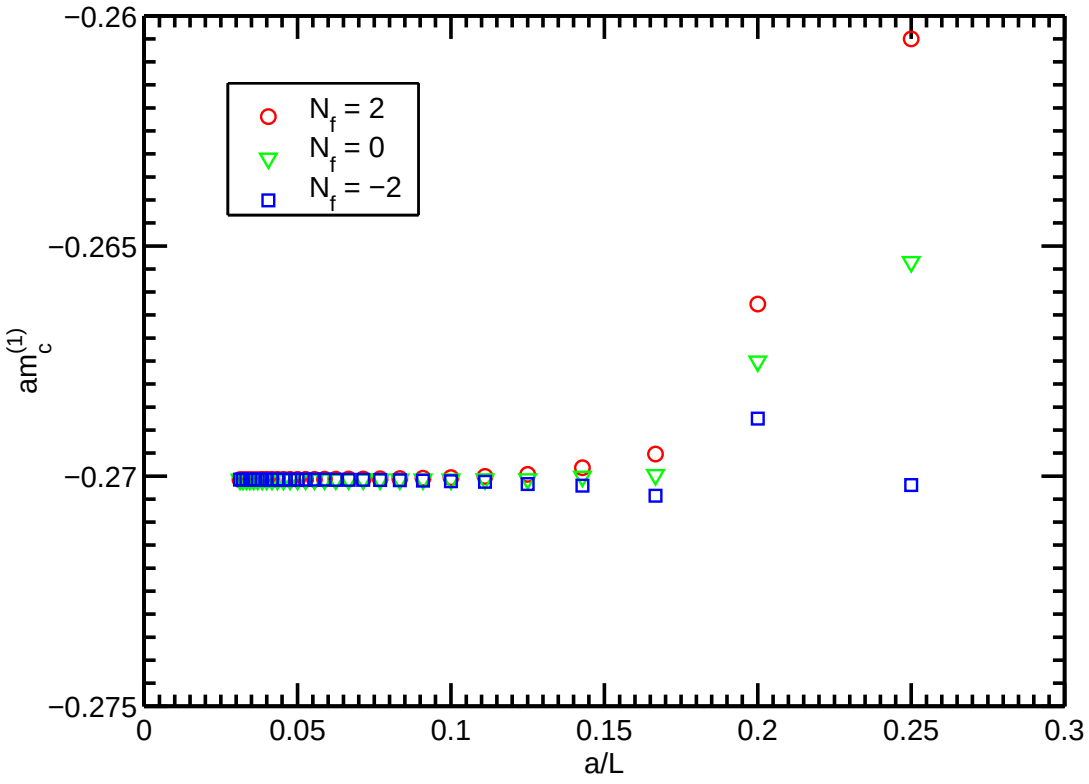

Figure 7.1: *The critical quark mass m_c at 1–loop order*

7.1.2 Lattice artefacts of the current mass up to 1–loop order

Using the expansion of f_A and f_P, it is possible to compute the lattice artefacts d and e defined in (5.23) and (5.24). Here again, the 1–loop coefficients get a linear N_f dependence from diagrams 8a and 8b in figure 5.4 and may hence be written as

$$d^{(1)} = d_0^{(1)} + d_1^{(1)} N_\mathrm{f}, \tag{7.3}$$

$$e^{(1)} = e_0^{(1)} + e_1^{(1)} N_\mathrm{f}. \tag{7.4}$$

The results at tree and 1–loop level can be found in table 7.2, the 1–loop coefficients are also shown in figure 7.2 for different values of N_f. They are obviously small and converge quickly to zero. The expected behaviour in the improved theory is a convergence at rate proportional to $(a/L)^2$. Figure 7.2, where the 1–loop coefficients are plotted with respect to $(a/L)^2$, does however show that, for $N_\mathrm{f} \neq 0$, they are dominated by terms of higher order. In [27], the perturbative results up to 1–loop order are compared to results obtained by Monte Carlo simulations. While the values for e are approximated by perturbation theory remarkably well, the perturbative values for d are significantly larger than the simulation results, especially at large values of the renormalised coupling ($\bar{g}^2(L) = 3.334$).

An important question in this context is the dependence of the results on the improvement term proportional to $c_\mathrm{t}^{(1)}$, which was missing in previous publications. As already stated in chapter 5, this term is absent in zero background field calculations and irrelevant for the extrapolation both of $c_\mathrm{sw}^{(1)}$ and $m_\mathrm{c}^{(1)}$. It has, however, to be taken into account in the results for $d(L/a)$ and $e(L/a)$ published in [27]. There, the perturbative results including tree and 1–loop level are plotted for different values of the renormalised coupling $\bar{g}^2$. The results for the same values of $\bar{g}^2$ are shown in figure 7.3, where the symbols denote the results with full improvement, while the lines show the results without the $c_\mathrm{t}^{(1)}$–term, i.e. the values presented in [27]. The picture shows that the additional term only gives considerable changes in the case $\bar{g}^2 = 3.334$ for $N_\mathrm{f} = 0$ and $N_\mathrm{f} = -2$. Since, for this coupling, only the results for $N_\mathrm{f} = 2$ are plotted in [27], the corrections to the plots presented there are almost invisible.

7.2 Lattice artefacts of the step scaling function of the coupling

One of the reasons to compute the critical quark mass up to 1–loop order was to get the correct discretisation errors for the coupling up to 2–loop order. To this end, one has to use (4.45)–(4.49) with the current mass properly set to zero, $m_1(L) = 0$. Since the critical mass converges quickly to its continuum limit,

L/a	$Ld^{(0)}$	$Ld_0^{(1)}$	$Ld_1^{(1)}$	$Le^{(0)}$	$Le_0^{(1)}$	$Le_1^{(1)}$
4	0.1123	0.00752	0.01929	-0.004981	0.01931	0.00990
5	0.0522	0.00535	0.00653	-0.007783	0.01252	0.00309
6	0.0258	0.00378	0.00348	-0.003204	0.00032	0.00133
7	0.0140	0.00320	0.00172	-0.003550	0.00011	0.00066
8	0.0078	0.00277	0.00112	-0.002165	-0.00015	0.00040
9	0.0044	0.00224	0.00071	-0.002149	-0.00012	0.00025
10	0.0025	0.00180	0.00053	-0.001558	-0.00013	0.00018
11	0.0014	0.00149	0.00038	-0.001483	-0.00009	0.00013
12	0.0007	0.00122	0.00030	-0.001172	-0.00008	0.00010
13	0.0002	0.00104	0.00023	-0.001098	-0.00006	0.00008
14	-0.0001	0.00087	0.00019	-0.000913	-0.00005	0.00006
15	-0.0002	0.00076	0.00016	-0.000850	-0.00004	0.00005
16	-0.0003	0.00065	0.00014	-0.000730	-0.00003	0.00004
17	-0.0004	0.00057	0.00011			
18	-0.0005	0.00050	0.00010			
19	-0.0005	0.00045	0.00008			
20	-0.0005	0.00040	0.00007			
21	-0.0005	0.00036	0.00007			
22	-0.0005	0.00032	0.00006			
23	-0.0005	0.00029	0.00005			
24	-0.0005	0.00026	0.00005			
25	-0.0005	0.00024	0.00004			
26	-0.0004	0.00022	0.00004			
27	-0.0004	0.00020	0.00003			
28	-0.0004	0.00019	0.00003			
29	-0.0004	0.00017	0.00003			
30	-0.0004	0.00016	0.00003			
31	-0.0004	0.00015	0.00002			
32	-0.0003	0.00014	0.00002			

Table 7.2: *The lattice artefacts* $d = m_2(L) - m_1(L)$ *and* $e = m_1(2L) - m_1(L)$ *up to 1–loop order*

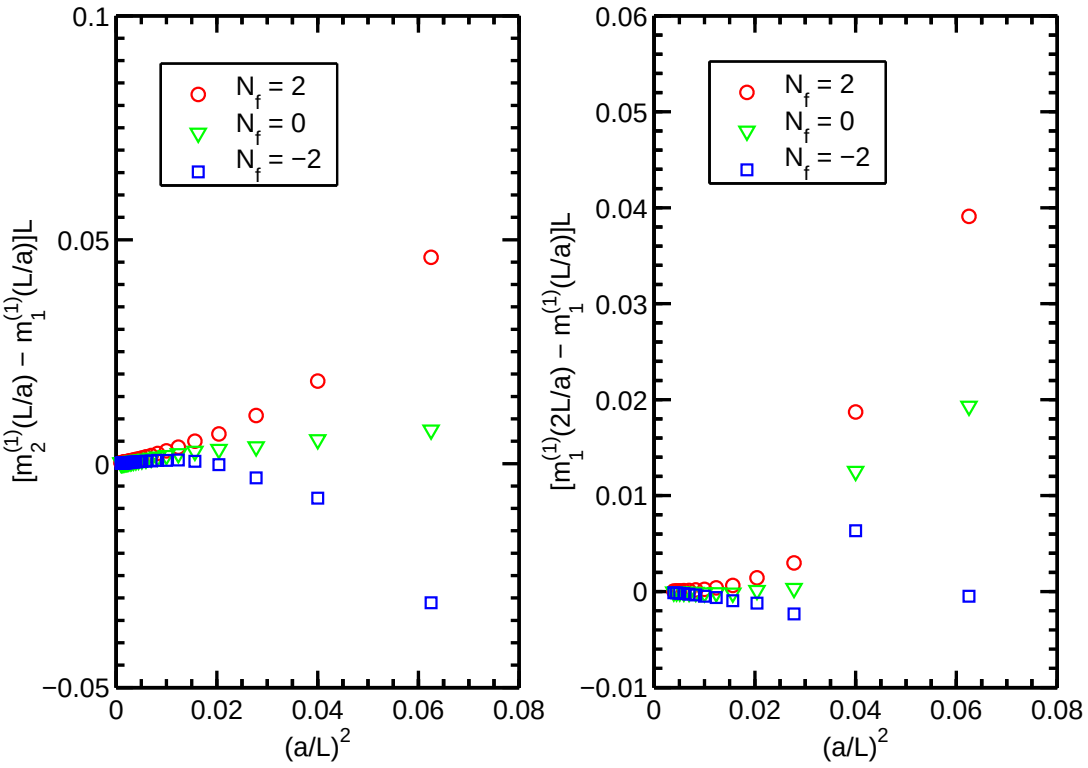

Figure 7.2: *The lattice artefacts* $d = m_2(L/a) - m_1(L/a)$ *and* $e = m_1(2L/a) - m_1(L/a)$ *at 1–loop order*

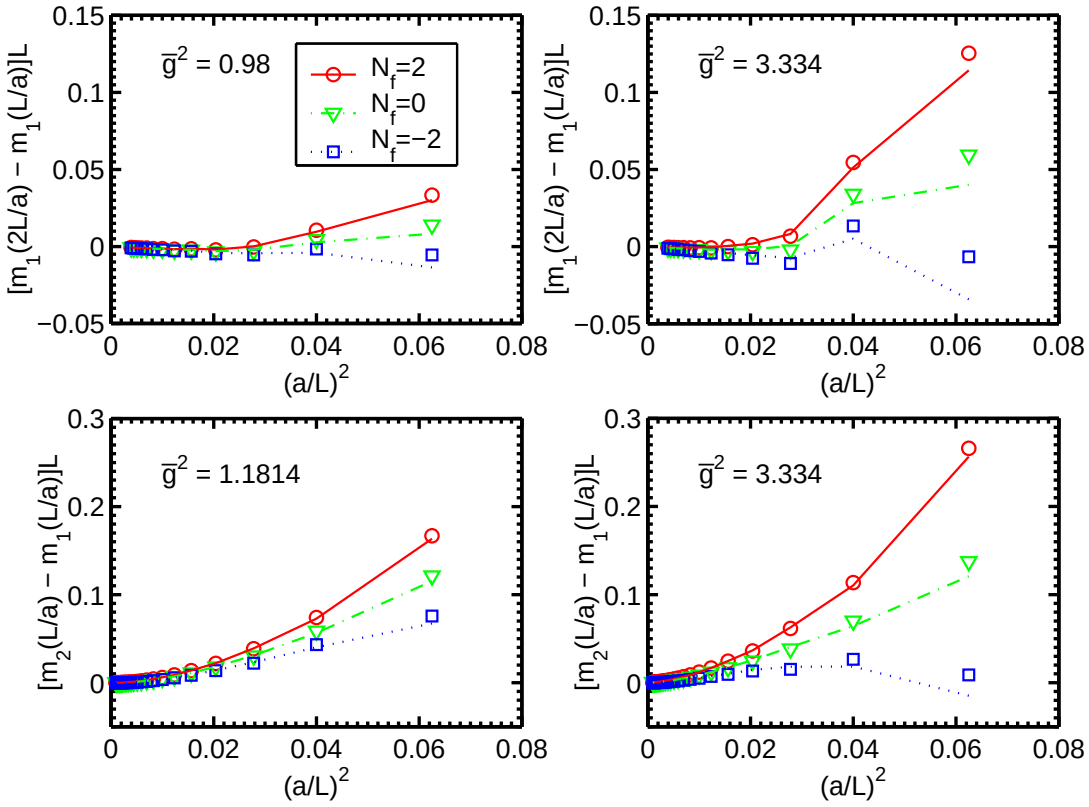

Figure 7.3: *The lattice artefacts* $e = m_1(2L/a) - m_1(L/a)$ *and* $d = m_2(L/a) - m_1(L/a)$ *up to 1–loop order at different values of the renormalised coupling* $\bar{g}^2$. *The lines show the values without the* $c_{\rm t}^{(1)}$*–term, while in the symbols, it is included.*

the discretisation errors δ_{ij}, shown in table 7.3 are expected to differ from the estimation in [34], which was obtained using the continuum limit value of the critical mass, only for small lattices. Since δ_{20} does not depend on the critical quark mass, the 2–loop coefficient will remain unaltered for $N_\mathrm{f} = 0$ when using the correct critical mass instead of its continuum limit. From the size of the critical mass (figure 7.1), one expects a small deviation for $N_\mathrm{f} = -2$ at $L/a = 6$, while for $N_\mathrm{f} = 2$, larger deviations are expected at $L/a = 4$ and $L/a = 6$. Figure 7.4 shows that this indeed is the case. The lines are the estimates from [34], while the symbols denote the values obtained with the proper $m_\mathrm{c}(L/a)$. In any case, the 2–loop coefficient δ_2 is small and does vanish at a rate proportional to $(a/L)^2$, as one should expect in the improved theory. Especially for $N_\mathrm{f} = 2$, it does get even smaller by using the correct critical mass.

L/a	δ_{10}	δ_{11}	δ_{20}	δ_{21}	δ_{22}
4	-0.01033	0.00002	-0.001588	-0.000630	0.000712
5	-0.00625	-0.00014	-0.000872	-0.000460	0.000407
6	-0.00394	-0.00014	-0.000550	-0.000341	0.000200
7	-0.00268	-0.00014	-0.000376	-0.000211	0.000103
8	-0.00194	-0.00011	-0.000268	-0.000138	0.000059
9	-0.00148	-0.00009	-0.000196	-0.000098	0.000038
10	-0.00117	-0.00007	-0.000147	-0.000073	0.000027
11	-0.00095	-0.00006	-0.000111	-0.000058	0.000020
12	-0.00079	-0.00005	-0.000085	-0.000047	0.000016

Table 7.3: *The discretisation errors δ_{ij} up to 2–loop order*

7.3 The renormalised quark mass

7.3.1 The renormalisation constant Z_P up to 1–loop order

In order to obtain the finite part z_p of Z_P defined in (6.7), one has to extrapolate the quantity

$$Y_\mathrm{P}(L/a) = \frac{1}{C_\mathrm{F}} \left(Z_\mathrm{P}^{(1)}(L/a) + d_0 \ln(L/a) \right) \tag{7.5}$$

to the continuum limit. Due to the N_f dependent tadpole graphs, one has a linear N_f dependence of Y_P,

$$Y_\mathrm{P} = Y_\mathrm{P0} + N_\mathrm{f} Y_\mathrm{P1}, \tag{7.6}$$

and thus the same dependence for z_p,

$$z_\mathrm{p} = z_\mathrm{p0} + N_\mathrm{f} z_\mathrm{p1}. \tag{7.7}$$

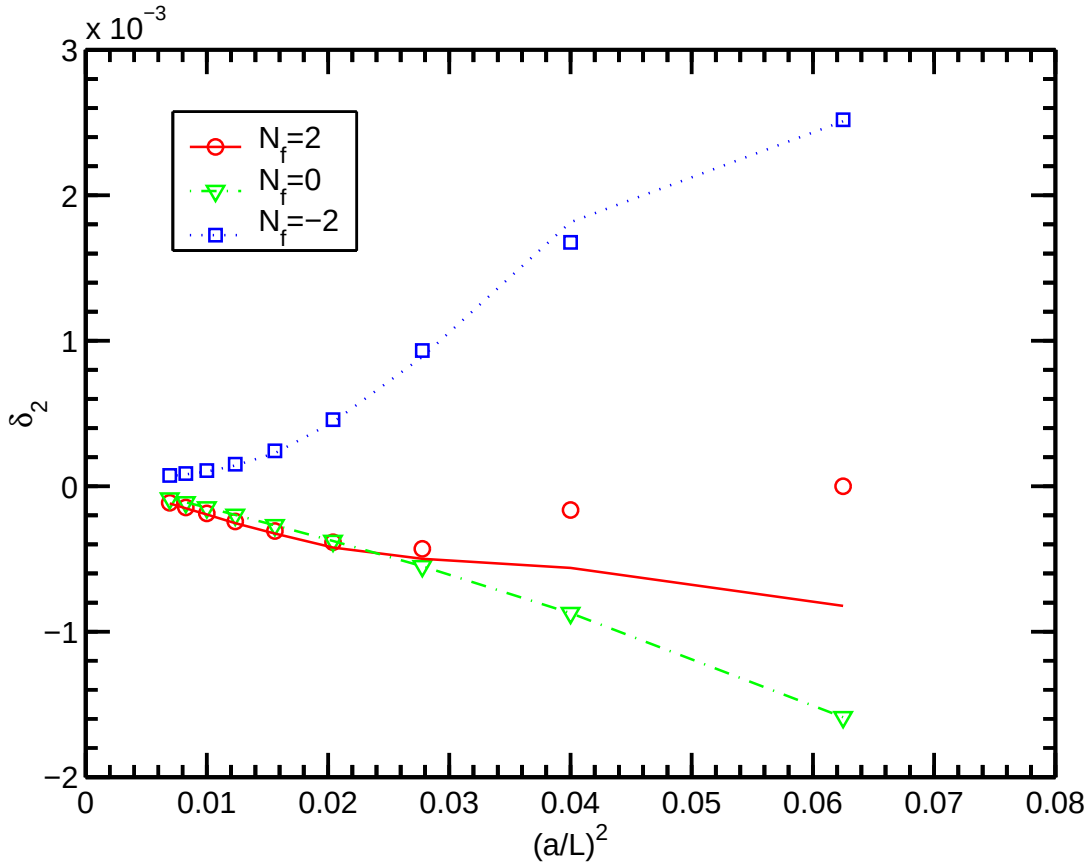

Figure 7.4: *The 2–loop discretisation error δ_2. The lines show the values for δ_2 if the continuum limit of the critical mass is used.*

L/a	Y_{P0}	Y_{P1}
4	-0.13990	0.025124
6	-0.14008	0.009000
8	-0.13757	0.005284
10	-0.13590	0.004070
12	-0.13476	0.003539
14	-0.13395	0.003254
16	-0.13336	0.003081
18	-0.13291	0.002966
20	-0.13256	0.002886
22	-0.13228	0.002828
24	-0.13205	0.002785
26	-0.13187	0.002751
28	-0.13172	0.002724
30	-0.13159	0.002703
32	-0.13148	0.002686

Table 7.4: *The N_{f} independent and N_{f} dependent part of $Y_{\mathrm{P}}(L/a)$*

The results for different lattice sizes are shown in table 7.4. The behaviour of Y_{P} is shown in figure 7.5 for different values of N_{f}.

For the extrapolation, the procedure described in appendix C may be used. Following [75], one expects an asymptotic expansion

$$Y_{\mathrm{P}}(L/a) = a_0 + \sum_{k=1}^{\infty} \left[a_k + b_k \ln(a/L)\right] (a/L)^k \tag{7.8}$$

to hold, where the terms linear in (a/L) are cancelled by improvement. Taking the functions 1, $(a/L)^2$, and $(a/L)^2 \ln(a/L)$ into the fit and using $(a/L)^3$ and $(a/L)^3 \ln(a/L)$ for the estimation of the systematic error yields the results

$$z_{\mathrm{p0}} = -0.13044(2), \qquad z_{\mathrm{p1}} = 0.002565(10). \tag{7.9}$$

Since Y_{P} depends on the improvement coefficients $c_{\mathrm{sw}}^{(1)}$, $\tilde{c}_{\mathrm{t}}^{(1)}$, $c_{\mathrm{t}}^{(1)}$, and via the critical mass also on $c_{\mathrm{A}}^{(1)}$, the errors of these coefficients have to be taken into account. However, varying the improvement coefficients within their error ranges shows that the change in z_{p0} and z_{p1} is smaller than the errors quoted in (7.9). The error due to the uncertainty in the improvement coefficients is thus negligible.

Taking $(a/L)^3$ and $(a/L)^3 \ln(a/L)$ into the fit and using the functions $(a/L)^4$ and $(a/L)^4 \ln(a/L)$ for the error estimation does not change the picture significantly. While one gets smaller systematic errors in the extrapolation, the errors of the improvement coefficients become more important. Taking everything into

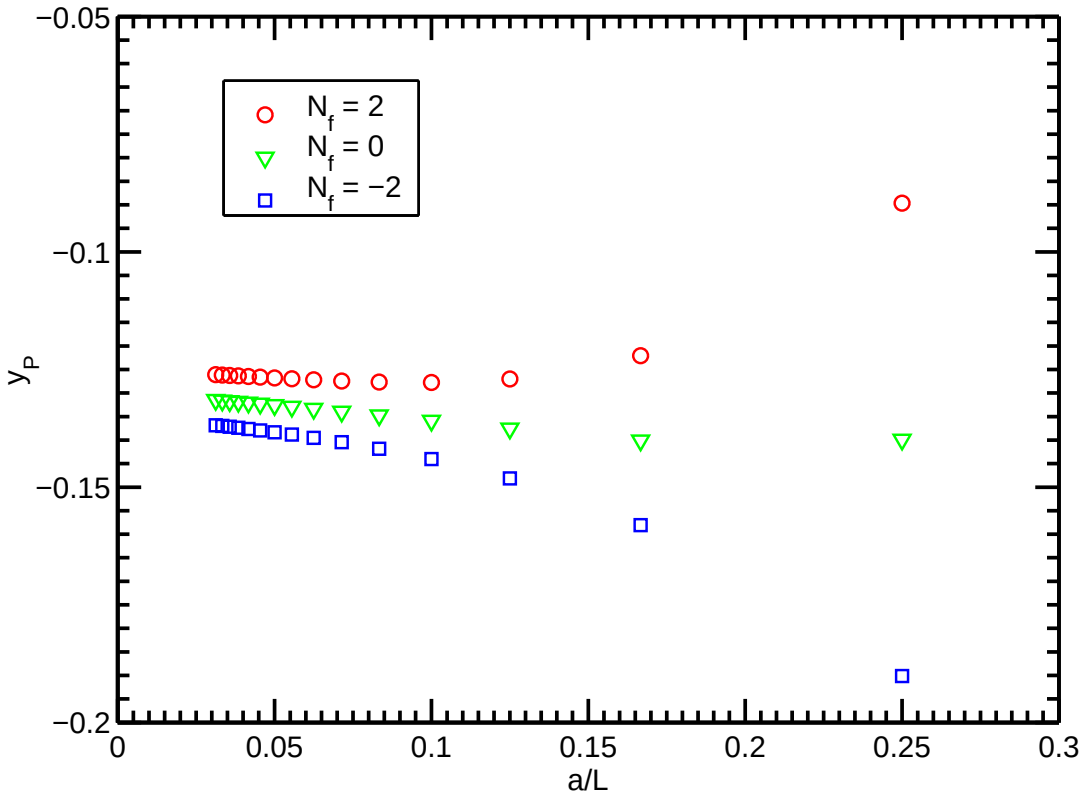

Figure 7.5: *The finite part Y_P of the renormalisation constant Z_P at 1–loop order*

account, the errors quoted in (7.9) seem to be reasonably conservative. Including (a/L) and $(a/L)\ln(a/L)$ in the fit shows that the coefficients of these functions are compatible with zero, as one should expect in the $\mathrm{O}(a)$ improved theory.

Inserting z_p into (6.21) and using (6.22), one now gets the 2–loop anomalous dimension d_1^SF. Due to the linear dependence of z_p on N_f, the anomalous dimension will get an N_f dependence up to order N_f^2, in contrast to order N_f in the case of a vanishing background field. Now, d_1^SF becomes

$$d_1^\mathrm{SF}/d_0 = 0.16508(8) - 0.00724(4)N_\mathrm{f} + 0.000570(2)N_\mathrm{f}^2. \tag{7.10}$$

This result for $\theta = \pi/5$ and $\rho = 1$ is small, but larger than the anomalous dimension with a vanishing background field computed in [35], which is $d_1^\mathrm{SF}/d_0 = 0.1251 + 0.0046N_\mathrm{f}$ for $\theta = 0$ and $d_1^\mathrm{SF}/d_0 = 0.0271 + 0.0105N_\mathrm{f}$ for $\theta = 0.5$.

7.3.2 Lattice artefacts of Σ_P up to 1–loop order

By computing the renormalisation constant Z_P both at L/a and $2L/a$ with $m_1(L/a) = 0$, one obtains the one loop coefficient $k(L/a)$ of the step scaling function Σ_P,

$$k(L/a) = Z_\mathrm{P}^{(1)}(2L/a) - Z_\mathrm{P}^{(1)}(L/a), \tag{7.11}$$

and its deviation δ_k from the continuum limit,

$$\delta_k(L/a) = \frac{k(L/a)}{k(\infty)} - 1, \tag{7.12}$$

with $k(\infty) = -d_0\ln(2)$. In contrast to the zero background field case, the tadpole graphs give a dependence on N_f,

$$\delta_k = \delta_{k0} + \delta_{k1}N_\mathrm{f}, \tag{7.13}$$

where the coefficients δ_{k0} and δ_{k1} (not to be confused with the δ_{ij} from section 7.2) are expected to vanish at a rate proportional to a^2. The results for δ_{k0} and δ_{k1} can be found in table 7.5. In figure 7.6, δ_k is shown for several flavour numbers. Compared to the results obtained with a vanishing background field in [35], these discretisation errors are very large, especially for $L/a = 4$ and $L/a = 6$. However, for $N_\mathrm{f} = 2$ and $L/a \geq 8$, the error seems to be reasonably small.

In order to get a direct impression of the change of the discretisation errors due to the presence of the background field, one should compare the values with and without background field at the same values of θ and ρ. This is done in table 7.6 and in figure 7.7, where the black lines represent the N_f independent results with a vanishing background field from [35], while the symbols denote the results obtained with the non–vanishing background field for several flavour numbers. For $N_\mathrm{f} = 0$, the discretisation errors with a non–vanishing background field are smaller than those with zero background field at $\theta = 0$, while at $\theta = 0.5$,

L/a	δ_{k0}	δ_{k1}
4	-0.3258	0.6248
6	-0.1998	0.1916
8	-0.1548	0.0790
10	-0.1229	0.0428
12	-0.0998	0.0274
14	-0.0826	0.0193
16	-0.0696	0.0144

Table 7.5: *The $N_{\rm f}$ independent and $N_{\rm f}$ dependent part of $\delta_k(L/a)$ for $\theta = \pi/5$ and $\rho = 1$*

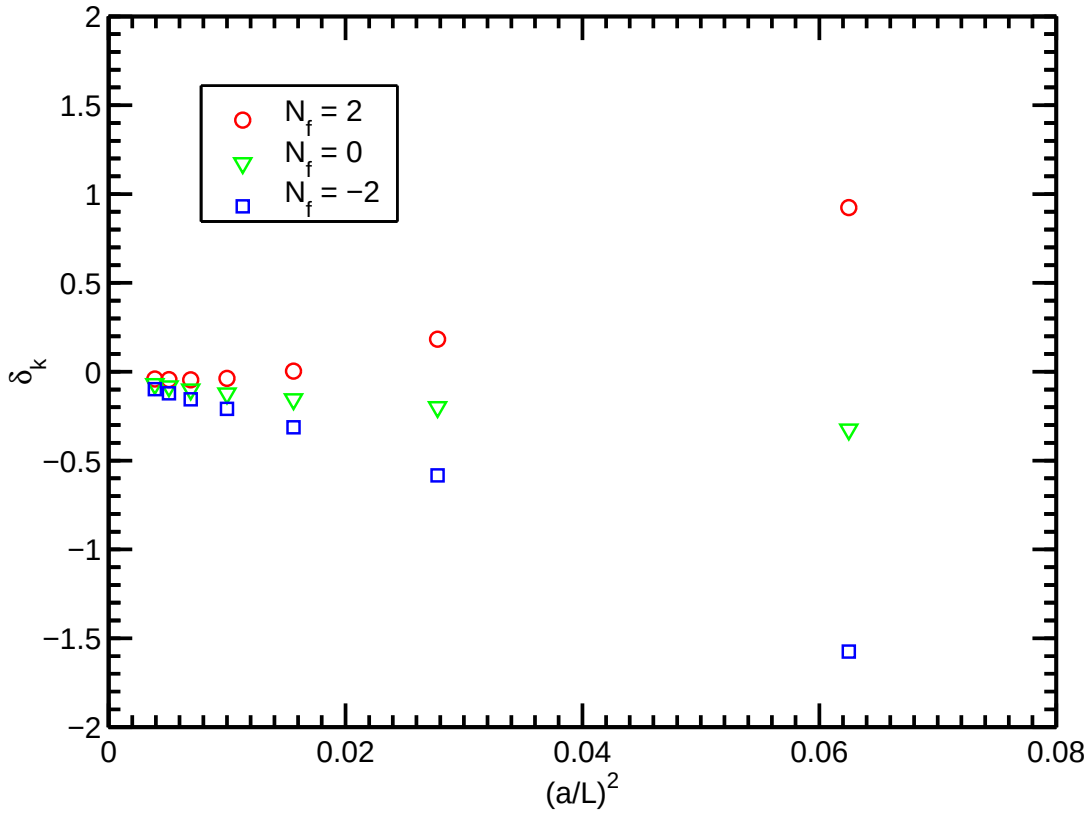

Figure 7.6: *The 1–loop order discretisation error δ_k of the step scaling function $\Sigma_{\rm P}$ for $\theta = \pi/5$ and $\rho = 1$*

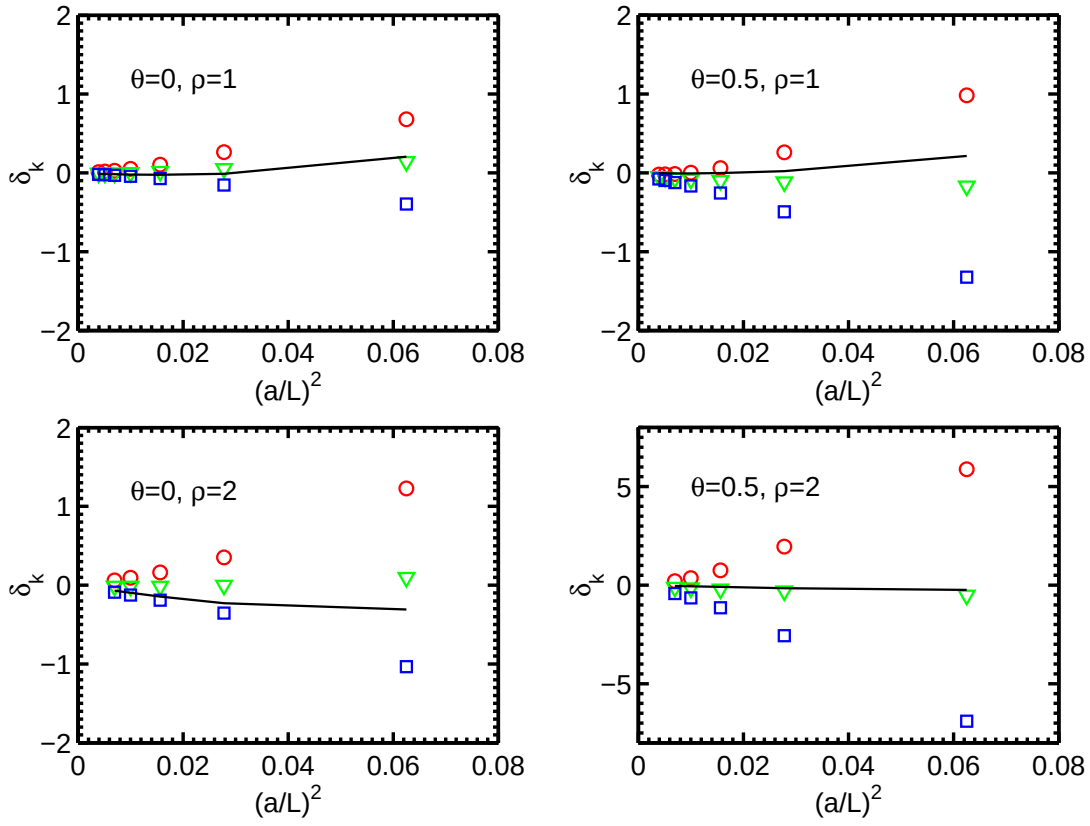

Figure 7.7: *The 1–loop order discretisation error δ_k of the step scaling function Σ_{P} for various values of θ and ρ at $N_{\mathrm{f}} = 2$ (○), $N_{\mathrm{f}} = 0$ (▽), and $N_{\mathrm{f}} = -2$ (□). The solid line (—) shows the values for a vanishing background field from [35].*

L/a	$\delta_{k0}\|_{\theta=0}$	$\delta_{k1}\|_{\theta=0}$	$\delta_k\|_{\theta=0,V=1}$	$\delta_{k0}\|_{\theta=0.5}$	$\delta_{k1}\|_{\theta=0.5}$	$\delta_k\|_{\theta=0.5,V=1}$
$\rho = 1$						
4	0.1425	0.2688	0.2040	-0.1697	0.5765	0.2136
6	0.0538	0.1046	-0.0121	-0.1167	0.1891	0.0208
8	0.0164	0.0442	-0.0253	-0.0983	0.0791	-0.0026
10	0.0033	0.0231	-0.0215	-0.0815	0.0425	-0.0062
12	-0.0019	0.0144	-0.0171	-0.0680	0.0270	-0.0064
14	-0.0040	0.0100	-0.0137	-0.0573	0.0190	-0.0058
16	-0.0049	0.0074	-0.0111	-0.0489	0.0141	-0.0052
$\rho = 2$						
4	0.0963	0.5651	-0.3084	-0.5116	3.1960	-0.2456
6	-0.0020	0.1768	-0.2292	-0.3020	1.1311	-0.1499
8	-0.0144	0.0880	-0.1449	-0.2007	0.4744	-0.0893
10	-0.0155	0.0546	-0.0974	-0.1472	0.2502	-0.0584
12	-0.0142	0.0377	-0.0696	-0.1137	0.1567	-0.0412

Table 7.6: The $N_{\rm f}$ independent and $N_{\rm f}$ dependent part of $\delta_k(L/a)$ for various values of θ and ρ compared to the zero background field ($V = 1$) values from [35]

they are larger. For $N_{\rm f} \neq 0$, the discretisation errors become drastically larger due to the large $N_{\rm f}$–term, which is not present in the case of a vanishing background field. This effect is particularly large at $\theta = 0.5$ and $\rho = 2$.

7.4 Numerical checks of the results

In order to check the programs, they were used to compute the tree level and 1–loop coefficients at $m_0 = 0$ and $L/a = 6$, where the results can be compared to non perturbative results obtained in Monte Carlo simulations by Juri Rolf. The simulations were done at small bare couplings ranging from 0.075 to 0.6 using the tree level values for the improvement coefficients. The results are shown in figure 7.8. The tree level values of $f_{\rm P}(T/2)$ and f_1 are obtained as the constant parts in polynomial fits up to order g_0^4. (The results do, of course, depend on the fit ansatz. Using a polynomial of the form $a_0 + a_1 g_0^2 + a_2 g_0^4$ turned out to give results with reasonable errors.) Fitting the polynomials to the filled symbols in figure 7.8 yields

$$f_{\rm P}^{(0)}(T/2) = 0.8586(11), \qquad f_1^{(0)} = 0.1312(3), \tag{7.14}$$

compared to the perturbative results

$$f_{\rm P}^{(0)}(T/2) = 0.8587, \qquad f_1^{(0)} = 0.1310. \tag{7.15}$$

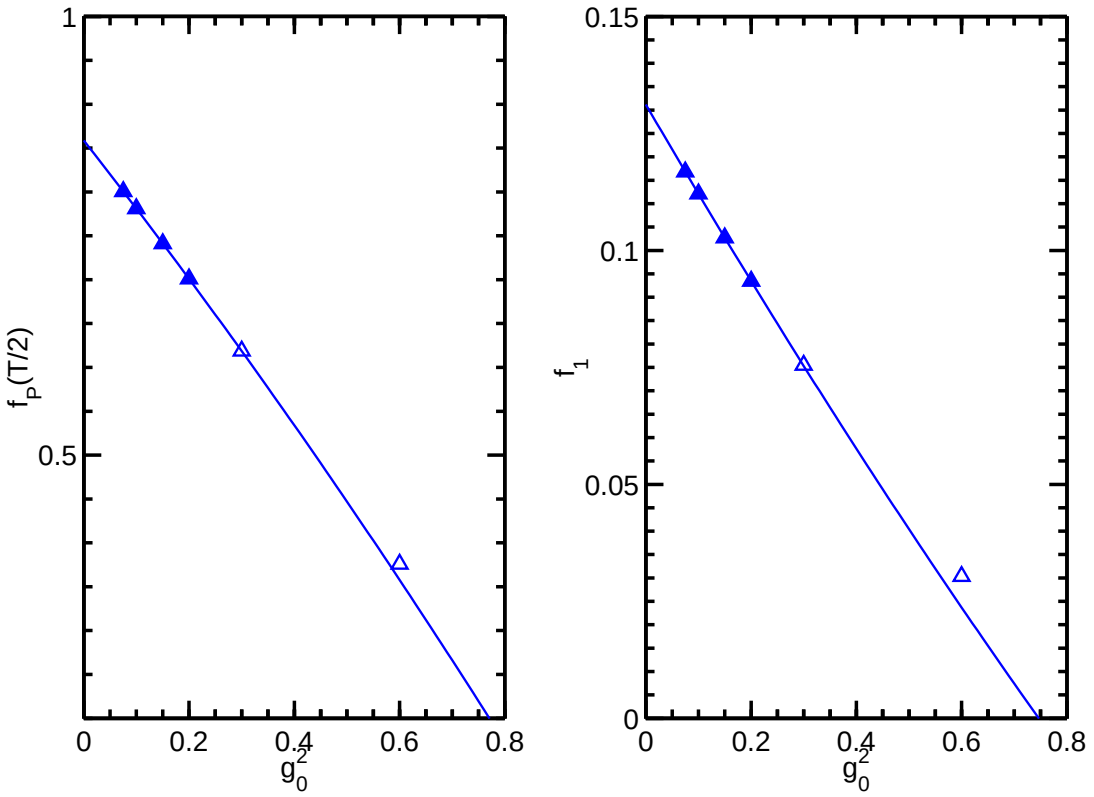

Figure 7.8: *Monte Carlo results for $f_{\rm P}(T/2)$ and f_1 at $L/a = 6$. The error bars are smaller than the symbols. The lines are polynomial fits up to order g_0^4 including the filled symbols, while the open symbols were disregarded.*

Obviously, these results agree perfectly well.

For the one loop coefficients, one could in principle use the coefficient of g_0^2 obtained in the fit. However, assuming the tree level values of $f_{\rm P}$ and f_1 to be correct, one achieves more precise results doing the fit on $(f_{\rm P}(T/2) - f_{\rm P}^{(0)}(T/2))/g_0^2$ and $(f_1 - f_1^{(0)})/g_0^2$, where the 1–loop coefficients get the constant parts in the fit. These functions are shown in figure 7.9 both for tree level improvement and for $c_{\rm t}^{(1)} = 2$, which was used to check the $c_{\rm t}^{(1)}$-term. In this case, the results for bigger g_0^2 seem to be dominated by terms of higher order than g_0^4.

For $c_{\rm t}^{(1)} = 0$, the extrapolation yields

$$f_{\rm P}^{(1)}(T/2) = -0.765(11), \qquad f_1^{(1)} = -0.188(3), \tag{7.16}$$

compared to

$$f_{\rm P}^{(1)}(T/2) = -0.760, \qquad f_1^{(1)} = -0.189, \tag{7.17}$$

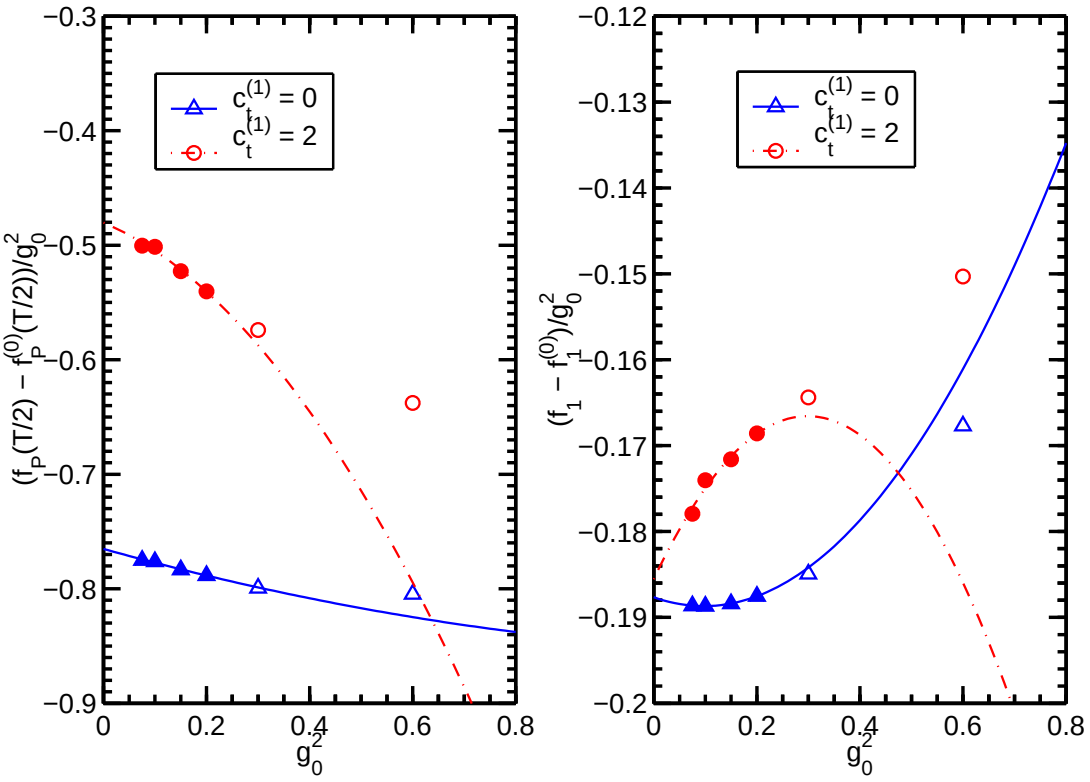

Figure 7.9: *Monte Carlo results for* $(f_{\rm P}(T/2) - f_{\rm P}^{(0)}(T/2))/g_0^2$ *and* $(f_1 - f_1^{(0)})/g_0^2$ *at* $L/a = 6$. *The error bars are smaller than the symbols. The lines are polynomial fits up to order* g_0^4 *including the filled symbols.*

obtained by perturbation theory, while for $c_{\rm t}^{(1)} = 2$ one gets

$$f_{\rm P}^{(1)}(T/2) = -0.480(10), \qquad f_1^{(1)} = -0.186(3), \tag{7.18}$$

compared to the perturbative results

$$f_{\rm P}^{(1)}(T/2) = -0.466, \qquad f_1^{(1)} = -0.183. \tag{7.19}$$

These results seem to agree well enough to state that the perturbative results could be confirmed by the simulations.

Chapter 8

Summary

In this thesis, a part of the programme of the ALPHA collaboration to renormalise QCD has been presented.

The basic ideas of the Schrödinger functional as a method to compute renormalised quantities have been outlined and it has been explained how this scheme avoids computations on very large lattices by using the length of the space time box as the renormalisation scale. Furthermore, Symanzik's improvement programme has been introduced as a method to reduce discretisation errors to $\mathrm{O}(a^2)$.

The main purpose of the Schrödinger functional method, the renormalisation of parameters, has been studied in detail. The definition of the renormalised coupling has been outlined, and it was shown how a renormalised quark mass can be introduced via the PCAC relation.

In order to do several 1–loop calculations, perturbation theory in the Schrödinger functional has been discussed. Perturbation theory has then been used to do a variety of calculations with a non–vanishing background field, which so far had only been done in the zero background field case. In particular, the following calculations have been done:

- The correlation functions f_{A}, f_{P}, and f_1 have been expanded up to 1–loop order.
- In these expansions, it was found that, with a non–vanishing background field, an improvement term proportional to $c_{\mathrm{t}}^{(1)}$ arises, which was missing in previous publications.
- The critical quark mass has been computed up to 1–loop order and was used to calculate the discretisation errors of the coupling's step scaling function up to 2–loop order.
- Several discretisation errors of the current quark mass have been calculated.
- The renormalisation constant Z_{P} has been computed at 1–loop order, giving the 2–loop anomalous dimension.

- The discretisation error of the step scaling function of the quark mass has been computed at 1–loop order.

These computations turned out to be time consuming, so that lattices larger than $L/a = 32$ could not be reached. Up to $L/a = 32$, calculations could however be done in reasonable time. In these calculations, the following results have been obtained:

- The critical quark mass was shown to converge quickly towards its continuum limit. Considerable deviations from this limit were only observed for very small lattices.
- The discretisation errors of the coupling's step scaling function turned out to be small and close to those computed with the continuum limit of the critical quark mass. Where the results using the correct critical mass deviate from the previous results, they were shown to make the discretisation errors smaller.
- The discretisation errors of the current quark mass turned out to be small.
- The effect of the previously missing $c_{\mathrm{t}}^{(1)}$–term on results published so far was shown to be negligible.
- The 2–loop anomalous dimension was shown to be small but larger than in the case of a vanishing background field.
- The discretisation error of the step scaling function of the renormalised quark mass turned out to be much larger than with a vanishing background field for $N_{\mathrm{f}} \neq 0$, while for $N_{\mathrm{f}} = 0$, it is smaller or larger, depending on θ. For the case of $\theta = \pi/5$, $\rho = 1$, and $N_{\mathrm{f}} = 2$, it turned however out to be reasonably small for $L/a \geq 8$.
- The results obtained perturbatively could be shown to agree well with non–perturbative results from Monte Carlo simulations in the small coupling limit on small lattices ($L/a = 6$).

With these calculations, the perturbative treatment of the quark mass renormalisation up to 1–loop order at vanishing renormalised mass is completed. The programs are, however, written such that they can be used for calculations at different quark masses without too much effort.

What has not yet been done are non–perturbative calculations of the renormalised mass with a non–vanishing background field. However, due to the large discretisation errors found in this thesis for small lattices, safe extrapolations to the continuum limit could turn out to be difficult.

Appendix A

Notations and conventions

A.1 The Dirac matrices

The Dirac matrices in Euclidean space may be obtained from those in Minkowski space by

$$\gamma_0^{\text{Euclidean}} = \gamma_0^{\text{Minkowski}}, \tag{A.1}$$
$$\gamma_{1,2,3}^{\text{Euclidean}} = -i\gamma_{1,2,3}^{\text{Minkowski}}, \tag{A.2}$$

giving

$$\gamma_0 = \begin{pmatrix} 1 & 0 \\ 0 & -1 \end{pmatrix}, \tag{A.3}$$
$$\gamma_{1,2,3} = \begin{pmatrix} 0 & -i\sigma_{1,2,3} \\ i\sigma_{1,2,3} & 0 \end{pmatrix}, \tag{A.4}$$

with the Pauli matrices

$$\sigma_1 = \begin{pmatrix} 0 & 1 \\ 1 & 0 \end{pmatrix}, \quad \sigma_2 = \begin{pmatrix} 0 & -i \\ i & 0 \end{pmatrix}, \quad \sigma_3 = \begin{pmatrix} 1 & 0 \\ 0 & -1 \end{pmatrix}. \tag{A.5}$$

In this representation, $\gamma_5 = \gamma_1\gamma_2\gamma_3\gamma_4$ is given by

$$\gamma_5 = \begin{pmatrix} 0 & -1 \\ -1 & 0 \end{pmatrix}. \tag{A.6}$$

The projectors $P_+ = \frac{1}{2}(1+\gamma_0)$ and $P_- = \frac{1}{2}(1-\gamma_0)$ become

$$P_+ = \begin{pmatrix} 1 & 0 \\ 0 & 0 \end{pmatrix}, \qquad P_- = \begin{pmatrix} 0 & 0 \\ 0 & 1 \end{pmatrix}. \tag{A.7}$$

A.2 The basis of the Lie algebra su(3)

One possible choice for a basis of $su(3)$ are the well known Gell-Mann matrices [76]. For the calculations in this thesis, it is however more convenient to use the same basis as in [51]. To this end, we introduce colour matrices $\tilde{\lambda}_a$, which coincide with the Gell-Mann matrices λ_a in all cases except for the two diagonal matrices, for which we choose

$$\tilde{\lambda}_3 = -\frac{1}{2}\lambda_3 + \frac{\sqrt{3}}{2}\lambda_8, \tag{A.8}$$

$$\tilde{\lambda}_8 = \frac{\sqrt{3}}{2}\lambda_3 + \frac{1}{2}\lambda_8. \tag{A.9}$$

Then, the matrices $\tilde{\lambda}_a$ are

$$\begin{aligned}
\tilde{\lambda}_1 &= \begin{pmatrix} 0 & 1 & 0 \\ 1 & 0 & 0 \\ 0 & 0 & 0 \end{pmatrix}, & \tilde{\lambda}_2 &= \begin{pmatrix} 0 & -i & 0 \\ i & 0 & 0 \\ 0 & 0 & 0 \end{pmatrix}, \\
\tilde{\lambda}_4 &= \begin{pmatrix} 0 & 0 & 1 \\ 0 & 0 & 0 \\ 1 & 0 & 0 \end{pmatrix}, & \tilde{\lambda}_5 &= \begin{pmatrix} 0 & 0 & -i \\ 0 & 0 & 0 \\ i & 0 & 0 \end{pmatrix}, \\
\tilde{\lambda}_6 &= \begin{pmatrix} 0 & 0 & 0 \\ 0 & 0 & 1 \\ 0 & 1 & 0 \end{pmatrix}, & \tilde{\lambda}_7 &= \begin{pmatrix} 0 & 0 & 0 \\ 0 & 0 & -i \\ 0 & i & 0 \end{pmatrix}, \\
\tilde{\lambda}_3 &= \begin{pmatrix} 0 & 0 & 0 \\ 0 & 1 & 0 \\ 0 & 0 & -1 \end{pmatrix}, & \tilde{\lambda}_8 &= \frac{1}{\sqrt{3}} \begin{pmatrix} 2 & 0 & 0 \\ 0 & -1 & 0 \\ 0 & 0 & -1 \end{pmatrix}.
\end{aligned} \tag{A.10}$$

After normalisation,

$$T_a = \frac{1}{2i}\tilde{\lambda}_a, \tag{A.11}$$

these matrices may be used to define a new basis I^a, which is given by

$$\begin{aligned}
I^1 = T_+ &= \frac{1}{\sqrt{2}}(T_1 + iT_2), & I^2 = T_- &= \frac{1}{\sqrt{2}}(T_1 - iT_2), \\
I^4 = U_+ &= \frac{1}{\sqrt{2}}(T_4 + iT_5), & I^5 = U_- &= \frac{1}{\sqrt{2}}(T_4 - iT_5), \\
I^6 = V_+ &= \frac{1}{\sqrt{2}}(T_6 + iT_7), & I^7 = V_- &= \frac{1}{\sqrt{2}}(T_6 - iT_7),
\end{aligned} \tag{A.12}$$

for the non–diagonal matrices and

$$I^3 = T_3, \qquad I^8 = T_8 \tag{A.13}$$

a	C_a	S_a
1	$\frac{1}{2}(\cos 2\gamma + \cos\gamma)$	$-i\frac{1}{2}(\sin 2\gamma + \sin\gamma)$
3	$\cos\gamma$	0
4	$\frac{1}{2}(\cos 2\gamma + \cos\gamma)$	$-i\frac{1}{2}(\sin 2\gamma + \sin\gamma)$
6	$\cos\gamma$	0
8	$\frac{1}{3}(2\cos 2\gamma + \cos\gamma)$	0

Table A.1: *C_a and S_a for the gauge group $SU(3)$. The other coefficients are $C_2 = C_1$, $C_5 = C_4$, $C_7 = C_6$, $S_2 = -S_1$, $S_5 = -S_4$, and $S_7 = -S_6$.*

for the diagonal ones. For this basis, one has

$$I^{a\dagger} = -I^{\bar{a}}, \tag{A.14}$$

where $\bar{1} = 2$, $\bar{4} = 5$, $\bar{6} = 7$, and vice versa. For the diagonal matrices, one has $\bar{3} = 3$ and $\bar{8} = 8$. The normalisation is chosen such that

$$\mathrm{Tr}\left(I^a I^b\right) = -\frac{1}{2}\delta_{b\bar{a}}. \tag{A.15}$$

A.3 The background field

In the chosen basis, the constant colour electric background field $\mathcal{E}$ is proportional to I^8. It can be written as

$$\mathcal{E} = -\gamma \begin{pmatrix} 2 & 0 & 0 \\ 0 & -1 & 0 \\ 0 & 0 & -1 \end{pmatrix} = -\gamma\sqrt{3}\tilde{\lambda}_8, \tag{A.16}$$

with

$$\gamma = \frac{1}{LT}\left(\eta + \frac{\pi}{3}\right). \tag{A.17}$$

A special feature of the chosen basis is that the star operation defined by

$$M \star G = \frac{1}{2}\left[(MG + GM^\dagger) - \frac{1}{N}\mathrm{tr}(MG + GM^\dagger)\right] \tag{A.18}$$

acts diagonally,

$$\cosh G_{0k} \star I^a = C_a I^a, \tag{A.19}$$

$$\sinh G_{0k} \star I^a = S_a I^a. \tag{A.20}$$

The values of C_a and S_a can be found in table A.1.

a	$\phi_a(x_0)$	R_a
1	$-3\gamma x_0 + \frac{1}{L}(\eta[\frac{3}{2} - \nu] - \frac{\pi}{3})$	$\cos\frac{\gamma}{2}$
3	0	$\cos\gamma$
4	$-3\gamma x_0 + \frac{1}{L}(\eta[\frac{3}{2} + \nu] - \frac{2\pi}{3})$	$\cos\frac{\gamma}{2}$
6	$\frac{1}{L}(2\eta\nu - \frac{\pi}{3})$	$\cos\gamma$
8	0	$\frac{1}{3}(2\cos 2\gamma + \cos\gamma)$

Table A.2: $\phi_a(x_0)$ *and* R_a *for the gauge group* $SU(3)$*. The other coefficients are* $\phi_2 = -\phi_1$, $\phi_5 = -\phi_4$, $\phi_7 = -\phi_6$, $R_2 = R_1$, $R_5 = R_4$, *and* $R_7 = R_6$.

The covariant derivative may be decomposed in the basis I^a, giving

$$(D_k f)(x) = \sum_a \Big[\Omega_a(x_0) f^a(x + \hat{k}) - f^a(x)\Big] I^a, \tag{A.21}$$

$$(D_k^* f)(x) = \sum_a \Big[f^a(x) - \Omega_a(x_0)^* f^a(x - \hat{k})\Big] I^a, \tag{A.22}$$

where $\Omega_a(x_0)$ is a phase factor and can thus be written as

$$\Omega_a(x_0) = e^{i\phi_a(x_0)}. \tag{A.23}$$

The values of ϕ_a are shown in table A.2. Another quantity useful for the calculation of the gluon propagator is

$$R_a = (C_a - S_a) e^{i\partial_0 \phi_a(x_0)/2}. \tag{A.24}$$

Also the values of R_a can be found in table A.2.

Appendix B

The numerical construction of the propagators

B.1 The gluon and ghost propagators

In order to obtain the gluon and ghost propagators, one has to invert the operators K^a and F^a from (5.51), (5.52), (5.53), (5.54), and (5.58). A very convenient way to do this is described in [64] and will be briefly outlined.

For the gluon propagator, one has to solve the difference equation

$$\sum_{y_0}\sum_{\nu} K^a_{\mu\nu}(\mathbf{p};x_0,y_0)D^a_{\nu\sigma}(\mathbf{p};y_0,z_0) = \delta_{x_0,z_0}\delta_{\mu\sigma}. \tag{B.1}$$

This is particularly simple for $a = 3, 8$ with $\mathbf{p} = \mathbf{0}$. In this case, one simply has

$$D^a_{\mu\nu}(\mathbf{0};x_0,y_0) = \begin{cases} \frac{1}{\lambda_0}(1+\min(x_0,y_0)) & \text{if } \mu=\nu=0, \\ \frac{1}{R_a}(\min(x_0,y_0) - \frac{x_0y_0}{T}) & \text{if } \mu=\nu=k, \\ 0 & \text{if } \mu\neq\nu. \end{cases} \tag{B.2}$$

In all other cases, the difference equation has to be solved numerically. To simplify the notation, we denote the propagator at fixed values for $\mathbf{p}$ and a by

$$D^a_{\mu\nu}(\mathbf{p};x_0,y_0) = Q_{\mu\nu}(x_0,y_0). \tag{B.3}$$

The operator K^a may be decomposed according to

$$K^a_{\mu\nu}(\mathbf{p};x_0,y_0) = \mathcal{A}_{\mu\nu}(x_0)\delta_{x_0+1,y_0} + \mathcal{B}_{\mu\nu}(x_0)\delta_{x_0,y_0} + \mathcal{A}_{\nu\mu}(x_0-1)\delta_{x_0-1,y_0}. \tag{B.4}$$

Using this notation, the difference equation (B.1) becomes

$$\begin{aligned} \mathcal{A}_{\mu\sigma}(x_0)Q_{\sigma\nu}(x_0+1,y_0) + \mathcal{B}_{\mu\sigma}(x_0)Q_{\sigma\nu}(x_0,y_0) & \\ +\mathcal{A}_{\sigma\mu}(x_0-1)Q_{\sigma\mu}(x_0-1,y_0) &= \delta_{\mu\nu}\delta_{x_0,y_0}. \end{aligned} \tag{B.5}$$

In order to solve this equation, we now construct two solutions $\psi^f(x_0)$ and $\psi^b(x_0)$ of the homogeneous equation by two step recursion forward and backward in time. The forward solution ψ^f starts from

$$\begin{aligned} \psi^f_{0\nu}(-1) = \psi^f_{0\nu}(0) &= \delta_{0\nu}, & \text{(B.6)} \\ \psi^f_{k\nu}(0) &= 0, & \text{(B.7)} \\ \psi^f_{k\nu}(1) &= \delta_{k\nu}, & \text{(B.8)} \end{aligned}$$

while the backward solution ψ^b starts from

$$\begin{aligned} \psi^b_{0\nu}(T) = \psi^b_{0\nu}(T-1) &= \delta_{0\nu}, & \text{(B.9)} \\ \psi^b_{k\nu}(T) &= 0, & \text{(B.10)} \\ \psi^b_{k\nu}(T-1) &= \delta_{k\nu}. & \text{(B.11)} \end{aligned}$$

(B.5) expresses the fact that Q is the right–inverse of K^a expressed in terms of $\mathcal{A}$ and $\mathcal{B}$. Then, Q is also the left–inverse, leading to the difference equation

$$\begin{aligned} Q_{\mu\sigma}(x_0, y_0+1)\mathcal{A}_{\nu\sigma}(y_0) + Q_{\mu\sigma}(x_0, y_0)\mathcal{B}_{\sigma\nu}(y_0) & \\ +Q_{\mu\sigma}(x_0, y_0-1)\mathcal{A}_{\sigma\nu}(y_0-1) &= \delta_{\mu\nu}\delta_{x_0,y_0}. \qquad \text{(B.12)} \end{aligned}$$

The homogeneous solutions of (B.12) are also given by ψ^f and ψ^b. Assuming the validity of (B.5) and (B.12) for $x_0 \neq y_0$ and demanding the symmetry

$$Q_{\mu\nu}(x_0, y_0) = Q_{\nu\mu}(y_0, x_0) \qquad \text{(B.13)}$$

leads to

$$Q_{\mu\nu}(x_0, y_0) = \begin{cases} \psi^f_{\mu\sigma}(x_0)\mathcal{W}^{-1}_{\lambda\sigma}\psi^b_{\nu\lambda}(y_0) & \text{for } x_0 \leq y_0 \\ \psi^b_{\mu\sigma}(x_0)\mathcal{W}^{-1}_{\sigma\lambda}\psi^f_{\nu\lambda}(y_0) & \text{for } x_0 \geq y_0 \end{cases} \qquad \text{(B.14)}$$

We now demand that the matrix $\mathcal{W}$ makes this definition consistent and also for $x_0 = y_0$ solves (B.5) and (B.12). These requirements can be shown to imply

$$\mathcal{W}_{\mu\nu} = \psi^f_{\sigma\mu}(x_0)\mathcal{A}_{\sigma\lambda}(x_0)\psi^b_{\lambda\nu}(x_0+1) - \psi^f_{\sigma\mu}(x_0+1)\mathcal{A}_{\lambda\sigma}(x_0)\psi^b_{\lambda\nu}(x_0). \qquad \text{(B.15)}$$

This is a Wronskian form which is easy to compute. Using (B.5) and the fact that $\psi^f_{\sigma\mu}(x_0)\mathcal{A}_{\sigma\lambda}(x_0)\psi^b_{\lambda\nu}(x_0+1)$ is symmetric in μ and ν, $\mathcal{W}$ can easily be shown to be independent of x_0. A particularly simple choice is $x_0 = 0$, which gives after some algebra

$$\begin{aligned} \mathcal{W}_{0\nu} &= \mathcal{A}_{0\sigma}(0)\psi^b_{\sigma\nu}(1) + (\mathcal{B}_{00}(0) + \mathcal{A}_{00}(-1))\psi^b_{0\nu}(0), & \text{(B.16)} \\ \mathcal{W}_{k\nu} &= -\mathcal{A}_{jk}(0)\psi^b_{j\nu}(0). & \text{(B.17)} \end{aligned}$$

Now one only has to insert $\mathcal{W}$ into (B.14) to get the propagator.

The computation of the ghost propagator proceeds along the same lines. Due to the absence of the spin matrix structure, it is, however, much simpler.

B.2 The quark propagator

The quark propagator is computed by carrying over the methods used for the gluon and ghost fields. The propagator S is the inverse of the Dirac–Wilson operator $\tilde{D}$ from (5.61), which means one has to solve the equation

$$\sum_{y_0} \tilde{D}(\mathbf{p}; x_0, y_0) S(\mathbf{p}; y_0, z_0) = \delta_{x_0, z_0}, \tag{B.18}$$

with the boundary conditions

$$P_+ S(\mathbf{p}; x_0, y_0)\big|_{x_0=0} = P_- S(\mathbf{p}; x_0, y_0)\big|_{x_0=T} = 0, \tag{B.19}$$

$$S(\mathbf{p}; x_0, y_0) P_-\big|_{y_0=0} = S(\mathbf{p}; x_0, y_0) P_+\big|_{y_0=T} = 0, \tag{B.20}$$

which are obtained by setting the boundary quark fields to zero.

In analogy to the gluon case, one first constructs solutions of the homogeneous equation by forward and backward recursion. This means one solves

$$\sum_{y_0} \tilde{D}(\mathbf{p}; x_0, y_0) \psi^f(\mathbf{p}, y_0) = 0 \tag{B.21}$$

and

$$\sum_{y_0} \tilde{D}(\mathbf{p}; x_0, y_0) \psi^b(\mathbf{p}, y_0) = 0, \tag{B.22}$$

starting from

$$P_+ \psi^f(\mathbf{p}, x_0)\big|_{x_0=0} = 0 \tag{B.23}$$

and

$$P_- \psi^b(\mathbf{p}, x_0)\big|_{x_0=T} = 0. \tag{B.24}$$

Here, only one starting value per solution is required, since one only has to solve a first order difference equation. This is easily seen by defining

$$F^{f/b}(x_0) = P_- \psi^{f/b}(\mathbf{p}, x_0) + P_+ \psi^{f/b}(\mathbf{p}, x_0 - 1). \tag{B.25}$$

Writing down the Dirac–Wilson operator in the form of (5.61),

$$\tilde{D}(\mathbf{p}; x_0, y_0) = -P_- \delta_{x_0+1, y_0} + B(\mathbf{p}^+, x_0) \delta_{x_0, y_0} - P_+ \delta_{x_0-1, y_0}, \tag{B.26}$$

then gives

$$\left[B(\mathbf{p}^+, x_0) P_+ - P_-\right] F^{f/b}(x_0 + 1) + \left[B(\mathbf{p}^+, x_0) P_- - P_+\right] F^{f/b}(x_0) = 0, \tag{B.27}$$

which is solvable by one–step recursion.

Having computed the solutions ψ^f and ψ^b, one can construct the propagator for $x_0 \neq y_0$,

$$S(\mathbf{p}; x_0, y_0) = \begin{cases} \psi^f(\mathbf{p}, x_0) N^f(\mathbf{p}, y_0) \gamma_5 & \text{for } x_0 < y_0, \\ \psi^b(\mathbf{p}, x_0) N^b(\mathbf{p}, y_0) \gamma_5 & \text{for } x_0 > y_0. \end{cases} \tag{B.28}$$

In order to determine N^f and N^b, one has to impose the required symmetry of the propagator,

$$\gamma_5 S(\mathbf{p}; x_0, y_0)\gamma_5 = S(\mathbf{p}; y_0, x_0)^\dagger, \tag{B.29}$$

which yields

$$\begin{aligned} N^f(\mathbf{p}, y_0) &= \mathcal{V}(\mathbf{p}, y_0)\psi^b(\mathbf{p}, y_0)^\dagger, & \text{(B.30)} \\ N^b(\mathbf{p}, y_0) &= \mathcal{V}(\mathbf{p}, y_0)^\dagger\psi^f(\mathbf{p}, y_0)^\dagger. & \text{(B.31)} \end{aligned}$$

Knowing that (B.18) is valid especially for $z_0 = x_0 + 1$ and $z_0 = x_0 - 1$ and using (B.29), one now concludes that, for the case $x_0 = y_0$, one has

$$\begin{aligned} S(\mathbf{p}; x_0, x_0) &= P_-\psi^f(\mathbf{p}, x_0)\mathcal{V}(\mathbf{p}, x_0)\psi^b(\mathbf{p}, x_0)^\dagger\gamma_5 \\ &\quad + P_+\psi^b(\mathbf{p}, x_0)\mathcal{V}(\mathbf{p}, x_0)^\dagger\psi^f(\mathbf{p}, x_0)^\dagger\gamma_5. \end{aligned} \tag{B.32}$$

Now, one is left with the task to determine $\mathcal{V}(\mathbf{p}, x_0)$. A lengthy calculation shows that one has

$$\begin{aligned} \left[\mathcal{V}(\mathbf{p}, x_0)^\dagger\right]^{-1} &= [P_-\psi^f(\mathbf{p}, x_0)]^\dagger\gamma_5 P_+\psi^b(\mathbf{p}, x_0 - 1) \\ &\quad - [P_+\psi^f(\mathbf{p}, x_0 - 1)]^\dagger\gamma_5 P_-\psi^b(\mathbf{p}, x_0). \end{aligned} \tag{B.33}$$

Furthermore, this expression can be shown to be independent of x_0,

$$\mathcal{V}(\mathbf{p}, x_0) = \mathcal{V}(\mathbf{p}). \tag{B.34}$$

(B.33) may hence be evaluated at an arbitrarily chosen x_0. Due to the boundary conditions, the expression becomes particularly simple for $x_0 = 1$, where one has

$$\left[\mathcal{V}(\mathbf{p})^\dagger\right]^{-1} = [P_-\psi^f(\mathbf{p}, 1)]^\dagger\gamma_5 P_+\psi^b(\mathbf{p}, 0). \tag{B.35}$$

Having computed $\mathcal{V}$, one can now construct the whole propagator,

$$S(\mathbf{p}; x_0, y_0) = \begin{cases} \psi^f(\mathbf{p}, x_0)\mathcal{V}(\mathbf{p})\psi^b(\mathbf{p}, y_0)^\dagger\gamma_5 & \text{for } x_0 < y_0, \\ \psi^b(\mathbf{p}, x_0)\mathcal{V}(\mathbf{p})^\dagger\psi^f(\mathbf{p}, y_0)^\dagger\gamma_5 & \text{for } x_0 > y_0, \\ P_-\psi^f(\mathbf{p}, x_0)\mathcal{V}(\mathbf{p})\psi^b(\mathbf{p}, x_0)^\dagger\gamma_5 & \\ \quad + P_+\psi^b(\mathbf{p}, x_0)\mathcal{V}(\mathbf{p})^\dagger\psi^f(\mathbf{p}, x_0)^\dagger\gamma_5 & \text{for } x_0 = y_0. \end{cases} \tag{B.36}$$

Appendix C

The extrapolation procedure

For the extrapolation of the 1–loop data to the continuum limit, the method described in [34] was used, which is a generalisation of the blocking technique used in [75].

In order to simplify the notation, the following description is given in lattice units, i. e. $a = 1$. The results which are to be extrapolated are n numbers $F(L)$ for a given range $L_1 < L_2 \ldots < L_n$. The aim is to extract the leading coefficient for $L \to \infty$.

One source of errors are roundoff effects. Optimistically, one may assume that the values $F(L)$ are correct up to machine precision,

$$\delta_F(L) = \epsilon |F(L)|, \tag{C.1}$$

with $\epsilon \sim 10^{-14}$ for double precision arithmetic, which was used for all computations in this thesis. Since the calculation of the Feynman diagrams involves large sums of terms of different sign, this is clearly an underestimation. In order to get a more realistic idea of the size of the roundoff errors, one could compare double precision to single (or quadruple) precision results and estimate the L–dependence of ϵ. This was done, for example, with the 2–loop results for the coupling in [34], where one found a growth of the roundoff error proportional to L^3 for most contributions. However, experience shows that the error of the extrapolation usually is completely dominated by the systematic error, so that this procedure for estimating the roundoff error did not seem to be necessary for our calculations.

For the extrapolation, we assume $F(L)$ to have an asymptotic expansion in functions $f_k(L)$ with $k = 1, 2, \ldots, n_f$,

$$F(L) = \sum_{k=1}^{n_f} \alpha_k f_k(L) + R(L), \tag{C.2}$$

where the rest $R(L)$ behaves like

$$\left| \frac{R(L)}{f_{n_f}(L)} \right| \to 0 \quad \text{as} \quad L \to \infty. \tag{C.3}$$

For improved 1–loop quantities, one would choose the functions $f_k(L)$ to be $1, \ln L/L^2, 1/L^2, \ln L/L^3, 1/L^3 \ldots$. Writing the n data values $F(L)$ as an n–dimensional column vector, (C.2) becomes

$$F = f\alpha + R, \tag{C.4}$$

where f is an $n \times n_f$ matrix and α is the n_f dimensional vector one wants to determine.

In order to get α, one has to minimise the quadratic form

$$\chi^2 = (F - f\alpha)^\top W^2 (F - f\alpha). \tag{C.5}$$

Here, W^2 is an $n \times n$ matrix of positive weights. It can be used to put an emphasis on small or large L. While the values at small L are less affected by roundoff errors, the asymptotic expansion is expected to hold to a better degree at large L, resulting in a smaller systematic error. In this thesis, all extrapolations where done with $W = 1$, and the behaviour of the systematic errors was examined by taking an L range from $L_{\min}$ to $L_{\max}$ and varying $L_{\min}$ at fixed $L_{\max}$. However, for reasons of generality, the procedure will be outlined here for arbitrary W^2.

Minimisation of (C.5) yields

$$f^\top W^2 f\alpha = f^\top W^2 F. \tag{C.6}$$

The columns of Wf, which are assumed to be linearly independent, span an n_f–dimensional subspace. Denoting the projector onto this subspace by P, one gets

$$Wf\alpha = PWF. \tag{C.7}$$

This equation has to be solved for α. As a suitable way to do this, the singular value decomposition [77] for Wf turned out to give stable results. To this end, one uses the factorisation

$$Wf = USV^\top, \tag{C.8}$$

where U is an $n \times n_f$ matrix with orthonormal columns and

$$U^\top U = 1, \qquad UU^\top = P. \tag{C.9}$$

S and V are both $n_f \times n_f$ matrices, S being diagonal and V orthonormal. Thus one gets the solution for α,

$$\alpha = VS^{-1}U^\top WF. \tag{C.10}$$

Now, one has to determine the error of α_k. The roundoff error δ_{α_k} is obtained from (C.1) by simple error propagation,

$$\delta^2_{\alpha_k} = \sum_L (VS^{-1}U^\top)^2_{kL} \delta^2_{F(L)}. \tag{C.11}$$

The determination of the systematic error is a more delicate problem. In [34], it was found that a convenient method is the following.

One assumes that the remainder R can be modelled by a linear combination of n_r functions $f_{n_f+1}, \ldots, f_{n_f+n_r}$. For the 1–loop calculations in this thesis, one may choose the functions $1, \ln L/L, 1/L, \ldots, \ln L/L^m, 1/L^m$ with some positive integer m for the fit and take the $n_r = 2$ functions $\ln L/L^{m+1}$ and $1/L^{m+1}$ to model the remainder. Now, one does n_r separate fits including the n_f functions used before and *one* of the n_r extra functions. In these fits, one gets coefficients $A_1, \ldots A_{n_r}$ for the extra functions. In order to estimate the error, one repeats the original fit, this time not using the data $F(L)$ but the function $A_1 f_{n_f+1}(L)$. In this fit, each of the n_f functions f_k will get a coefficient β_k. The same is done with the other $n_r - 1$ extra functions. For each function f_k, one thus gets n_r coefficients β_k. The largest of these β_k is then taken as the systematic error d_{α_k} of the coefficient α_k.

Appendix D

Tables of expansion coefficients

The 1–loop coefficient $m_1^{(1)}$, which is set to zero in order to compute the critical bare mass, can be decomposed into

$$am_1^{(1)} = u_1 + N_\mathrm{f}u_2 + c_\mathrm{sw}^{(1)}u_3 + \tilde{c}_\mathrm{t}^{(1)}u_4 + c_\mathrm{A}^{(1)}u_5 + am_\mathrm{c}^{(1)}u_6 + c_\mathrm{t}^{(1)}u_7. \tag{D.1}$$

The coefficients u_i are shown in tables D.1 and D.2 for $\theta = \pi/5$ and $\rho = 1$ and in tables D.3 and D.4 for the other values of θ and ρ.

In the same way, $m_1^{(1)}(2L)$ and m' (defined using the upper boundary quark fields) may be decomposed according to

$$am_1^{(1)}(2L/a) = v_1 + N_\mathrm{f}v_2 + c_\mathrm{sw}^{(1)}v_3 + \tilde{c}_\mathrm{t}^{(1)}v_4 + c_\mathrm{A}^{(1)}v_5 + am_\mathrm{c}^{(1)}(L/a)v_6 + c_\mathrm{t}^{(1)}v_7, \tag{D.2}$$

with the coefficients v_i for $\theta = \pi/5$ and $\rho = 1$ in tables D.5 and D.6, and

$$am'^{(1)} = w_1 + N_\mathrm{f}w_2 + c_\mathrm{sw}^{(1)}w_3 + \tilde{c}_\mathrm{t}^{(1)}w_4 + c_\mathrm{A}^{(1)}w_5 + am_\mathrm{c}^{(1)}w_6 + c_\mathrm{t}^{(1)}w_7, \tag{D.3}$$

with the coefficients w_i for $\theta = \pi/5$ and $\rho = 1$ in tables D.7 and D.8.

The renormalisation constant Z_P has the coefficients

$$Z_\mathrm{P}^{(1)} = z_1 + N_\mathrm{f}z_2 + c_\mathrm{sw}^{(1)}z_3 + \tilde{c}_\mathrm{t}^{(1)}z_4 + am_\mathrm{c}^{(1)}z_6 + c_\mathrm{t}^{(1)}z_7, \tag{D.4}$$

where the coefficients z_i can be found in tables D.9 and D.10 for $\theta = \pi/5$ and $\rho = 1$ and in tables D.11 and D.12 for different values of θ and ρ. Finally, the renormalisation constant Z_P at $2L$ such that $m_1(L) = 0$ may be expanded according to

$$Z_\mathrm{P}^{(1)}(2L/a) = \tilde{z}_1 + N_\mathrm{f}\tilde{z}_2 + c_\mathrm{sw}^{(1)}\tilde{z}_3 + \tilde{c}_\mathrm{t}^{(1)}\tilde{z}_4 + am_\mathrm{c}^{(1)}(L/a)\tilde{z}_6 + c_\mathrm{t}^{(1)}\tilde{z}_7, \tag{D.5}$$

with the coefficients $\tilde{z}_i$ in tables D.13 and D.14 for $\theta = \pi/5$ and $\rho = 1$ and in tables D.15 and D.16 for the other values of θ and ρ.

In the tables, up to ten digits of the coefficients are shown. Since they have been computed using double precision arithmetic and experience shows that up

to $L/a = 32$, one looses two to three digits due to roundoff errors, all digits shown here should be significant. To get a better estimate for the roundoff errors, one would have to compare the results for some small lattices with single or quadruple precision results and extract the scaling behaviour of the errors for increasing L/a. In this thesis, however, we are only interested in discretisation errors, where the last digits are irrelevant, and in extrapolations, which are dominated by the systematic errors due to higher order terms in the expansion. Therefore, a precise determination of the roundoff errors did not seem to be necessary.

L/a	u_1	u_2	u_3
4	0.3602839939	-0.003225474813	-0.09605428870
5	0.3232002646	-0.000774641219	-0.05739586792
6	0.3037717960	-0.000214828175	-0.03886722333
7	0.2945227639	-0.000090081829	-0.02788612762
8	0.2886435020	-0.000047062385	-0.02116169433
9	0.2846484024	-0.000027131359	-0.01653724923
10	0.2818166195	-0.000017284660	-0.01334401178
11	0.2797403581	-0.000011720940	-0.01096120300
12	0.2781681231	-0.000008284863	-0.00919331010
13	0.2769535573	-0.000006129109	-0.00780391809
14	0.2759917826	-0.000004608993	-0.00672232221
15	0.2752204783	-0.000003596909	-0.00584115805
16	0.2745896768	-0.000002820717	-0.00513109826
17	0.2740694316	-0.000002283224	-0.00453708978
18	0.2736334509	-0.000001846627	-0.00404578595
19	0.2732659914	-0.000001535330	-0.00362632773
20	0.2729521158	-0.000001271725	-0.00327224614
21	0.2726829531	-0.000001079336	-0.00296502249
22	0.2724494848	-0.000000911236	-0.00270139289
23	0.2722464289	-0.000000786142	-0.00246962788
24	0.2720680657	-0.000000674154	-0.00226804856
25	0.2719111055	-0.000000589418	-0.00208889322
26	0.2717717705	-0.000000512088	-0.00193130204
27	0.2716479341	-0.000000452721	-0.00178994940
28	0.2715370145	-0.000000397695	-0.00166441225
29	0.2714375933	-0.000000354905	-0.00155092337
30	0.2713478540	-0.000000314740	-0.00144929720
31	0.2712668249	-0.000000283144	-0.00135679872
32	0.2711931957	-0.000000253175	-0.00127337243

Table D.1: *Parts of the 1–loop coefficient* $m_1^{(1)}$ *for* $\theta = \pi/5$ *and* $\rho = 1$

L/a	u_4	u_5	u_6	u_7
4	0.7316730490	0.6084363759	1.188647276	0.01803922007
5	0.3210591192	0.3878385759	1.117262157	0.00413349286
6	0.0042189812	0.2631884549	1.079778023	-0.00157603839
7	0.0024050333	0.1935221158	1.057964363	-0.00069723702
8	0.0012919050	0.1464623871	1.043886577	-0.00038756353
9	0.0008286417	0.1158988293	1.034483484	-0.00020611832
10	0.0005124163	0.0932417601	1.027741909	-0.00012753286
11	0.0003555287	0.0771715444	1.022853029	-0.00007616582
12	0.0002404411	0.0645591187	1.019116087	-0.00005074611
13	0.0001763427	0.0550783445	1.016254342	-0.00003280704
14	0.0001268701	0.0473445009	1.013970372	-0.00002306893
15	0.0000969510	0.0412863218	1.012152254	-0.00001579511
16	0.0000729793	0.0362045275	1.010655337	-0.00001157037
17	0.0000575581	0.0320993397	1.009428779	-0.00000827330
18	0.0000448460	0.0285822227	1.008394882	-0.00000625754
19	0.0000362650	0.0256723716	1.007528515	-0.00000462840
20	0.0000290320	0.0231377112	1.006784665	-0.00000359173
21	0.0000239575	0.0210003357	1.006150100	-0.00000272952
22	0.0000196031	0.0191135425	1.005597146	-0.00000216309
23	0.0000164500	0.0174975213	1.005118494	-0.00000168054
24	0.0000137045	0.0160552118	1.004696293	-0.00000135523
25	0.0000116632	0.0148037736	1.004326361	-0.00000107234
26	0.0000098641	0.0136765405	1.003996718	-0.00000087756
27	0.0000084961	0.0126877084	1.003704907	-0.00000070513
28	0.0000072780	0.0117900311	1.003442618	-0.00000058430
29	0.0000063338	0.0109951461	1.003208384	-0.00000047564
30	0.0000054857	0.0102686695	1.002996274	-0.00000039839
31	0.0000048172	0.0096201313	1.002805407	-0.00000032793
32	0.0000042121	0.0090239315	1.002631448	-0.00000027722

Table D.2: *Parts of the 1–loop coefficient* $m_1^{(1)}$ *for* $\theta = \pi/5$ *and* $\rho = 1$ *(cont.)*

L/a	u_1	u_2	u_3
$\theta = 0,\ \rho = 1$			
4	0.3117291700	-0.001413989874	-0.06325439280
6	0.2851814233	-0.000072348720	-0.02653692904
8	0.2786313238	-0.000015427643	-0.01462634537
10	0.2755771628	-0.000005279182	-0.00927252482
12	0.2739097717	-0.000002238838	-0.00640604311
14	0.2729004050	-0.000001074282	-0.00469179577
16	0.2722432007	-0.000000559106	-0.00358486772
$\theta = 0.5,\ \rho = 1$			
4	0.3527716036	-0.003134326041	-0.08882286240
6	0.3009793922	-0.000203934067	-0.03600623562
8	0.2872085538	-0.000044256296	-0.01960752669
10	0.2809505241	-0.000016156714	-0.01236285801
12	0.2775900272	-0.000007687118	-0.00851637431
14	0.2755788098	-0.000004247030	-0.00622673813
16	0.2742799815	-0.000002584214	-0.00475246807
$\theta = 0,\ \rho = 2$			
4	0.2890122981	-0.000466276200	-0.02966169499
6	0.2776917924	-0.000096885717	-0.01285486035
8	0.2742017998	-0.000032373848	-0.00717204102
10	0.2726668499	-0.000014117091	-0.00457353269
12	0.2718544505	-0.000007249144	-0.00317000300
$\theta = 0.5,\ \rho = 2$			
4	0.3230287075	0.004646415684	-0.04091643990
6	0.2928573371	0.000682358234	-0.01682956807
8	0.2827493514	0.000177104745	-0.00920123428
10	0.2781432425	0.000066678908	-0.00581015860
12	0.2756603756	0.000030966376	-0.00400514977

Table D.3: *Parts of the 1–loop coefficient* $m_1^{(1)}$ *for various values of* θ *and* ρ

L/a	u_4	u_5	u_6	u_7
$\theta = 0,\ \rho = 1$				
4	0.5887651776	0.2773460352	1.060808688	0.01414891282
6	0.0007741031	0.1200813871	1.027928002	-0.00039927726
8	0.0001985526	0.0670949370	1.016024884	-0.00007249879
10	0.0000659113	0.0428310908	1.010376100	-0.00001642414
12	0.0000255381	0.0297073108	1.007259112	-0.00000361335
14	0.0000108268	0.0218109132	1.005360129	-0.00000027458
16	0.0000047721	0.0166920181	1.004118703	0.00000058142
$\theta = 0.5,\ \rho = 1$				
4	0.7136493082	0.5749737393	1.168810060	0.01714141379
6	0.0030661542	0.2495987793	1.072695582	-0.00138698280
8	0.0009267006	0.1391978462	1.040386927	-0.00033684366
10	0.0003656376	0.0887236823	1.025677627	-0.00010975186
12	0.0001711788	0.0614750484	1.017759437	-0.00004324006
14	0.0000902366	0.0451034411	1.013012168	-0.00001945044
16	0.0000518894	0.0345013971	1.009943004	-0.00000964499
$\theta = 0,\ \rho = 2$				
4	0.0032392824	0.0936449462	1.036188030	-0.00040229454
6	0.0005702345	0.0394953561	1.014454343	-0.00004485954
8	0.0001630428	0.0217769672	1.007693781	-0.00000952668
10	0.0000612800	0.0138044243	1.004761213	-0.00000285504
12	0.0000273938	0.0095357430	1.003232426	-0.00000105727
$\theta = 0.5,\ \rho = 2$				
4	0.0011902517	0.4959636094	1.137886597	-0.00272630910
6	0.0001742293	0.2178875276	1.060855811	-0.00034621022
8	0.0000433483	0.1220946720	1.034142311	-0.00008143737
10	0.0000147043	0.0780067469	1.021817535	-0.00002664492
12	0.0000060319	0.0541217346	1.015134789	-0.00001071394

Table D.4: *Parts of the 1–loop coefficient $m_1^{(1)}$ for various values of θ and ρ (cont.)*

L/a	v_1	v_2	v_3
4	0.2888594021	-0.00005058908107	-0.02117043086
5	0.2820887015	-0.00001972144488	-0.01335256814
6	0.2782616600	-0.00000882525879	-0.00919576341
7	0.2760809582	-0.00000497218858	-0.00672431079
8	0.2746373747	-0.00000296561503	-0.00513202789
9	0.2736756316	-0.00000194609439	-0.00404651418
10	0.2729796791	-0.00000132369711	-0.00327267396
11	0.2724733713	-0.00000094810144	-0.00270172931
12	0.2720853970	-0.00000069646118	-0.00226827213
13	0.2717867718	-0.00000052844286	-0.00193148046
14	0.2715486018	-0.00000040853487	-0.00166454014
15	0.2713579394	-0.00000032292580	-0.00144940101
16	0.2712013150	-0.00000025894756	-0.00127345074

Table D.5: *Parts of the 1–loop coefficient* $m_1^{(1)}(2L)$ *with* $m_1(L) = 0$ *for* $\theta = \pi/5$ *and* $\rho = 1$

L/a	v_4	v_5	v_6	v_7
4	0.001291461837	0.1463868229	1.045074777	-0.0003869872089
5	0.000511742035	0.0931663422	1.029247500	-0.0001269718170
6	0.000240252491	0.0645364689	1.019635452	-0.0000506118783
7	0.000126734771	0.0473260174	1.014466186	-0.0000229801784
8	0.000072924806	0.0361957674	1.010920783	-0.0000115365918
9	0.000044809374	0.0285753372	1.008629730	-0.0000062357257
10	0.000029013497	0.0231336427	1.006938179	-0.0000035810441
11	0.000019590549	0.0191103368	1.005730206	-0.0000021559966
12	0.000013697243	0.0160530751	1.004792851	-0.0000013512045
13	0.000009858993	0.0136748331	1.004080301	-0.0000008747879
14	0.000007274769	0.0117888051	1.003507183	-0.0000005825718
15	0.000005483328	0.0102676735	1.003052472	-0.0000003971558
16	0.000004210539	0.0090231792	1.002676692	-0.0000002763990

Table D.6: *Parts of the 1–loop coefficient* $m_1^{(1)}(2L)$ *with* $m_1(L) = 0$ *for* $\theta = \pi/5$ *and* $\rho = 1$ *(cont.)*

L/a	w_1	w_2	w_3
4	0.2971376852	0.007159453631	0.07069378144
5	0.2930551099	0.002002507543	0.04435489541
6	0.2845876866	0.000904887361	0.03097531507
7	0.2820563435	0.000384152314	0.02227017749
8	0.2796089169	0.000228377566	0.01706219846
9	0.2779500101	0.000127950492	0.01329286954
10	0.2764995647	0.000087862653	0.01077351137
11	0.2755037279	0.000057206374	0.00882189295
12	0.2746365666	0.000042530198	0.00741823947
13	0.2740124775	0.000030217871	0.00628082481
14	0.2734635897	0.000023601409	0.00541982387
15	0.2730515248	0.000017755117	0.00469970451
16	0.2726849153	0.000014352239	0.00413374337
17	0.2724001308	0.000011245712	0.00364919780
18	0.2721440627	0.000009327024	0.00325731535
19	0.2719396253	0.000007535561	0.00291573391
20	0.2717540932	0.000006376663	0.00263317208
21	0.2716026412	0.000005276671	0.00238335648
22	0.2714640928	0.000004537982	0.00217290423
23	0.2713489030	0.000003828045	0.00198468504
24	0.2712427988	0.000003336311	0.00182372283
25	0.2711532200	0.000002859114	0.00167838569
26	0.2710702125	0.000002519843	0.00155251931
27	0.2709992153	0.000002188062	0.00143795523
28	0.2709330829	0.000001946840	0.00133766988
29	0.2708758835	0.000001709481	0.00124576235
30	0.2708223594	0.000001533525	0.00116456364
31	0.2707756142	0.000001359513	0.00108970680
32	0.2707316956	0.000001228300	0.00102303872

Table D.7: *Parts of m' at 1–loop order with $m_1(L) = 0$ for $\theta = \pi/5$ and $\rho = 1$*

L/a	w_4	w_5	w_6	w_7
4	0.6670524594	0.8104561493	1.111943322	-0.01095404633
5	0.3903966722	0.5388856057	1.091349905	-0.00357819396
6	-0.0022730281	0.3747386559	1.069419226	0.00063957047
7	-0.0010901031	0.2781810491	1.055379436	0.00017422876
8	-0.0006270025	0.2119249521	1.043698522	-0.00008757089
9	-0.0003743296	0.1681735583	1.035783207	-0.00008690205
10	-0.0002493311	0.1356020041	1.029322006	-0.00009872911
11	-0.0001683210	0.1123440306	1.024688617	-0.00007582581
12	-0.0001217515	0.0940684807	1.020845628	-0.00006576171
13	-0.0000885627	0.0802868921	1.017957986	-0.00005052598
14	-0.0000674800	0.0690416443	1.015515375	-0.00004195232
15	-0.0000515736	0.0602178847	1.013611180	-0.00003293300
16	-0.0000407400	0.0528164319	1.011971652	-0.00002726629
17	-0.0000322524	0.0468314608	1.010655815	-0.00002188842
18	-0.0000261695	0.0417044433	1.009505714	-0.00001826479
19	-0.0000212731	0.0374600536	1.008560908	-0.00001495738
20	-0.0000176252	0.0337634280	1.007724628	-0.00001261428
21	-0.0000146275	0.0306449645	1.007024441	-0.00001050889
22	-0.0000123250	0.0278924569	1.006398071	-0.00000895924
23	-0.0000104015	0.0255343162	1.005865307	-0.00000757449
24	-0.0000088871	0.0234298978	1.005384399	-0.00000652389
25	-0.0000076047	0.0216036230	1.004969907	-0.00000558578
26	-0.0000065743	0.0199587646	1.004592861	-0.00000485624
27	-0.0000056916	0.0185156623	1.004264203	-0.00000420373
28	-0.0000049703	0.0172056983	1.003963238	-0.00000368576
29	-0.0000043461	0.0160456199	1.003698336	-0.00000322116
30	-0.0000038285	0.0149854514	1.003454342	-0.00000284588
31	-0.0000033768	0.0140389494	1.003237764	-0.00000250813
32	-0.0000029975	0.0131688820	1.003037259	-0.00000223120

Table D.8: *Parts of m' at 1–loop order with $m_1(L) = 0$ for $\theta = \pi/5$ and $\rho = 1$ (cont.)*

L/a	z_1	z_2	z_3
4	0.09550891946	0.03423528831	-0.1341134935
6	0.16565857330	0.01473258948	-0.0932504829
8	0.22869553805	0.00949691345	-0.0711779334
10	0.28916821812	0.00753246481	-0.0574507258
12	0.34887762674	0.00654228932	-0.0481191321
14	0.40849882024	0.00594073122	-0.0413752997
16	0.46828819102	0.00553322566	-0.0362791400
18	0.52833626903	0.00523794769	-0.0322950506
20	0.58866515448	0.00501397159	-0.0290961208
22	0.64926855814	0.00483827767	-0.0264717741
24	0.71012902785	0.00469683169	-0.0242803679
26	0.77122555828	0.00458056303	-0.0224231782
28	0.83253695525	0.00448334105	-0.0208293183
30	0.89404326241	0.00440087155	-0.0194465900
32	0.95572628769	0.00433005700	-0.0182357146

Table D.9: *Parts of the 1–loop coefficient* $Z_{\mathrm{P}}^{(1)}$ *at* $\theta = \pi/5$ *and* $\rho = 1$

L/a	z_4	z_6	z_7
4	0.2752077673	1.240156503	-0.1954547977
6	0.3024134295	1.582932389	-0.1615028450
8	0.2903043621	1.870599424	-0.1331757885
10	0.2677764380	2.136141388	-0.1121302285
12	0.2446013168	2.391341118	-0.0964095495
14	0.2234839233	2.641100707	-0.0843763356
16	0.2049375164	2.887730110	-0.0749275370
18	0.1888173394	3.132429195	-0.0673363702
20	0.1748109198	3.375870929	-0.0611160764
22	0.1625955840	3.618456709	-0.0559323228
24	0.1518850825	3.860438271	-0.0515494198
26	0.1424386316	4.101980209	-0.0477971213
28	0.1340577488	4.343193976	-0.0445497094
30	0.1265798562	4.584157332	-0.0417124957
32	0.1198717596	4.824925943	-0.0392128935

Table D.10: *Parts of the 1–loop coefficient* $Z_{\mathrm{P}}^{(1)}$ *at* $\theta = \pi/5$ *and* $\rho = 1$ *(cont.)*

L/a	z_1	z_2	z_3
$\theta = 0,\ \rho = 1$			
4	0.1326808072	0.01528384278	-0.1168458223
6	0.1474652524	0.00728806063	-0.0779791840
8	0.1731329290	0.00439645001	-0.0585101791
10	0.2035733306	0.00321873110	-0.0468218991
12	0.2367057252	0.00262320959	-0.0390261029
14	0.2715872938	0.00226224002	-0.0334556609
16	0.3077062797	0.00201667075	-0.0292766717
$\theta = 0.5,\ \rho = 1$			
4	0.0824520269	0.03143610800	-0.1238972498
6	0.1271965066	0.01394010853	-0.0857279226
8	0.1683678316	0.00887347640	-0.0652575226
10	0.2089123772	0.00693665488	-0.0525900075
12	0.2497370083	0.00597030160	-0.0440062052
14	0.2910727552	0.00538995423	-0.0378156722
16	0.3329441002	0.00499976060	-0.0331442026
$\theta = 0,\ \rho = 2$			
4	0.6521364999	0.02993994420	-0.1209100243
6	0.9221596868	0.01125513464	-0.0810128062
8	1.1964703064	0.00632783134	-0.0608921086
10	1.4728928412	0.00424833271	-0.0487675434
12	1.7507932870	0.00311330602	-0.0406652864
$\theta = 0.5,\ \rho = 2$			
4	0.0665300894	0.16011586673	-0.0811127180
6	0.1791766558	0.07550278985	-0.0548862358
8	0.2766417147	0.04877505559	-0.0413683000
10	0.3693268329	0.03915526808	-0.0331678255
12	0.4605318775	0.03486305919	-0.0276723609

Table D.11: *Parts of the 1–loop coefficient* $Z_{\mathrm{P}}^{(1)}$ *at various values of* θ *and* ρ

L/a	z_4	z_6	z_7
$\theta = 0,\ \rho = 1$			
4	0.2448721196	1.297122470	-0.1526509731
6	0.1942219137	1.476291125	-0.1197969999
8	0.1640794499	1.643098574	-0.0965623402
10	0.1420781526	1.806546577	-0.0803607200
12	0.1251135646	1.968711620	-0.0686367894
14	0.1116498521	2.130300176	-0.0598239325
16	0.1007298970	2.291603872	-0.0529813561
$\theta = 0.5,\ \rho = 1$			
4	0.2334171022	1.189005361	-0.1834591369
6	0.2443514694	1.448427447	-0.1510297236
8	0.2314225501	1.659729841	-0.1241302945
10	0.2123099369	1.853796129	-0.1042991779
12	0.1934250942	2.040359892	-0.0895616671
14	0.1764740188	2.223182810	-0.0783182317
16	0.1616952383	2.403947754	-0.0695088918
$\theta = 0,\ \rho = 2$			
4	0.5124378929	2.975968192	-0.1883730541
6	0.4114552065	4.088045527	-0.1353705625
8	0.3378163059	5.172972867	-0.1049844154
10	0.2849616955	6.247086041	-0.0855561121
12	0.2458461197	7.315968086	-0.0721305763
$\theta = 0.5,\ \rho = 2$			
4	0.2819915539	1.490852756	-0.2128630913
6	0.2895835015	1.938807978	-0.1612690338
8	0.2645149383	2.334410619	-0.1275581165
10	0.2365500613	2.709957987	-0.1049282241
12	0.2116794602	3.076362839	-0.0889178266

Table D.12: *Parts of the 1–loop coefficient* $Z_{\rm P}^{(1)}$ *at various values of* θ *and* ρ *(cont.)*

L/a	$\tilde{z}_1$	$\tilde{z}_2$	$\tilde{z}_3$
4	0.2293123742	0.009573101967	-0.07147065652
6	0.3494732430	0.006579092370	-0.04825027064
8	0.4688244330	0.005555581838	-0.03634661389
10	0.5891478869	0.005029207837	-0.02913523296
12	0.7105656939	0.004707933201	-0.02430499001
14	0.8329343379	0.004491803200	-0.02084578712
16	0.9560901651	0.004336724846	-0.01824725568

Table D.13: *Parts of the 1–loop coefficient* $Z_{\mathrm{P}}^{(1)}(2L)$ *with* $m_1(L) = 0$ *at* $\theta = \pi/5$ *and* $\rho = 1$

L/a	$\tilde{z}_4$	$\tilde{z}_6$	$\tilde{z}_7$
4	0.2911905373	1.874547330	-0.1335040402
6	0.2450740029	2.394596702	-0.0965677693
8	0.2051995671	2.890423111	-0.0750119316
10	0.1749691162	3.378169482	-0.0611660627
12	0.1519872262	3.862442505	-0.0515813433
14	0.1341272577	4.344969442	-0.0445712831
16	0.1199210816	4.826518506	-0.0392281295

Table D.14: *Parts of the 1–loop coefficient* $Z_{\mathrm{P}}^{(1)}(2L)$ *with* $m_1(L) = 0$ *at* $\theta = \pi/5$ *and* $\rho = 1$ *(cont.)*

L/a	$\tilde{z}_1$	$\tilde{z}_2$	$\tilde{z}_3$
$\theta = 0,\ \rho = 1$			
4	0.1844808442	0.004372112061	-0.05984829671
6	0.2453504776	0.002601676822	-0.03949477059
8	0.3142628791	0.002001926120	-0.02947930729
10	0.3877224203	0.001689952794	-0.02352815290
12	0.4639602752	0.001496341488	-0.01958158454
14	0.5420480669	0.001364127036	-0.01677124455
16	0.6214500817	0.001268049176	-0.01466752787
$\theta = 0.5,\ \rho = 1$			
4	0.1689995368	0.008923199948	-0.06548732132
6	0.2505009004	0.005999143948	-0.04413591317
8	0.3336383383	0.005016999229	-0.03321155407
10	0.4187398577	0.004517026013	-0.02660691792
12	0.5054112010	0.004213452330	-0.02218859089
14	0.5932918622	0.004009910129	-0.01902679794
16	0.6821137770	0.003864208278	-0.01665284161
$\theta = 0,\ \rho = 2$			
4	1.2060785837	0.007491917291	-0.06149659905
6	1.7559778103	0.003528122640	-0.04081983117
8	2.3131197146	0.002140383509	-0.03057928797
10	2.8738200566	0.001463496442	-0.02445228153
12	3.4366941330	0.001073113077	-0.02037239719
$\theta = 0.5,\ \rho = 2$			
4	0.2773639094	0.049707671735	-0.04185048543
6	0.4609370909	0.035128446020	-0.02778302053
8	0.6423873199	0.031226685817	-0.02081561802
10	0.8244441384	0.029527745468	-0.01664726569
12	1.0074272069	0.028606927366	-0.01387127057

Table D.15: *Parts of the 1–loop coefficient* $Z_{\mathrm{P}}^{(1)}(2L)$ *with* $m_1(L) = 0$ *at various values of* θ *and* ρ

L/a	$\tilde{z}_4$	$\tilde{z}_6$	$\tilde{z}_7$
$\theta = 0,\ \rho = 1$			
4	0.1718305672	1.687871282	-0.09775258579
6	0.1280139314	2.002040662	-0.06907686487
8	0.1020232090	2.316619630	-0.05317715374
10	0.0848215601	2.633590801	-0.04317899772
12	0.0725826258	2.952117432	-0.03632993149
14	0.0634269015	3.271619233	-0.03134989520
16	0.0563194892	3.591757515	-0.02756760705
$\theta = 0.5,\ \rho = 1$			
4	0.2321338155	1.663348371	-0.12438362939
6	0.1938923565	2.044179271	-0.08971537396
8	0.1619544256	2.407180440	-0.06959163712
10	0.1379679076	2.765026025	-0.05670609836
12	0.1198008298	3.120873229	-0.04780137447
14	0.1057072432	3.475803721	-0.04129513010
16	0.0945069004	3.830264175	-0.03633907736
$\theta = 0,\ \rho = 2$			
4	0.3405246084	5.207874762	-0.10562217877
6	0.2465730856	7.335024524	-0.07229922856
8	0.1926801273	9.459097330	-0.05491154830
10	0.1579528577	11.581344073	-0.04425113515
12	0.1337701693	13.702563787	-0.03705152726
$\theta = 0.5,\ \rho = 2$			
4	0.2661600367	2.343188522	-0.12821614899
6	0.2121269758	3.079864030	-0.08907791880
8	0.1730920116	3.798786095	-0.06801232921
10	0.1454143632	4.511560279	-0.05494446490
12	0.1251028064	5.221609660	-0.04606774596

Table D.16: *Parts of the 1–loop coefficient* $Z_{\rm P}^{(1)}(2L)$ *with* $m_1(L) = 0$ *at various values of* θ *and* ρ *(cont.)*

Bibliography

[1] S.L. Glashow, Nucl. Phys. 22 (1961) 579.

[2] J. Goldstone, A. Salam and S. Weinberg, Phys. Rev. 127 (1962) 965.

[3] S. Weinberg, Phys. Rev. Lett. 19 (1967) 1264.

[4] P.W. Higgs, Phys. Lett. 12 (1964) 132.

[5] J.D. Bjorken, Phys. Rev. 179 (1969) 1547.

[6] J.D. Bjorken and E.A. Paschos, Phys. Rev. 185 (1969) 1975.

[7] R.P. Feynman, Phys. Rev. Lett. 23 (1969) 1415.

[8] M. Gell-Mann, Phys. Lett. 8 (1964) 214.

[9] G. Zweig, CERN-TH-412.

[10] H. Fritzsch, M. Gell-Mann and H. Leutwyler, Phys. Lett. B47 (1973) 365.

[11] R.P. Feynman, The Principle of Least Action in Quantum Mechanics, PhD thesis, Princeton University, 1942.

[12] R.P. Feynman, Rev. Mod. Phys. 20 (1948) 367.

[13] G. 't Hooft, unpublished, see *Proc. Coll. on Renormalization of Yang-Mills Fields and Applications to Particle Physics*, Marseilles, 1972 (ed. C. P. Korthals-Altes).

[14] G. 't Hooft, Nucl. Phys. B254 (1985) 11.

[15] H.D. Politzer, Phys. Rev. Lett. 30 (1973) 1346.

[16] G. Altarelli and G. Parisi, Nucl. Phys. B126 (1977) 298.

[17] A. Peterman, Phys. Rept. 53 (1979) 157.

[18] G. Altarelli, Phys. Rept. 81 (1982) 1.

[19] M. Dine and J.R. Sapirstein, Phys. Rev. Lett. 43 (1979) 668.

[20] K.G. Chetyrkin, A.L. Kataev and F.V. Tkachov, Phys. Lett. B85 (1979) 277.

[21] W. Celmaster and R.J. Gonsalves, Phys. Rev. Lett. 44 (1980) 560.

[22] K.G. Wilson, Phys. Rev. (1974).

[23] K. Symanzik, Nucl. Phys. B226 (1983) 187.

[24] K. Symanzik, Nucl. Phys. B226 (1983) 205.

[25] M. Lüscher, P. Weisz and U. Wolff, Nucl. Phys. B359 (1991) 221.

[26] M. Lüscher, R. Sommer, P. Weisz and U. Wolff, Nucl. Phys. B413 (1994) 481, hep-lat/9309005.

[27] ALPHA, A. Bode et al., Phys. Lett. B515 (2001) 49, hep-lat/0105003.

[28] S.J. Anthony, C.H. Llewellyn Smith and J.F. Wheater, Phys. Lett. B116 (1982) 287.

[29] G.M. de Divitiis, R. Frezzotti, M. Guagnelli, M. Masetti and R. Petronzio, Nucl. Phys. B455 (1995) 274, hep-lat/9507020.

[30] J. Rolf and U. Wolff, Nucl. Phys. Proc. Suppl. 83 (2000) 899, hep-lat/9907007.

[31] B. Gehrmann, J. Rolf, S. Kurth and U. Wolff, Nucl. Phys. B612 (2001) 3, hep-lat/0106025.

[32] S. Sint and R. Sommer, Nucl. Phys. B465 (1996) 71, hep-lat/9508012.

[33] Alpha, A. Bode, U. Wolff and P. Weisz, Nucl. Phys. B540 (1999) 491, hep-lat/9809175.

[34] ALPHA, A. Bode, P. Weisz and U. Wolff, Nucl. Phys. B576 (2000) 517, hep-lat/9911018.

[35] ALPHA, S. Sint and P. Weisz, Nucl. Phys. B545 (1999) 529, hep-lat/9808013.

[36] I. Montvay and G. Münster, Quantum Fields on a Lattice (Cambridge Univ. Press, 1994).

[37] M. Creutz, Quarks, Gluons, Lattices (Cambridge Univ. Press, 1983).

[38] H.J. Rothe, Lattice Gauge Theories: An Introduction (World Scientific, 1992).

[39] M. Lüscher, Advanced lattice QCD, Talk given at Les Houches Summer School in Theoretical Physics: Probing the Standard Model of Particle Interactions, Les Houches, France, 28 Jul - 5 Sep 1997; hep-lat/9802029.

[40] R. Gupta, (1997), hep-lat/9807028.

[41] J.B. Kogut and L. Susskind, Phys. Rev. D11 (1975) 395.

[42] L. Susskind, Phys. Rev. D16 (1977) 3031.

[43] K.G. Wilson, New Phenomena In Subnuclear Physics. Part A. Proceedings of the First Half of the 1975 International School of Subnuclear Physics, Erice, Sicily, July 11 - August 1, 1975, ed. A. Zichichi, Plenum Press, New York, 1977, p. 69, CLNS-321.

[44] H.B. Nielsen and M. Ninomiya, Nucl. Phys. B185 (1981) 20.

[45] P. Hasenfratz, Nucl. Phys. B525 (1998) 401, hep-lat/9802007.

[46] P.H. Ginsparg and K.G. Wilson, Phys. Rev. D25 (1982) 2649.

[47] M. Lüscher, Phys. Lett. B428 (1998) 342, hep-lat/9802011.

[48] B. Sheikholeslami and R. Wohlert, Nucl. Phys. B259 (1985) 572.

[49] R. Wohlert, DESY 87/069.

[50] M. Lüscher and P. Weisz, Nucl. Phys. B479 (1996) 429, hep-lat/9606016.

[51] P. Weisz, internal notes (1996).

[52] M. Lüscher, S. Sint, R. Sommer, P. Weisz and U. Wolff, Nucl. Phys. B491 (1997) 323, hep-lat/9609035.

[53] ALPHA, K. Jansen and R. Sommer, Nucl. Phys. B530 (1998) 185, hep-lat/9803017.

[54] M. Lüscher, S. Sint, R. Sommer and P. Weisz, Nucl. Phys. B478 (1996) 365, hep-lat/9605038.

[55] W. Celmaster and R.J. Gonsalves, Phys. Rev. Lett. 42 (1979) 1435.

[56] G. 't Hooft, Nucl. Phys. B61 (1973) 455.

[57] W.A. Bardeen, A.J. Buras, D.W. Duke and T. Muta, Phys. Rev. D18 (1978) 3998.

[58] S. Capitani et al., Nucl. Phys. Proc. Suppl. 63 (1998) 153, hep-lat/9709125.

[59] S. Sint, Nucl. Phys. B451 (1995) 416, hep-lat/9504005.

[60] M. Lüscher, R. Narayanan, P. Weisz and U. Wolff, Nucl. Phys. B384 (1992) 168, hep-lat/9207009.

[61] A. Bode, Nucl. Phys. Proc. Suppl. 63 (1998) 796, hep-lat/9710043.

[62] S. Sint and P. Weisz, Nucl. Phys. B502 (1997) 251, hep-lat/9704001.

[63] M. Lüscher, Selected topics in lattice field theory, Lectures given at Summer School 'Fields, Strings and Critical Phenomena', Les Houches, France, Jun 28 - Aug 5, 1988.

[64] R. Narayanan and U. Wolff, Nucl. Phys. B444 (1995) 425, hep-lat/9502021.

[65] A. Bode, P. Weisz and U. Wolff, Nucl. Phys. Proc. Suppl. 83 (2000) 920, hep-lat/9908044.

[66] R. Sommer, The step scaling function with two flavours of massless Wilson quarks, 1998, unpublished.

[67] G. Heatlie, G. Martinelli, C. Pittori, G.C. Rossi and C.T. Sachrajda, Nucl. Phys. B352 (1991) 266.

[68] M. Bochicchio, L. Maiani, G. Martinelli, G.C. Rossi and M. Testa, Nucl. Phys. B262 (1985) 331.

[69] L. Maiani and G. Martinelli, Phys. Lett. B178 (1986) 265.

[70] E. Gabrielli, G. Martinelli, C. Pittori, G. Heatlie and C.T. Sachrajda, Nucl. Phys. B362 (1991) 475.

[71] M. Lüscher, S. Sint, R. Sommer and H. Wittig, Nucl. Phys. B491 (1997) 344, hep-lat/9611015.

[72] P. Weisz, internal notes (1995).

[73] K. Jansen et al., Phys. Lett. B372 (1996) 275, hep-lat/9512009.

[74] ALPHA, S. Capitani, M. Luscher, R. Sommer and H. Wittig, Nucl. Phys. B544 (1999) 669, hep-lat/9810063.

[75] M. Lüscher and P. Weisz, Nucl. Phys. B266 (1986) 309.

[76] M. Gell-Mann, Phys. Rev. 125 (1962) 1067.

[77] W.H. Press, S.A. Teukolsky, W.T. Vetterling and B.P. Flannery, Numerical recipes: The art of scientific computing (Cambridge Univ. Press, 1992).

Lebenslauf

Name:	Stefan Kurth
geboren am	10.04.1971 in Berlin
Nationalität:	Deutsch

6/1991	Abitur an der Lessing-Oberschule (Gymnasium) in Berlin-Wedding
10/1991 - 01/1997	Studium an der Technischen Universität Berlin in der Fachrichtung Physik
05/1997 - 06/1998	Wissenschaftlicher Mitarbeiter beim Deutschen Elektronensynchrotron DESY, Zeuthen
seit 07/1998	Wissenschaftlicher Mitarbeiter am Institut für Physik der Humboldt-Universität zu Berlin

Publikationen

[a] Johannes Blümlein and Stefan Kurth, *On the Mellin transform of the coefficient functions of* $F_L(x, Q^2)$, hep-ph/9708388, 1998.

[b] Johannes Blümlein and Stefan Kurth, *Harmonic sums and Mellin transforms up to two-loop order*, Phys. Rev. D60:014–018, 1999.

[c] ALPHA Collaboration (Achim Bode et al.), *First results on the running coupling in QCD with two massless flavors*, Phys. Lett. B515:49–56, 2001.

[d] Bernd Gehrmann, Stefan Kurth, Juri Rolf, Ulli Wolff, *Schrödinger functional at negative flavour number*, Nucl. Phys. B612:3–24, 2001.

[e] Stefan Kurth, *Properties of the renormalized quark mass in the Schrödinger functional with a non-vanishing background field*, Nucl. Phys. Proc. Suppl. 106: 850–852, 2002.

[f] Bernd Gehrmann, Stefan Kurth, Juri Rolf, Ulli Wolff, *Schrödinger functional at* $N_{\mathrm{f}} = -2$, Nucl. Phys. Proc. Suppl. 106:793–795, 2002.

Selbständigkeitserklärung

Hiermit erkläre ich, die vorliegende Arbeit selbständig ohne fremde Hilfe verfasst zu haben und nur die angegebene Literatur und Hilfsmittel verwendet zu haben.

Stefan Kurth
06.06.2002